UNIVERSITY OF SOUTHAMPTON

FACULTY OF PHYSICAL AND APPLIED SCIENCES

Electronics and Computer Science

Towards Smartphone-Aided Electrochemical Detection for Point-of-Care Diagnostics

by

Nikolaos G. Pechlivanidis

An MPhil thesis submitted

Supervisor: Prof. Hywel Morgan

Co-Supervisor: Dr. Daniel Spencer

Examiner: Dr. Helen Bridle

Examiner: Dr. Nicolas G Green

June 19, 2020

UNIVERSITY OF SOUTHAMPTON

ABSTRACT

FACULTY OF PHYSICAL AND APPLIED SCIENCES
Electronics and Computer Science

An MPhil thesis submitted

TOWARDS SMARTPHONE-AIDED ELECTROCHEMICAL DETECTION FOR POINT-OF-CARE DIAGNOSTICS

by Nikolaos G. Pechlivanidis

A novel portable amperometric bio-instrumentation platform that utilises the processing power of a smartphone is developed. The system rapidly reports the results of electrochemical measurement and requires small sample volumes (<15 μl). This diagnostic platform can be beneficial in developing countries, where there is limited access to medical centres. This lab-on-PCB system exploits commercial PCB manufacturing processes to make the system inexpensive. The electronic readout board connects to an Android-based smartphone for data processing and acts as a power source for the instrumentation. The results of the electrochemical reactions are reported through a simple to use, custom designed App. The electronic instrumentation platform has a wide dynamic range, measuring currents with a range of few nA to +2.5mA, allowing it to be able to reliably measure a wide range of electrochemical reactions. An automatic range-adjustment system is also implemented to adjust the input signal range maintain a high resolution in the system (122 pA resolution for input current range +/- 2.5 μA). This automatic algorithm provides better results in comparison to the constant range measurements. Furthermore, different sensing designs are performed investigating the effect of electrode's design and size on the system's sensitivity and accuracy. Finally, the system is evaluated using NaCl, H_2O_2 and an enzymatic assay: horseradish peroxidase acting on the substrate TMB (a common reporter for ELISA colorimetric detection) in the presence of H_2O_2. Results show that the amperometric data correlate well with the colorimetric for the above reaction. The promising results encourage further development of the system by adding a more complicated microfluidic design and detecting the concentration of the IFN-γ into solution.

Contents

Declaration of Authorship xiii

Acknowledgements xv

Nomenclature xvii

1 Introduction 1
- 1.1 Background and motivation . . . 1
- 1.2 Aims . . . 3
- 1.3 Thesis objectives . . . 3
- 1.4 Structure of the thesis . . . 4

2 Introduction to Point of Care diagnostic devices 7
- 2.1 Point of Care diagnostic devices . . . 7
- 2.2 Material and method of detections used in POC platforms . . . 9
  - 2.2.1 Material that are used on POC . . . 9
  - 2.2.2 Methods of detection using POC diagnostic tools . . . 10
  - 2.2.3 Microfluidics . . . 13
- 2.3 Biosensors . . . 15
- 2.4 Print Circuit Board . . . 17
- 2.5 POC Implementations . . . 18
  - 2.5.1 TB diagnostic devices . . . 18
  - 2.5.2 PCB-based applications . . . 21
  - 2.5.3 Applications based on Smartphone . . . 25
    - 2.5.3.1 Applications based on Smartphone's components . . . 25
    - 2.5.3.2 Applications based on external components . . . 28

3 Smartphone-aided bio-instrumentation platform 37
- 3.1 Design of PCB implementation . . . 37
  - 3.1.1 Layout of board . . . 40
- 3.2 Android-based App . . . 42
- 3.3 PCB-Based Sensing Platform . . . 43
  - 3.3.1 Commercial manufacturing PCB-Based Sensing Platform . . . 43
  - 3.3.2 Biosensors Geometries and Clean-room Fabrication technique . . . 44

4 Characterisation and Experimental measurements 53
- 4.1 Electronic Board Characterisation . . . 53
- 4.2 Cyclic Voltammetry . . . 55

4.3 Biological Measurements 58
4.4 Comparison with other relevant studies 70

5 Conclusions and Future work **73**
5.1 Overview and Contributions of the accomplished work 73
5.2 Future work, ideas and applications 74

A Publication record **77**

B Schematic of the bioinstrumentation board **79**

C Biosensor Parameters Definitions **85**

References **87**

List of Figures

2.1 Basic Amperometric method configuration (33). 11
2.2 Potentiometric biosensor. 12
2.3 Absorbance spectroscopy (38). 13
2.4 PCB-based micropump (43). 14
2.5 Equivalent circuit model of an electrochemical cell (Randles circuit) (52). 16
2.6 Multilayer PCB Structure. 18
2.7 Common Elisa formats (57). 19
2.8 PCB-based gold electrode array for DNA detection (67). 22
2.9 PCB sensor integrated with PMMA microfluidic channel (67). 22
2.10 Amperometric enzyme sensor for glucose, glutamate and glutamine detection (69). 23
2.11 A) PCB-based 8 independent assay areas and electrochemical cells, B) 3D representation of assay area, C) 3D representation of final phase (assay flow into the electrochemical sensor) and D) 3D representation of electrodes connections (15). 24
2.12 Heart rate algorithm based on smartphone (77). 26
2.13 Steps of a heart rate measurement (77). 26
2.14 Colorimetric detection for pH based on Smartphone (75). 27
2.15 pH reference table based on RGB values and the intensity of them (75). . 28
2.16 Immunoassay detection PCB device (78). 29
2.17 POC Electrochemical biosensor based on smartphone (79). 30
2.18 Smartphone-aided instrument for infectious diseases detection (80). 32
2.19 A simple schematic diagram of Smartphone-based instrument for infectious pathogens detection (80). 32
2.20 A 3D-printed microscope. A) An internal view of the illumination tunnel, B) A cross-section view of the illumination tunnel (external of the microscope), C) A cross-section view of the illumination tunnel (internal of the microscope) and D) The entire 3D-printed microscope (81). 33
2.21 A 3D-printed microscope and smartphone assembly. A) Insert the objective lens into the microscope, B) Place the objective lens further into the recess, C) Verify the objective lens is pushed into friction-fit recess, D) Squeeze the microscope, E) Insert the smartphone and the sample into the microscope and F) Observe the captured image using the flash mode of the smartphone's camera (81). 34
2.22 A) SERS chip on glass surface and B) SERS detection with the smartphone-based Raman analyzer (82). 35
2.23 Smartphone-aided Health Care Products: A) Blood pressure monitor, B) Wireless scale, C) Glucose meter and D) Fitness (83). 35

3.1 A simplified schematic diagram of the fabricated bioinstrumentation board that interfaces with the PCB-based sensor. . . . 38
3.2 The smartphone-aided "*eELISA*" bioinstrumentation board. . . . 39
3.3 Top Layer of the Board. . . . 41
3.4 Bottom Layer of the Board. . . . 41
3.5 Two snapshots of the designed Android-based App. On the left, the welcoming screen can be seen, while on the right a snapshot of a real-time NaCl measurement can be found. . . . 42
3.6 The proposed PCB-based sensing platform. A) The top view of the sensor with its three electrodes, B) the bottom view of the sensor with its three electrodes and C) the final assembly clamped within an aluminium frame. 44
3.7 Different Biosensors Geometries (mask size 70mm x 70mm). . . . 45
3.8 Different Biosensors Geometries (mm scale). . . . 46
3.9 Lift-off precess steps. . . . 47
3.10 Photolithography pattern of Working and Counter electrodes. . . . 48
3.11 Fabrication of different sensor's designs. . . . 49
3.12 Electroplating setup. . . . 51
3.13 AFM height image of an Au electro-deposited on FR-4 substrate with thickness almost 2.5 μm. . . . 51
3.14 PCB-based sensing platform. . . . 52

4.1 Investigation of the resolution properties of the instrument. The graphs demonstrate adequate, visible readings with 500pA and 1nA step changes. 54
4.2 Automatic adaptation of the instrument's current reading range, as the input current increases from 10nA - 50μA. . . . 55
4.3 Potentiostat characterisation: A) Manual current input and B) Standard sine wave. . . . 55
4.4 Cyclic Voltammetry of gold electrodes in Ferricyanide solution. . . . 56
4.5 Cyclic Voltammetry of 6.4 mM H_2O_2 in different scan rates. . . . 57
4.6 Cyclic Voltammetry of different concentrations of H_2O_2. . . . 57
4.7 Amperometric measurement of NaCl concentrations (high and low) with the fabricated board. The system exhibits high degree of linearity with coefficients of determination (R^2) equal to 0.9883 and 0.9950 for the high and low NaCl concentration measurements, respectively (OPC voltage: -600mV). . . . 58
4.8 Amperometric measurement of H_2O_2 concentrations, using the commercial PCB-based sensor of Figure 3.6. The system exhibits high degree of linearity with coefficient of determination (R^2) equal to 0.9953 (OPC voltage: -600mV). . . . 60
4.9 Amperometric measurement of H_2O_2 concentrations, using the fabricated PCB-based sensor of Figure 3.14. Again, the system exhibits high degree of linearity with coefficient of determination (R^2) equal to 0.94552 (OPC voltage: -600mV). . . . 60
4.10 Amperometric measurement of H_2O_2 concentrations, using the fabricated PCB-based sensor of Figure 3.14. The system shows a further increase in linearity with coefficient of determination (R^2) equal to 0.98875 (OPC voltage: -800mV). . . . 61

4.11 Amperometric measurement of H_2O_2 concentrations, using different biosensors geometries of the fabricated PCB-based sensors of Figure 3.8(OPC voltage: -800mV): A)Figure 3.8A, B)Figure 3.8C, C)Figure 3.8D, D)Figure 3.8E and E)Figure 3.8F. 62
4.12 TMB tablet dissolved in: A)DI water and B)DMSO. 63
4.13 Colorimetric detection of HRP concentrations. 64
4.14 Biological plate including TMB and HRP solutions. 64
4.15 Comparison of colorimetric and amperometric detection of HRP concentrations. 65
4.16 Steady-state kinetic assay and catalytic mechanism of TMB. 66
4.17 Current-time curve corresponding to TMB concentrations (31.25 μM - 1 mM). 67
4.18 Amperometric detection of TMB concentrations (15.625 μM - 1 mM). . . 67
4.19 Standard ELISA detection method. 69
4.20 Colorimetric measurements detecting different IFN-γ concentrations. . . . 69
4.21 Colorimetric measurements detecting different IFN-γ concentrations dissolving TMB tablet in DMSO and DI. 70

B.1 Schematic diagram of the TIAs (Input Channels 1-4). 79
B.2 Schematic diagram of the TIAs (Input Channels 5-8). 80
B.3 Schematic diagram of ADC and Power Supplies/Inverter. 80
B.4 Schematic diagram of the DDC118. 81
B.5 Schematic diagram of the μC , USB/Jack connectors and DAC. 81
B.6 Topology of the potentiostat and CE/RE connectors. 82
B.7 Top schematic diagram of the bioinstrumentation board. 82
B.8 4-Layers layout of the bioinstrumentation board. 83

List of Tables

2.1 POC requirements according to the WHO. 8
2.2 Advantages and disadvantages of POC diagnostic devices. 8
2.3 Advantages and disadvantages of Sensor's methods (51). 15
2.4 PoC diagnostic devices for TB (9). 21

3.1 Bio-instrumentation Board's Characteristics 39

4.1 Summary of the characterisation experiments 54

Declaration of Authorship

I, Nikolaos G. Pechlivanidis , declare that the thesis entitled *Towards Smartphone-Aided Electrochemical Detection for Point-of-Care Diagnostics* and the work presented in the thesis are both my own, and have been generated by me as the result of my own original research. I confirm that:

- this work was done wholly or mainly while in candidature for a research degree at this University;
- where any part of this thesis has previously been submitted for a degree or any other qualification at this University or any other institution, this has been clearly stated;
- where I have consulted the published work of others, this is always clearly attributed;
- where I have quoted from the work of others, the source is always given. With the exception of such quotations, this thesis is entirely my own work;
- I have acknowledged all main sources of help;
- where the thesis is based on work done by myself jointly with others, I have made clear exactly what was done by others and what I have contributed myself;
  - The PCB electronic platform (presented in Figure 3.2) was designed under Dr. K. Papadimitriou guidance.
  - The TMB assay and the IFN-γ protocols of Dr. D. Evans (Prof. T. Prodromakis group) were used for biological experiments. However, these protocols were replaced by Sigma-Aldritch protocols.
  - The Android based App uses open source libraries to plot data in real-time.
- parts of this work have been published as listed in Appendix A

Signed:

Date:

Acknowledgements

Firstly, I would like to express my gratitude to my family for supporting me all these difficult years of my studies, especially my parents (Dr. George Pechlivanidis and Eleni Pechlivanidou), my brother Dr. Ilias Pechlivanidis and my sister Georgia Pechlivanidou. I appreciate everything you have done.
Moreover, Dr. Nikolaos Vasilakis for his support, guidance, advices and the knowledge that transfered me about microfluidics.
Finally, I would like to thank my religious father (Metropolitan Nikodemos of Kassandreia), my cousin Dr. Ilias Pagkalos, my best friend Thodoris Voutsikakis, Elina Zoumpoulidou, Maria Papadopoulou, Eirini Vorniotaki and my friends (from Greece and the UK) for their willingness to help in all the difficulties I faced and who have always been there to share all this experience.
I feel blessed that you are all part of my life.

PS.
What does not kill me makes me stronger.

Nomenclature

ADC	Analog to Digital Converter
AFM	Atomic Force Microscopy
Ag	Silver material
$Ag/AgCl$	Silver / Silver Chloride material
App	Mobile Software Application
Au	Gold material
$CMOS$	Complementary Metal Oxide Semiconductor
CV	Cyclic Voltammetry
DAC	Digital to Analog Converter
$DMSO$	Dimethyl Sulfoxide
ECG	Electrocardiagram
$ELISA$	Enzyme-Linked Immunosorbent Assay
$eELISA$	Electronic ELISA
FSK	Frequency Shift Keying
HIV	Human Immunodeficiency Viruses
HRP	Horseradish Peroxidase
H_2O_2	Hydrogen peroxide
$IFN-\gamma$	Interferon Gamma target
$IGRAs$	Interferon Gamma Release Assays
LAM	Lipoarabinomannan
LOC	Lab on a Chip
LoD	Limit of Detection
mA	Milliampere
MG	Malachite Green
$MLPA$	Multiple Ligation-dependent Probe Amplification technique
$MOSFET$	Metal Oxide Semiconductor Field Effect Transistor
nA	Nanoampere
$NaCl$	Sodium Chloride
OPC	Open Circuit
PCB	Printed Circuit Board
PDI	Program / Debug Interface
$PDMS$	Poly-dimethylsiloxane

$pk - pk$	Peak to Peak
$PMMA$	Poly (Methyl Methacrylate)
POC	Point of Care
$RH6G$	Rhodamine 6G
$SERS$	Surface-Enhanced Raman Spectroscopy
SPI	Serial Peripheral Interface
SPS	Sample per Second
TB	Tuberculosis
TIA	Transimpedance Amplifiers
TMB	3,3',5,5'-Tetramethylbenzidine
$UART$	Universal Asynchronous Receiver/Transmitter
USB	Universal Serial Bus
WHO	World Health Organisation
μC	Microcontroller

Chapter 1

Introduction

1.1 Background and motivation

Diagnostic testing devices are essential tools of a health system, providing important information about the disease and/or treatment of a patient. Over the last decades, diagnostic devices have been developing rapidly reducing the size and cost of the device (1). However, these platforms remain expensive and bulky for personal uses. Point of Care (POC) diagnostic devices are widespread in the medical field with plenty of applications. POC provides a "first-cut" diagnosis on the patient's health condition. According to the World Health Organisation (WHO), POC diagnostic devices should follow specific requirements such as portability, rapid test results, small sample volume, robust and be cost effective (see Table 1) (2). These devices are used by clinician experts for complex analysis or even by patients, if the analysis does not require the presence of a clinician expert. For instance, diabetes requires daily monitoring of blood glucose levels. Nevertheless it is almost impossible for a patient to visit a hospital on a daily basis and therefore a POC diabetes device can easily be used.

POC diagnostic devices find uses in different countries, including both developed and developing. In tests that take place in a centralised environment, the differences in Lab-on-a-Chip (LOC) methods are easier to detect than in point-of-care tests performed at high-income versus low-income settings (3). According to WHO, the most common diseases that threat human life, in high-income countries, are heart and diabetes diseases (4). In contrast, in developing countries, human lives are threatened by infectious diseases. In 2015 10.4 million people (including 1 million children) suffered by *tuberculosis* (TB) whilst 1.8 million died. Surveys have shown that 95% of these deaths occurred in developing countries (5). Therefore, inexpensive and accurate diagnostics have a high potential to contribute to the reduction of deaths in low-income countries. For instance, in the period between 2000 and 2015, TB diagnosis and treatment saved 49 million lives (5).

Particularly in the past decade, interest in TB diagnostic devices has risen, especially with a focus on developing countries, where deaths are increasing. The diagnostic devices are classified based on the detection method (Optical, Mechanical and Electrochemical) (6) as well as the detection sample (Blood, Urine and Sputum) (7). However, current TB diagnostic applications still face unresolved issues (bulky, expensive, insensitive devices) that do not allow a market uptake in undeveloped environments (8). Skin test and serological antibody methods are widely used to detect TB, but both are inaccurate. On the other hand, fluorescence microscopy and urine methods provide more accurate results, but still face challenges such as sensitivity and the need for bulky equipment (9).

Electronic-based diagnostic devices based on electrochemical biosensors, are found in many applications in the medical field. The electrochemical detection can be readily employed in diagnostic methodologies through the translation of biological reporter signals to electrical signals, which can then be digitised and processed appropriately. Furthermore, with the inclusion of microfluidic sample processing, electrochemical biosensors require smaller sample volumes than without the inclusion and demonstrate improved assay speed through the reduction of required diffusion times. *Enzyme-Linked Immuno-Sorbent Assay* (ELISA) with colorimetric detection remains the prevailing technique in medical diagnostics with the majority of contemporary advancement focusing on high-throughput sample processing and automation (10). However, reporter components of enzymatic assays often provide signals detectable by electrochemical means, eliminating bulky spectrophotometric apparatus.

The capabilities of Printed Circuit Board (PCB) technology allow to solve problems as the integration of functional electronics and microfluidics on a single device. This technology is a promising technology in the medical field. Furthermore, PCB is a standardized platform ideal for complex biosensing process in parallel (11). PCB technology provides advantages such as high precision, electronics integration, biocompatible (biochemical sensors), microfluidics integration and lower manufacturing cost than other materials (glass and silicon) (12). Electronics and microfluidics integrations as well as the manipulation of the signal (signal processing) allow PCB technology to be used as a Lab-on-a-PCB for POC diagnostic devices, combining all the components into a cost effective device without any compromises in accuracy. For instance, the cost of the four layer PCB is almost £0.067 per cm^2 (13).

Inspired by PCB advantages in medical field and specifically in POC diagnostic devices, this thesis looking to exploit these advantages and to combine them with the capabilities that a smartphone offers. Herein, this investigation employs microfluidic amperometric detection of *Hydrogen peroxide* (H_2O_2), *Horseradish Peroxidase* (HRP) and *"3,3',5,5'-Tetramethylbenzidine"* (TMB) using *lab-on-PCB* (LoPCB) sensors, manufactured entirely by standard commercial techniques, to demonstrate a unique PoC approach to medical diagnostics. This is supported by recent results showing that the

ELISA PCB-based TB detection could provide comparable results with the standard colorimetric detection technique (14).

1.2 Aims

The aim of this thesis is the design and fabrication of a portable, smartphone-integrated electronic platform towards to reading-out electronic ELISA (eELISA) data from printed circuit board (PCB)-based sensors. The purpose of this instrumentation is to detect different concentrations of enzyme product TMB/HRP (TMB product is proportional to Interferon Gamma target (IFN-γ) for TB detection) through amperometry, reducing the total volume of the sample and the time of the measurement with an external battery independent of the instrument. Comparing to other relevant projects, this thesis presents a portable (no external battery requirement), automatic adapted (increasing the accuracy) smartphone-aided and PCB-based bio-instrument. This instrument measures different concentrations of biological samples, i.e. HRP and TMB, in real-time, requiring only 15 μl and total time of 60 seconds, as opposed to recent relevant research that requires 200μl (15). Moreover, in contrast to other relevant investigations (14)(16), the significant reduction in volume and detection time, using the same initial sample volume, allows multiple measurements, resulting in a significant increase in the accuracy of the measurements. The platform doesn't require external power supply or a bulky computer, as the other above relevant investigations. It can be easily connected to a smartphone through a USB-C port monitoring the data of the measurement in real-time while powered by the smartphone. Finally, this thesis also investigates how the size and the design of electrodes effect the sensitivity and distinct detection of sample's concentrations.

1.3 Thesis objectives

The PCB manufacturing technology benefits as the low cost, biocompatible and high accuracy measurements are suitable for POC diagnostic devices. The current bio-instrumentation platform consists of the electronic board, the Mobile Software Application (App) and the bio-sensing platform. Driven by the above, the main objectives of this thesis are separated into the following pillars:

1. The design and manufacturing of a PCB-based electronic platform. The instrument features eight independent, re-configurable current input channels each consisting of a low-noise transimpedance amplifier (TIA) and filtering stage coupled to low-noise switch ICs for automatic current range detection. A bipolar, 16-bit resolution voltage-input analog-to-digital converter (ADC) is employed for digitisation

of converted current values received from the analogue front-end. In addition, a bipolar, 12-bit resolution digital-to-analog converter (DAC) combined with standard three-electrode potentiostat provides a wide range of biasing voltages to the amperometric sensors. The electronic components of the instrumentation board are chosen having as criterion the coverage of a wide range of current input signals from few nanoampere (nA) to 2 milliampere (mA) with high accuracy. This range allows the detection of any possible signals that the biosensor can provide (17).

2. The programming of an Android-based application that receives and processes the biological measurement data. The resulting data is transmitted by the electronic platform to an Android-based smartphone via a serial interface. An interface, which is designed to be easy to use, guides the operator through the detection process. The customised Android application (App) provides a real-time monitoring of the electrochemical cell and stores that return the biochemical data back to the device once the measurement is complete (18).

3. Finally, the sensing platform comprises of three electrodes (two gold (Au) and one silver/ silver chloride (Ag/ AgCl) electrodes) converting the biological reaction to a current signal. This sensing platform is designed and fabricated in order to measure different concentrations of H_2O_2, TMB and IFN-γ solutions. Herein, H_2O_2 concentrations measurements are provided using both commercial manufactured and cleanroom-fabricated sensors. The results of both types of sensors are comparable; however the fabricated sensors provide faster results and decrease the amount of the total sample (15 μl). Finally, HRP and TMB concentrations are compared using both colorimetric and amperometric techniques.

1.4 Structure of the thesis

Chapter1: Introduction

This Chapter presents the aims and the objectives of a *Smartphone-aided Electrochemical Detection Platform*, providing the main idea and the novelty of this thesis. It also briefly describes the chapters of this thesis.

Chapter2: Introduction to Point of Care diagnostic devices

This Chapter introduces the Point of Care diagnostic devices and specifically the materials and methods that the POC devices use in order to detect and analyse the different types of samples for the different diseases. Furthermore, the main part of this chapter introduces the POC implementations that are based on the electronic technologies, such as the PCB, and describes how a smartphone can be used as a tool of a POC device.

Chapter 3: Smartphone-aided bio-instrumentation platform

This Chapter presents the PCB technology and provides information about the design of a bio-instrumentation platform. Most importantly, it describes the connection among the PCB-based sensing platform, the electronic board and a smartphone for real-time plotting data of the board works and its main components. In addition, this chapter presents the board's design using the Altium professional designer program, the App on a smartphone for the data acquisition and two types of a sensing platform (commercial manufactured and fabricated for this thesis by individual process steps).

Chapter 4: Characterisation and Experimental measurements

In this Chapter, the characterisation of the electronic board is presented as well as the sensing platform. Artificial and biological measurements employing the board and external PCB-based amperometric biosensing platform for Sodium chloride (NaCl), H_2O_2, HRP and TMB concentrations, are also demonstrated. The measured results are provided in real-time through an android-based smartphone application. Furthermore, a colorimetric detection of HRP, TMB and IFN-γ concentrations is introduced.

Chapter 5: Conclusions and Future work

This Chapter concludes the accomplished work, the contributions of this thesis and provides suggestions about the future directions of this investigation.

Chapter 2

Introduction to Point of Care diagnostic devices

2.1 Point of Care diagnostic devices

POC diagnostic devices is a crucial component of healthcare, informing the patient about the state of his/her health with high accuracy. POC diagnostic devices have been developed during the last decades trying to cover the needs of the laboratory experiments in portable devices (19). Also, there is a tremendous number of applications that find use in the medical field. The main advantages of this tool that makes it widespread in the medical world is that is portable and handheld without the presence of a doctor or an expert being necessary, keeping the cost low (20). The majority of the POC devices are designed, manufactured and programmed in fact to be easy to use by everyone. As it is expected, there are several POC applications that cover different types of needs. For instance, each one of the POC devices are used to analyse samples; blood sample, spittle, sweat and urine, based on different technologies for each of those samples (21). Furthermore, except of the technologies, the same sample can be measured using another detection method. For example, glucose concentration into the blood can be measured using absorbance photometry, electrochemical biosensor and reflectance photometry (21). In contrast with the laboratories or hospitals, the commercial POC devices are usually use specific samples.However, according the WHO, every POC diagnostic device must satisfy specific requirements (see Table 2.1) (2).

Table 2.1 presents POC diagnostic device requirements according to World Health Organisation (2).

Requirements	Details
Cost Effective	Low cost (see Appendix C)
Portable	Without the presence of an expert
Robust	Can be transferred and stored without the need to refrigerated and maintenance
Sensitivity and Specificity (see Appendix C)	
User friendly	Can be used by health experts (doctors) and patients
Rapid test results	Reduce the time of the test
Small Sample Volume	Reduce the sample volume of the test (few μl)

Table 2.1: POC requirements according to the WHO.

Table 2.2 illustrates few advantages and disadvantages of POC testing (21). The aforementioned main advantages of POC are the portability, no needing of an expert and the low cost of the device. However, this useful tool has plenty of advantages. The time taken for the analyses and the detection of a sample depends on many variables as the sample, the detection method and the material that the POC is based on. However, the majority of them require only few minutes in order to complete the measurement and provide the results as the pregnancy test and the glucose concentration device. Moreover, there are POC devices that can be used to measure more than one sample, saving time. Nevertheless, these devices are more complex and expensive than the previous ones.

One the other hand, POC testing has also some disadvantages. The need to provide additional information on the health state of the patient resulted in production of more complex devices (multi-purpose) keeping the cost high. These types of POC devices are not easy to use by patients and they are used only by professionals. However, the majority of the commercial devices that use only one sample are cheap and simple to use, but they have limited range of measurements.

ADVANTAGES	DISADVANTAGES
Portability	Limited range of measurements
Low cost	Expensive for more complicated devices
No expert requirement	
User friendly	
Reduce the time of the diagnostic testing	

Table 2.2: Advantages and disadvantages of POC diagnostic devices.

2.2 Material and method of detections used in POC platforms

POC diagnostic devices differ from each other in the fact that they use different materials and detection methods between them. POC devices provide immediate information and use a number of elements that are used in LOC devices in micro scale such as micro-pumps, micro-filters, micro-valves, microarrays, micro-channels and bio-electronic chips (22).

2.2.1 Material that are used on POC

Manufacturers are currently using these specific materials, *polymer* (23), *glass* (23), *paper* (24) or *Complementary Metal Oxide Semiconductor* (CMOS) (25) in order to fabricate the above elements for POC implementations (26). Each one of these materials, present both advantages and disadvantages and are preferred for a unique reason according to the demands of the application.

Specifically, polymer is preferred in applications that need a transparent, flexible, elastic or biocompatible material. Furthermore, polymer is a low cost material but it cannot be compatible to electronics' integration. Inkjet printed *Bio-Field Effect Transistor* (BioFET) technology offers a low cost, portable and electronic integrated system (27). However, some disadvantages of this technique are the reduction of resolution when the speed increases and the fact that the printers are quite expensive (28). Another common material, which is biocompatible and transparent, is the *glass* but it still has the same disadvantage as the *polymer*, meaning that is not compatible with electronics keeping the cost high for mass production. *Paper-based* POCs are not compatible with the integration of microfluidics but the sample is transferred through the capillary using hydrophilic channels onto the surface, without pumps. In addition, paper is a cheap solution, which is a main advantage for the POC devices and it does not need big volume of samples (23). *CMOS* technology differs with the above materials, on the base that *CMOS* can be used in more complicated and sophisticated circuits. The fabrication cost of this technology is low (£0.04 per transistor with 14nm process node) (29). The minimisation of the process node contributes to: (1) the reduction of the total power consumption and integrated circuit's package size, and (2) the increase of the power process (high performance). Furthermore, the reduction of the integrated circuit's package size affects the reduction of the total size of a PCB (less area required). However, the fabrication cost of *CMOS* significantly increases for complete LOCs applications. There are several factors to consider during the LOC fabrication (chemical interactions, surface roughness, capillary forces etc.). These factors require complex equipments instead of a conventional one, which results of the increase of the fabrication cost (30).

Finally, *PCB* technology is an alternative POC implementation, which shows an increasing development in the last period of years in this field. Specifically, PCB technology finds fertile ground in POC diagnostic applications due to the fact that has the ability to combine the electronic components with microfluidics and sensing components at the same time (31). An extra advantage of PCB-based technology is that it provides the result of any electrochemical biological detection with high accuracy holding the cost low (£0.067 per cm^2) (13). This technology develops day by day, a fact that has as a result the development of applications and the combination of these with smartphones for further portability and flexibility of the POC diagnostic devices.

2.2.2 Methods of detection using POC diagnostic tools

The detection method that the POC tool uses, depends on the application and the sample, which will be used. There are plenty commercial biosensors that use different detection methods depending on the samples such as the electrochemical method or the colorimetric technique. This chapter provides an overview of electrochemical methods.

Amperometric technique:
Firstly, the amperometric method is the most common on the electrochemical biosensor. This method converts the biological reaction to current signal allowing to extract and process data from the reaction. This method uses two (working and reference electrodes) or three electrodes. When only two electrodes are used, it is difficult to keep stable the potential between working and reference electrodes in high currents. However, this disadvantage can be overcomed by using an extra electrode (counter electrode) with the same potential as the reference one. Using three electrodes, a constant voltage between reference and working electrode is achieved and the current flows between the counter and the working electrode (32). Figure 2.1 shows a basic configuration of the amperometric method (33). Amperometric method is used in many commercial applications. A most well known application is the glucose biosensor. Furthermore, other applications that based on amperometric method detect *Mycobacterium tuberculosis* (34), *Malaria*, *Chagas disease* (35), etc.

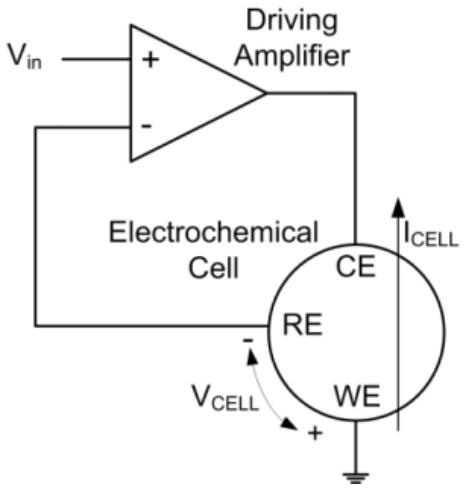

Figure 2.1: Basic Amperometric method configuration (33).

Potentiometric technique:
Another electrochemical technique that finds uses in plenty POC medical applications is the potentiometric method. Potentiometric biosensors differ from the amperometric ones converting the biological reaction to a voltage signal. This biosensor consists of two electrodes (working and reference) in order to measure the potential between them that is produced by the biological reaction. During the measurement the current that flows through the electrodes is zero avoiding interference with the reaction. Figure 2.2 shows how the most common potentiometric biosensor works using an ion selective membrane. In this biosensor there are two champers, one with a constant concentration of the ion as a reference and the other chamber, which includes the test solution. The chambers are separated by a membrane that allows specific ions to flow or to bind on it. An electrode is sunk in each chamber (Ag/AgCl) in order to measure the potential between these two using a voltmeter with high-input impedance (36). The potential between the working and the reference electrodes can be calculated by the Nernst equation (see Equation 2.1), where E^0 is a characteristic constant for ion selective electrode (V), T is the absolute temperature (K), R is the universal gas constant (J K^{-1} mol^{-1}), F is the Faraday constant (C mol^{-1}), n is the signed ionic charge and A is the concentration of the chemical species involved in a chemical reaction. In a room temperature the parameter RT/F is equal with 0.059 (36). One of the most well-known applications of the potentiometric method is the pH measurements.

$$E = E^0 + \frac{RT}{nF} ln[A] \tag{2.1}$$

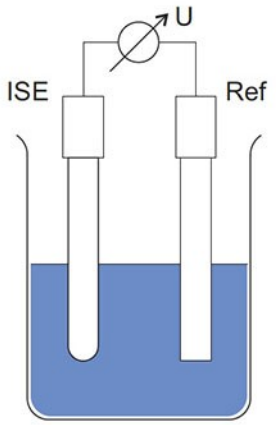

Figure 2.2: Potentiometric biosensor.

Impedimetric technique:
Impedimetric biosensor is another electrochemical biosensor, but less common than the amperometric and potentiometric biosensors (32). Impedimetric biosensor uses two interdigitated electrodes applying a small sinusoidal signal (few mV pk-pk amplitude) (36). Part of this biosensor usually is a Wheatstone bridge that is used as bio-recognition component for enzyme reactions (urea/urease and amino-acid oxidase reactions). During the enzyme reaction the biosensor measures the total charge that is produced unless an ion selective layer is used. The sensitivity of the impedimetric biosensor is measured by the change of the conductance before and during the enzyme reaction. However, the sensitivity can be improved using a reference electrode, which incorporates or isolates an inactive enzyme from the reaction in to the solution (36). Impedimetric biosensor methods find uses in *Samlonella* species, *E.coli* serotypes (36), ethanol level in alcoholic beverages, *ant-human IgG* (10 pg.ml in a sample) and in monitoring the hybridization of DNA fragments by *Polymerase Chain Reaction (PCR)* (32) detections.

Colorimetric technique:
Finally, over the past two decades, colorimetric method finds uses determining the concentration of the assay by measuring the absorbance of the solution in a wavelength light. This method is preferred due to low cost analysis per sample, the rapid results of the measurement and the specificity that provides in one chemical species analysis. However, at the same time there are limitations that this method faces as the cost increases for precise analysis of the solution (tighter wavelength required). Furthermore, similar colours of interfering substances as well as the present of a light could lead to error in results (37). Absorbance is the amount of specific wavelength light that the sample solution does not allow passing through. In Figure 2.3 you can find the steps of a spectrophotometer setup illustrated. The light source wavelength is separated in monochromatic wavelengths through a prism. Then this wavelength passes through the sample and is collected by a detector. The *Beer-Lambert law* presents the linear relationship of a sample's concentration ([C]) with its optical absorbance (A) (see Equation

2.2), where ε is the molar absorption coefficient (M^{-1} cm^{-1}) and l is the optical path length of the sample. However, the linearity of the Beer-Lamber law does not exist in high absorbance values that are related with the concentration of the sample and the molar absorbance coefficient (ε) (36).

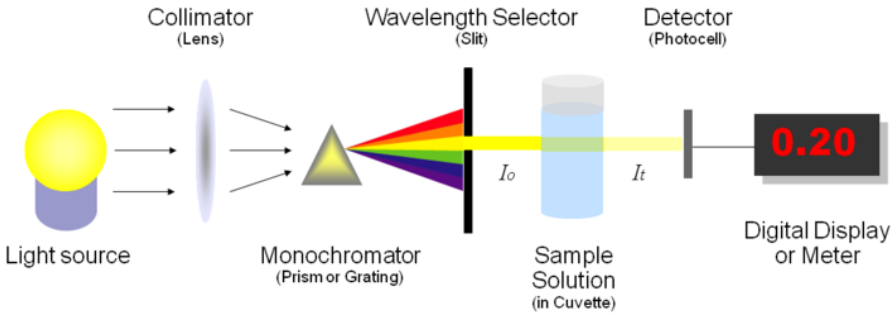

Figure 2.3: Absorbance spectroscopy (38).

$$A = \varepsilon l[C] \tag{2.2}$$

2.2.3 Microfluidics

Microfluidic technique on POC diagnostic devices allows the possibility to handle complicated laboratory experiments, using a small volume sample. The small volume of fluids leads to size reduction of the device and the time of diagnostic testing. The rapid diagnosis is resulting from the small volumes of sample and reagents (39). Over the past years, microfluidic technique has become widely known in POC devices having plenty applications based on as pH and chemical binding coefficients (40). This technique and the small volume of fluids provide the ability to use LOC devices miniaturizing the size and the cost of the device. The common components that the microfluidic system comprises are microchannels, micropumps, microvalves and micromixers (41). In particular, the microfluidic components can be either active or passive. These two categories differ in fact that the first one requires power from an external source. The available fabrication techniques for the microfluidic systems can be based on different materials as silicon (42), glass (42), polymers and paper (23).

In 2000, Wego and Paygel presented a novel PCB-based micropump (43). The PCB-based micropump comprised of four layers of PCB, two passive check valves and a thermopneymatically driven volume actuator. The maximum flow rate of the pump is 530 μl/min requiring only 1 Watt power consumption (see Figure 2.4). This flow rate is high enough in comparison to other relevant studies (100 μl/min, 135 μl/min and 138 μl/min) (15; 44; 45) to cover the needs of the current thesis (15 μl/min), as it is further described in details. Nevertheless, the application requires an external power source; a fact that is considered as a drawback for POC implementations. In addition, in

2016 Vasilakis et al. published a Lab-on-PCB electrochemical biosensor integrated with microfluidic for POC applications (46). This PCB-based microfluidic application is a passive microfluidic biosensing platform. The platform uses the PCB technique creating microfluid channels and gold ring as biosensing electrodes. The device is exposed to oxygen plasma converting the microfluidic surface to hydrophilic one, fact that allows the fluidic to flow into the microchannel passively. Another device published by the same group is a microfluidic diluter controlling actively the dilution ratio. This device consists of a microfluidic network and a metal–oxide–semiconductor field-effect transistor (MOSFET), which thermally regulates the dilution ratio.

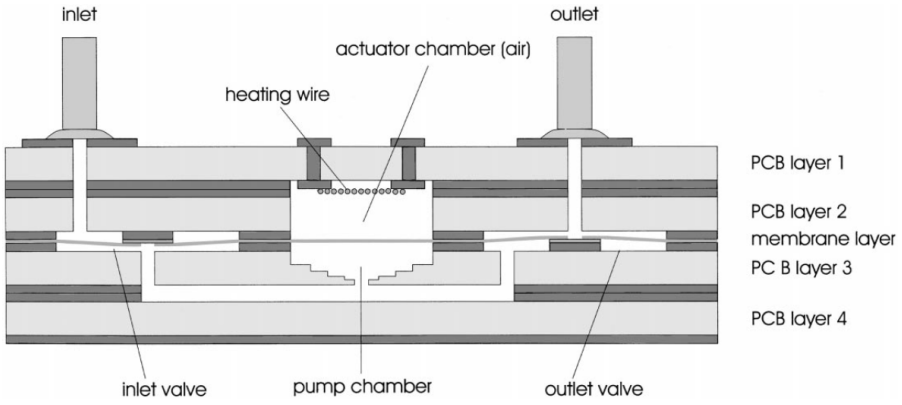

Figure 2.4: PCB-based micropump (43).

Hydrophilic microchannels allow the aqueous solutions to fill and flow through the microfluidic network without requiring external power source. The wettability of the surface is characterised as hydrophilic or hydrophobic and depends on the contact angle between the solution and the surface. The contact angle is higher than 90° for the hydrophobic surfaces and lower for the hydrophilic ones. The wettability of polymeric surfaces as Poly-dimethylsiloxane (PDMS), Polystyrene, etc. can be changed from hydrophobic to hydrophilic if the surface is exposed for a short period of time to *Plasma* (47). Another relevant study showed that a plastic surface can achieve a (more) hydrophilic feature through exposure to *Plasma*, while this feature could last for about 80 days (48).

The wettability of the surface allows the flow of the aqueous solution without an external power which is the aim of the passive microfluidics. Furthermore, capillary force could be used in microfluidic method and especially in passive microfluidic pumps. Capillary pressure on characteristic length creates a driving force that allows the fluid to flow through hydrophilic channels (49). In addition, the capillary force depends on the shape and the geometrical parameters of the capillary. In 2013, Madadi et al. designed different capillary shapes (elongated, circle, diamond and pine) in order to increase the flow rate in to microcapillary pump. The experiments show that the diamond shape for micropillar pumps has higher throughput performance than the other one (73% higher flow rate than circular-based microchannel integrated micropillar pump) (50).

2.3 Biosensors

Electrochemical sensors detect and measure the chemical or biological reaction converting one form of energy to another one. Some of the main performance factors of a biosensor considered to be the accuracy, sensitivity, selectivity, precision and the *Limit of Detection (LoD)* (see Appendix C). *LoD* is the lowest analyte concentration of the sample (see Equation 2.3), where *LoB* is the signal in reagent blank, k is the numerical factor and σ the standard deviation of the low concentration sample (lowest detectable concentration of the sample) (36). As it is mentioned in section 2.2.2, there are different detection methods based on the technique that the sample is analysed (Optical, Electrochemical, Mechanical etc.). Table 2.3 presents the main advantages and limitations of some of these methods.

$$LoD = LoB + k\sigma \tag{2.3}$$

Method	**ADVANTAGES**	**DISADVANTAGES**
Optical	Rapid Reproducible Sensitive Specific	High power requirement (see Appendix C) Expensive for precise analysis Life time of the reagents Lower respond time than Electrochemical sensor
Electrochemical	Rapid Reproducible	Low sensitivity Low specificity
Mechanical	Rapid	Low sensitivity Low specificity Reproducibility

Table 2.3: Advantages and disadvantages of Sensor's methods (51).

In electrochemistry the biological reaction is converted into an electrical signal. This conversion occurs when an electrode reacts with the solution. The electron transfer between the electrode and the solution is defined as *redox* (reduction-oxidation) reaction. Reduction or Oxidation is termed when the molecule receives or loses an electron, respectively. The electrode, which reacts with the solution providing electrons is called *anode* and the other electrode (receives electron) is called *cathode*. When a potential is applied to an electrode, a charged layer is formed in its surface attracting opposite charges. This charged layer (double layer) creates a capacity on the electrode's surface. In an actual measurement, when WE's potential is change, it appears that an oxidation/reduction reaction on the electrode's surface is producing a high current. Then this area is expanded to the solution fact that reduces the concentration gradient and the flow of the sample to the electrode. Equation 2.4 presents that the total current, which

is measured during an electrochemical experiment, is the sum of the capacitance current (I_C) and the Faraday current (I_F).

$$I = I_C + I_F \tag{2.4}$$

Electrochemical cells can be modeled by an equivalent network of passive electrical circuit elements. These elements can be resistors, capacitors and inductors that simulate the electrochemical reaction. Figure 2.5 presents the equivalent circuit of a simple electrochemical cell. When a potential is applied to an electrode, attracting forces are generated between the electrode and the solution, creating different layers (double layer, diffusion layer and bulk solution layer). The equivalent circuit consists of an uncompensated electrolyte (resistance) in series with the parallel combination of a double layer (capacitance) and an electron transfer (resistance) (see Figure 2.5) (52).

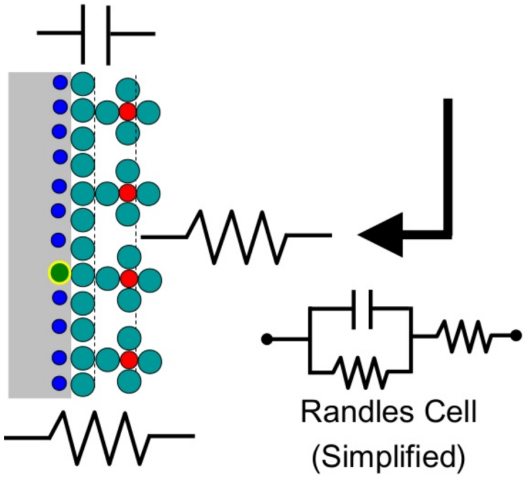

Figure 2.5: Equivalent circuit model of an electrochemical cell (Randles circuit) (52).

Randles-Sevcik equation defines the connection among the scan rate, the diffusion properties and the current that flows through the sample solution. The equation describes the dependence of the current-time for linear diffusion control at a working electrode. It is commonly used in redox reactions by also providing information about the electrode area. Equation 2.5 presents the calculated current, where n is the number of electrons that required for the redox, F is the Faraday constant (C mol^{-1}), A is the area of the electrode (cm^2), C is the concentration of the solution (mol/cm^3), v is the scan rate (V/s), D is the diffusion coefficient (cm^2/s), R is the universal gas constant (J K^{-1} mol^{-1}) and T is the absolute temperature (K). At room temperature, the equation is simplified to equation 2.6.

$$i_p = 0.4463nFAC(\frac{nFvD}{RT})^{\frac{1}{2}} \tag{2.5}$$

$$i_p = 268,600 n^{\frac{3}{2}} A D^{\frac{1}{2}} C v^{\frac{1}{2}} \tag{2.6}$$

2.4 Print Circuit Board

PCB technology first appeared in 1850 using wooden bases and metal strips in order to connect bulky electric components. Over the years, the electric components became smaller and wires were used to connect the pads of the components. In 1925, another method well known as Printed Circuit was developed by Charles Ducas of the United States using electrical path through the base's surface. The surface of the board, known as substrate, is consisted of an insulating material and the printed wires of a conducting one, transferring the signals that the components provide. Nowadays, this technology has significantly improved, allowing to print both sides of the board (double-sided) or to use more than one layer for the PCB devices (multi-layer PCB). PCB technology uses through holes connecting the above layer with the bottom one or blind vias when multi-layer technique is used (53). The number of layers on a PCB device differs from the application. Any implementation needs different functions, which determine the number of the layers and if the board will be single or double sided.

There are more than one building blocks to manufacture a PCB. When only one layer is used, the basic building block is an insulating substrate (usually reinforced glass is preferred, known as FR-4) between two layers of copper, which is used as a conductor. However, when the application requires more than one layer, another substrate is used (prepreg) that is impregnated with adhesion epoxy resin and helps to improve the characteristics of a PCB. The prepreg allows to create a multi-layer board increasing the functionality of the board by using more components (54). In Figure 2.6, a 4-layer PCB structure is presented that consisted of two FR-4 substrates and a prepreg substrate among them for their connection. There are metal tracks in each side of the FR-4 substrates connecting the electronic components. Vias holes (blind vias and through hole vias) connects electrically the layers. Blind and through hole via are used for the electrical interconnection of the both sides and among the FR-4 substrates, respectively. Finally, the solder mask is applied to protect the metal tracks of the FR-4 substrate against oxidation or solder bridges. Independently of the number of the layers, the cost of the device remains low without any compromises in accuracy. Furthermore, this technology uses commercially available components, a fact that reduces more the cost for mass production.

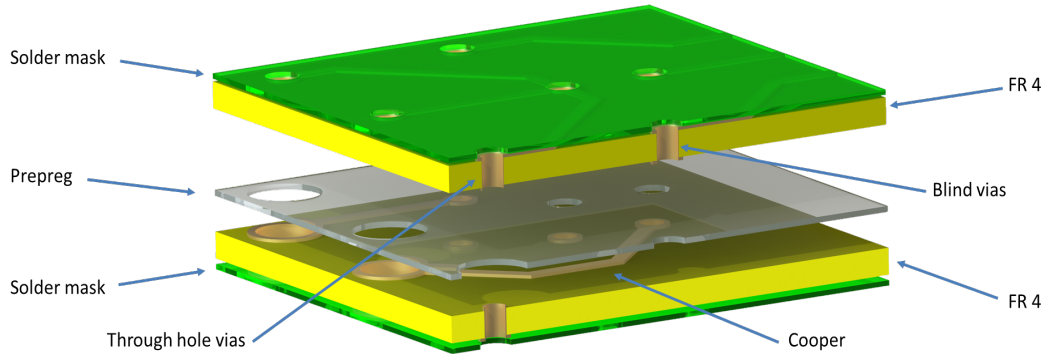

Figure 2.6: Multilayer PCB Structure.

2.5 POC Implementations

At this section few commercial and laboratory applications are presented, using several of the above materials and techniques. Firstly, TB diagnostic tests are mentioned based on different detection methods and samples. Then electronic applications and PCB based implementations are introduced detecting different targets or diseases. Finally, the last subsection is focused on POC devices that are based on a Smartphone, using internal and external components.

2.5.1 TB diagnostic devices

Immunoassay is a common protein assay suitable for point-of-care microfluidic-based diagnostics that benefits from the interactions among antigens and antibodies in order to identify protein markers from pathogen or host immune responses. *Immunoassays* are valuable for the detection of bacteria, parasites and viruses, etc. A well known technique for enzyme immunoassay detection is the ELISA. In most cases, the detection methods that ELISA uses are colorimetric or chemiluminescence-based, having detection limits (pM range), as a result of enzyme-mediated signal amplification and serial washing. The main drawback of ELISA is the fact that consists of several steps and after each step a washing step is required (24). Figure 2.7 shows the four most common ELISA principles (Direct, Indirect, Sandwich and Competitive) that use different detection methods. These ELISA methods find uses in many applications as Pregnancy Test, Food industry, West Nile Virus, *Human Immunodeficiency Viruses* (HIV) and TB (55; 56).

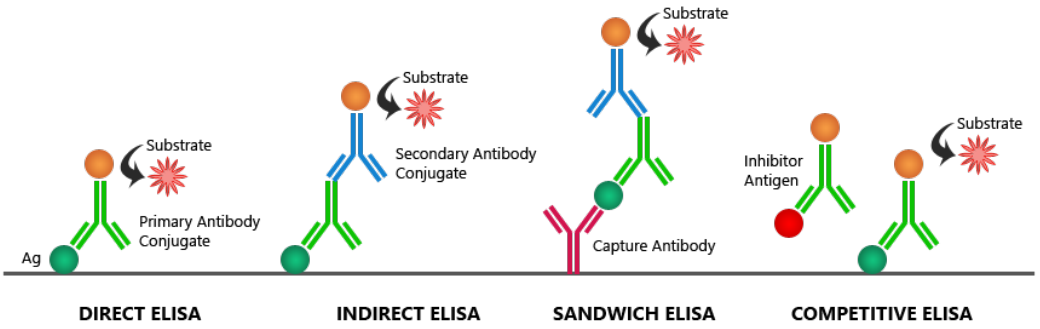

Figure 2.7: Common Elisa formats (57).

TB disease is one of the main threats to global health, especially in developing countries. TB is caused by *Mycobacterium tuberculosis* bacteria (58). TB can affect the lungs or throat (pulmonary TB) and it is difficult to be controlled due to the fact that can be easily transmitted through the air. Another form of TB infectious illness is the latent TB, in which the bacteria is "asleep" into the body and it does not pass the TB to others. However, in latent TB the bacteria could suddenly "wake up" bringing any symptom of the TB disease. WHO has been interested in TB detection using POC diagnostic devices. Tuberculosis can be detected using detection methods as ELISA and chemical luminescence immunity analysis (59). Current applications use blood, skin, urine or sputum as samples for TB detection.

Sputum smear microscopy is a method for pulmonary TB detection. This method uses sputum sample, which is produced in the lungs. A small amount of this sputum is placed on glass slide creating a smear. The smear is mixed with series of specific stains producing signs of TB bacteria that could be checked by a clinician through a microscope. The advantages of sputum smear microscopy are the low cost of the test and the rapid result of the measurements (several hours). This test provides low sensitivity (50-60%) that may be decreased for patients who suffer from HIV infection. Finally, smear microscopy requires laboratory infrastructures with a technician's presence (60). On the other hand, an alternative method is the *Fluorescent microscopy* which improves the previous limitations. Fluorescent microscopy optimizes the previous technique by measuring the illumination of the smear with a quartz halogen. This method could also be optimized using LED fluorescent microscopy providing significantly longer life than the standard mercury vapour lamps. However, the sensitivity of the fluorescent microscopy is still low (9).

Serological or serodiagnostic tests is another diagnostic method for the pulmonary TB using blood sample. This method detects a specific antibody in the blood of patients who suffer from TB. Serological test still faces difficulties due to the fact that this antibody may also be detected in healthy people (inconsistent and inaccurate). On the other hand, serodiagnostic tests are cost effective offering rabid results (61).

The unsuccessful efforts of antibody-based TB tests lead to the need for different detection markers. *Urine lipoarabinomannan (LAM)* was the first antigen-based test that produced promising results. Urine LAM test uses the ELISA method for antigen detection into the urine sample. Pulmonary TB LAM diagnostic test is an inexpensive commercial available PoC test (Alere Determine TB-LAM) providing rapid results (an hour). It does not require any special training for uses. On the other side, the sensitivity of TB-LAM is controversial. Specifically, it shows higher sensitivity in patients who suffer from both TB and HIV than only from TB (9).

Skin test is a well know diagnostic method for TB. A trained health care worker injects a small amount of tuberculin fluid in the lower part of the patient's arm skin (Mantoux TB test). After 3 days the patient should be checked at these areas looking for a raised hard area or swelling. If a raised hard area or swelling appears, the clinician expert will measure the size of this area. The larger the size, the higher the chance that the patient will suffer from TB. This test is suitable for and widely common, especially in developing countries, due to its low cost. However, this method is not accurate and does not provide any information about the type of the TB disease (active or latent) (62).

Finally, *Interferon gamma release assays (IGRAs)* is a latent TB test based on blood sample. IGRAs tests are a new type of TB test, measuring patient's immune response to TB bacteria. Interferon gamma cytokine is included into patient's blood and is produced by its immune system. The presence of the interferon gamma cytokine could be detected by mixing the blood sample with a specific substance. IGRAs use the optical method to detect the level of the interferon gamma cytokine into the solution as the colour of the solution changes when the cytokine is mixed with the substance. In contrast with serodiagnostic, IGRAs method offers rapid results with high accuracy. However, IGRAs require bulky equipments and sample preparation before each measurement. Furthermore, this method is suggested only in latent TB and the accuracy of the measurement is decreased for patients who suffer by HIV, too (63). Comparing to skin test, IGRAs requires only one healthcare visit of the patient. IGRAs test provides the diagnosis within 24 hours as opposed to the skin test that takes about 3 days (64). Studies have shown that IGRAs can detect patients with active TB among others suspected of having TB, with the sensitivity and selectivity ranging from 73-83% and 49-58% respectively (65). Overall, both IGRAs and *Tuberculin skin testing* TST have shown relatively adequate skill in detecting *Latent tuberculosis infection* (LTBI); however, due to the remaining uncertainty of their performance, results should be interpreted with caution (66).

Table 2.4 illustrates advantages and disadvantages of different TB detection methods providing few applications for each method.

Methods	**Applications**	**Advantages**	**Limitations**
Skin test	Mantoux TB test	Inexpensive	No accurate
Sputum smear/ Fluorescent microscopy	Fluorescence staining, Direct and concentrated Ziehl-Neelsen	Rapid, Inexpensive, Simple	Low sensitivity, Bulky equipment
Serological antibody	MycoDot, ICT TB, Anda-TB IgG	Rapid Inexpensive, User friendly	Inconsistent, Inaccurate
Urine	Determine TB-LAM	Rapid, Inexpensive, Minimal training	Low sensitivity
IGRAs	QuantiFERON T-SPOT	High accuracy, Rapid detection (within 24 hours)	Sample preparation, No suitable in the community

Table 2.4: PoC diagnostic devices for TB (9).

2.5.2 PCB-based applications

This section presents the state-of-the art in PCB based sensing and highlights how the work in the thesis contributes to challenges in this area.

Sánchez et al. demonstrated a multiplex electrochemical detection of seven breast cancer biomarkers (67). These cancer biomarkers are amplified through the multiple ligation-dependent probe amplification technique (MLPA). The device based on PCB technology is using a gold electrode array integrating with Poly Methyl Methacrylate (PMMA) microfluidic channels. Figure 2.8 presents a PCB-based 64 gold electrode array sensor with Pt counter electrode and Ag/AgCl, which are common for the 64-electrode array. The sensor is consisted by FR-4 glass substrate (1 mm) and 3 μm of Au (electrode's material) on a Ni layer (4 μm). This system uses an external potentiostat with 4 MUX module for the electrochemical characterisation.

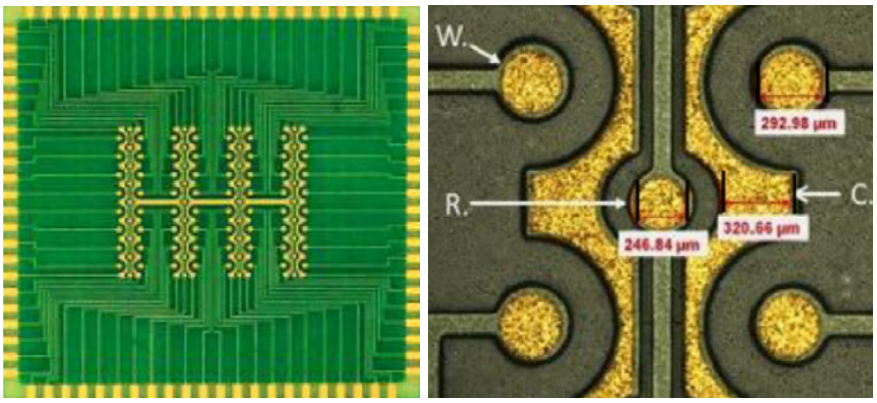

Figure 2.8: PCB-based gold electrode array for DNA detection (67).

In Figure 2.9, the assembly of a PCB-based sensor with PMMA microfluidic channels is illustrated. The instrument is based on the MLPA amplification method of seven genetic markers for the detection of breast cancer. The amplified markers are immobilized on the sensor's surface. Then several biological samples are injected to the sensor through the microfluidic with a wash step after each step (ELISA technique). Finally, for the simultaneous detection of these biomarkers, the amperometric technique was used providing high specificity and low limit of detection (25 pM) (67; 68).

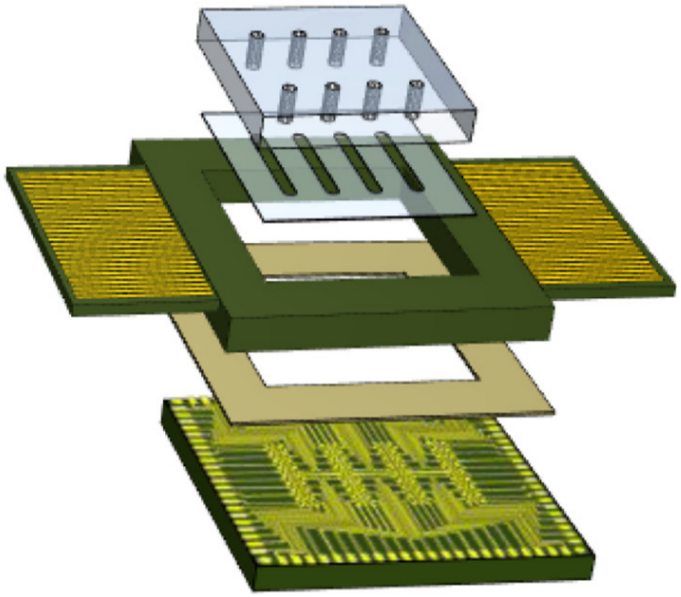

Figure 2.9: PCB sensor integrated with PMMA microfluidic channel (67).

In 2013, Bäcker et al. (69) presented an amperometric enzyme sensor for the measurement of three different concentrations of *glucose*, *glutamate* and *glutamine* in parallel. The sensor consists of thin platinum (Pt) electrodes on top of a Si substrate and an external Ag/AgCl reference electrode (Metrohm) (see Figure 2.10). These Pt electrodes were coupled with an enzyme membrane creating the biosensor's surface. Microfluidic

channel is integrated on the top of the sensor's surface based on SU-8 technology. Finally, this sensor chip is connected with a PCB by an ultrasonic wedge bonder.

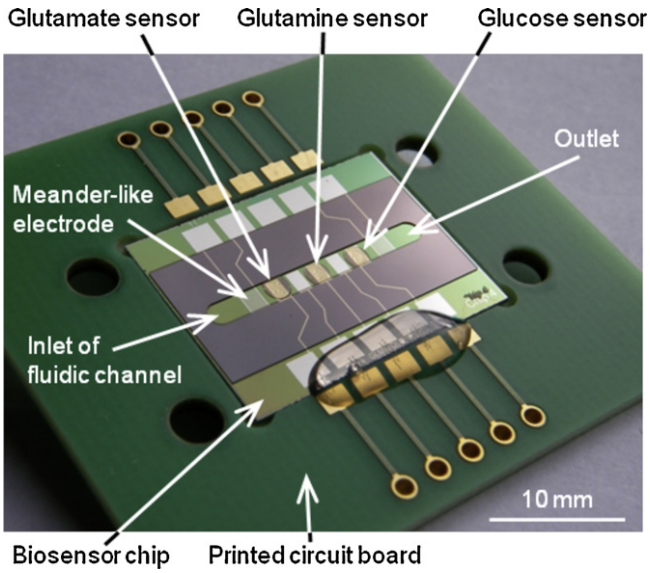

Figure 2.10: Amperometric enzyme sensor for glucose, glutamate and glutamine detection (69).

This enzyme sensor shows high sensitivity, 1.47 μA/mM and 3.68 μA/mM for the glucose and the glutamate sensors respectively. Besides, the small size of the sensor chip, a main drawback of this project is the external reference electrode that is expensive and bulky for POC diagnostic devices. The linearity of this sensor is up to 10 mM for the glutamate and 20 mM for glucose and glutamine. Finally, the lower detection limit of this sensor is 0.1 mM for the glutamine and 0.05 mM for glucose and glutamate.

Clinical chemistry comprises the measurement of an important variety of blood parameters (70). The need to reduce turnaround time of diagnostic testing led to the need for clinical chemistry tests at the point-of-care. Also, POC testing for clinical chemistry markers can be more accurate by avoiding analyte changes during sample transport to laboratories. Usually, the number amount of simultaneous reactions increases the complexity of the devices, fact that also increases the size and the cost of the device. For applications in which only a semi quantitative analysis is needed, paper-based devices probably appealing. However, the detection method that is preferred depends on the application (71).

Evans et al. (15; 72) demonstrated a microfluidic PCB-based Elisa PoC diagnostic device, providing promising results on IFN-γ detection. This project presents a PCB-based amperomentric sensor integrated with a microfluidic chamber (assay area) that takes place on Au-plated. The sensing platform consists of a microfluidic channel on Au surface, 3 Au working electrodes, Au counter electrode and Ag/AgCl reference electrode (see Figure 2.11). The PCB-based surface was covered by PMMA creating microfluidic

channels on top of Au or electrodes surfaces. This platform was used in several electrochemical reactions, as H2O2, TMB product and IFN-γ, to detect different concentrations levels of the samples.

The assay phases consist of the sample preparation and the sensing measurement. The different steps of the assay protocol are located on Au surface of the microfluidic chamber. After each step, sample is moved out of the microfluidic chamber, through an outlet, to a waste chamber (see Figure 2.11B). When the assay protocol completed, the sample is transferred to electrochemical sensor, where the electrochemical reaction take place (see Figure 2.11C).

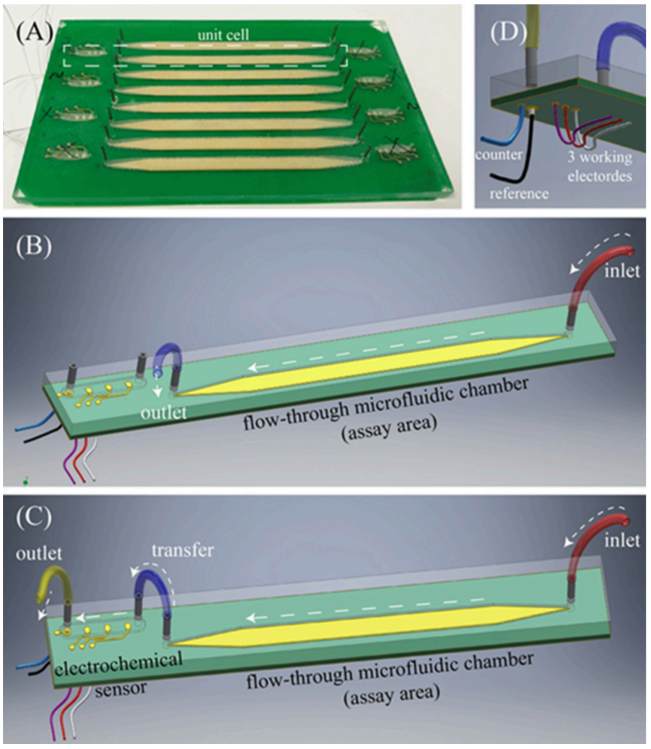

Figure 2.11: A) PCB-based 8 independent assay areas and electrochemical cells, B) 3D representation of assay area, C) 3D representation of final phase (assay flow into the electrochemical sensor) and D) 3D representation of electrodes connections (15).

The platform was used to detect amperometricaly different IFN-γ concentrations. This system requires 8 minutes for analysis of IFN-γ, Strepdavidin-HRP and TMB flow (100 μl/min for each sample). The data shows a nice reproducibility of 108 pg/ml and 325 pg/ml IFN-γ concentration detection (estimated accuracy 93-97%). This amperometric system reaches LoD of IFN-γ close to 40 pg/ml. The range of the current measurements is approximately 90 nA to 160 nA for 2048 pg/ml to 40 pg/ml IFN-γ concentration, respectively.

In this project a previously presented electronic platform was used (16; 73). This electronic board allows to measure a wide range of $\pm$2.5mA with ideal resolution 122nA.

However, on Figure 5 of this referenced paper (15) illustrated that the electronic board can detect different IFN-γ concentrations when the signal differs only 10nA. This signal difference is much smaller than the ideal value that the board can measure. Furthermore, the sensing platform uses three times bigger working electrode comparing to counter electrode. According to literature, the CE must me much greater than the WE to be able to provide electrons to WE if this is needed (74). Finally, following the "Sigma Aldrich" protocol, the TMB tablet must be dissolved into 1mL Dimethyl Sulfoxide (DMSO) and 9 mL deionized water. On Chapter 4.3 of the current report has been proven that the TMB tablet cannot be dissolved into 10 mL deionised water and 5 μL 30% (by volume) H2O2, even when the reagent was centrifuged at 16,000 RCF for 30 min.

2.5.3 Applications based on Smartphone

Several mobile medical applications using smartphone devices have been developed. Some of them rely on the internal hardware capabilities of the smartphone; whereas others, need an external component to perform their functionality.

2.5.3.1 Applications based on Smartphone's components

Nowadays, the majority of the population uses a smartphone to cover their personal needs. POC size and the possibilities of smartphones lead the manufacturers to combine them. Smartphones components have found such an increase that are currently being used in medical factors. Some of the main components that all the smartphones comprise are the camera and the microphone. These components, unsurprisingly, did not remain untapped in POC diagnostic detection. Plenty of POC applications, which take place in a smartphone, are based on in-built smartphone's sensors as camera and microphone, in order to detect biological signals and provide a result with high resolution. Nowadays, the camera on smartphones has significantly improved achieving the range of 5 Megapixel to 15 Megapixel (High and Full High definition). A smartphone's camera can be used in POC application for ophthalmology, dermatology and colorimetric diagnostics (75). The resolution of the camera can provide a quantitative solution of the detection's analysis that is not possible to be visible with naked eye. There is a major number of algorithms for image processing, which present a quantitative solution from an image. Furthermore, all the smartphones are equipped with data transmission protocols as Wireless Fidelity (Wi-Fi), Bluetooth, Universal Serial Bus (USB) and Global System Mobile Communication (GSM), in order to cover the data transmission between the phone and other devices in short and long distances. Finally, the advantages of using only the internal components are that either there is no need for another (external) device to detect or that the external device includes less components, which solution is significantly cheaper.

One of the most common applications that use the internal components of a smartphone is the *Electrocardiagram test (ECG)*. The first recording of a heartbeat (ECG) was 100 years ago. Willem Einthoven (Department of Cardiology, Jersey General Hospital) created a device for a ECG test, which weighed 600 pounds and its size was as big as 2 rooms (76). After a few decades, the size of the ECG tests decreased, having as a result, that nowadays we need only a smartphone in order to measure our heartbeat.

In 2013, Pal et al. published a heart rate project based on a smartphone (Tata consultancy Service, Kolkata, India). The project uses the camera, the flash led of a smartphone and an image-processing algorithm (77). The user put his/her finger in front of the camera following the application's advices for better results. Then the App records a video and process it using an algorithm. In Figure 2.12, it is observed how the algorithm works having as input the video and counting the average of the red pixels. Finally, a Finite State Machine rejects the noise of the signal keeping only the heart rate signal. Figure 2.13 shows the steps of a measurement and the results on the mobile screen using the App.

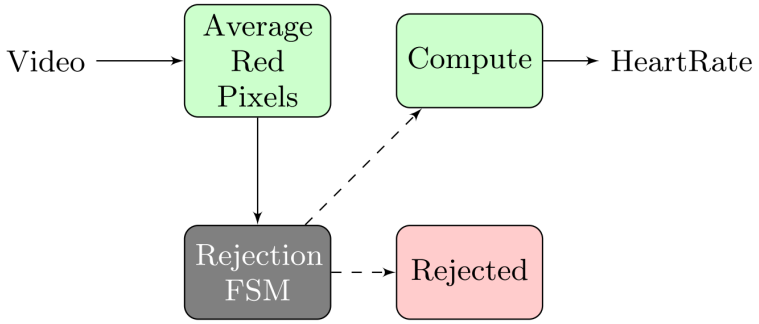

Figure 2.12: Heart rate algorithm based on smartphone (77).

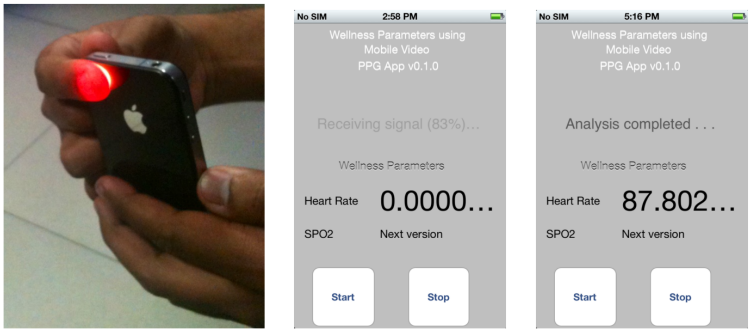

Figure 2.13: Steps of a heart rate measurement (77).

In 2012, Shen et al. designed a POC colorimetric detection using as main tools, a paper based microfluidic and the camera of the mobile phone (seeFigure 2.14) (75). This application can detect the pH value of a sample, which changes the colour of the paper after few minutes, by the time is dropped on the paper's surface. Then the camera takes a picture of the paper and recognizes the pH value of the test solution. Specifically, the application detects the pH scale using a reference chart that starts from 1 to 12. The colour of the pH paper changes from red (pH 1) to dark blue (pH 12), based on the RGB values of images in order to convert the image's colour to the pH value. However, the main disadvantage of this technique is that it cannot provide the qualitative detection, which is reduced to dark colours (75). This disadvantage can be solved by using CIE 1931 colour space code that uses two parameters to recognise the colour. In contrast, with the simple RGB analysis, which needs only colorimetric image, the CIE 1931 relies on another parameter that is the brightness of a colour (75). The new 2D reference chromaticity diagram can recognise changes in the luminance of a colour (see Figure 2.15). The main advantage of this technique is the linear response of the pH measurements into the range 1 to 12. This technique could be used for more complicated testing than the pH measurement that are not obvious by naked eye as paper microfluidic immunoassays and ELISA chips. It should be mentioned that the results of the same sample differed by 5% when they were used by HTC and BlackBerry phones, which is due to the variety of the cameras that the smartphones had. That can be solved by re-calibrating the smartphone, but is necessary only once (initial). The results can also be differed when the light conditions change.

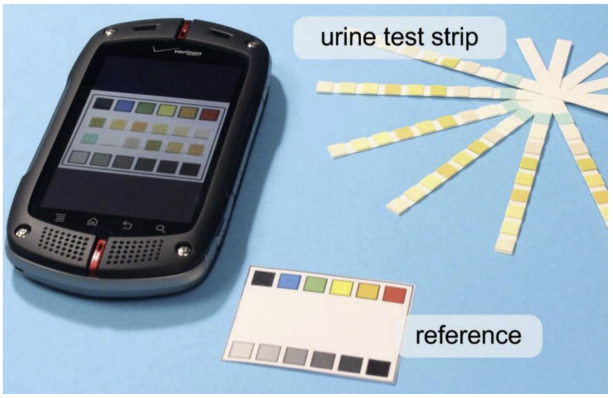

Figure 2.14: Colorimetric detection for pH based on Smartphone (75).

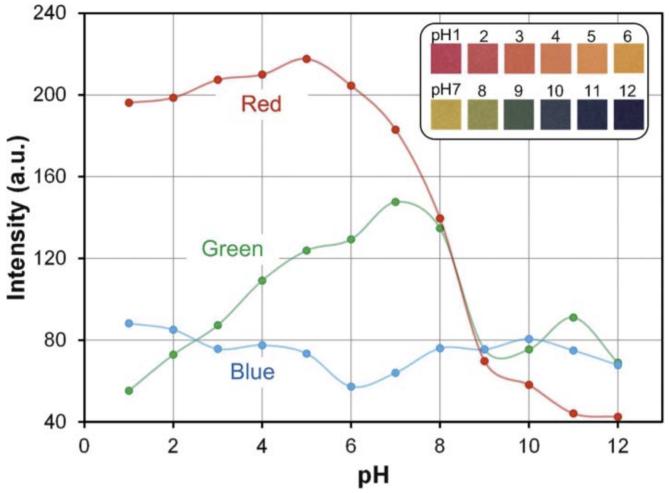

Figure 2.15: pH reference table based on RGB values and the intensity of them (75).

2.5.3.2 Applications based on external components

At the previous subsection POC applications were provided that were based only on the internal components of a smartphone, as the camera and the microphone. However, the combination of a smartphone and external components allows the expansion of diagnostic applications detecting more complicated biological samples and using microfluidic chips for biosensing. In this subsection several applications are mentioned that use microfluidic chips and PCB technology.

Firstly, Lillehoj et al. (78) presents a quantitative biomolecular detection application that uses an external device providing the result of the detection on the smartphone's display. Using this device, the user can detect the level of the *Plasmodium falciparum Histdine-rich protein 2 (PfHRP2)* in human serum. This system provides a user interface that is easy for every user (78).

Figure 2.16 presents the device of this application that is based on PCB technology and uses a second platform for microfluidics. The microfluidic chip uses a PDMS material in order to drive the samples through the capillary flow. The biomolecular detection is achieved by using an electrochemical method and specifically a high sensitivity amperometric measurement (16 ng mL^{-1}). Moreover, the device is connected with the smartphone by a micro-USB port in order to transfer and provide the result of the detection on the display by using a user interface (78).

Specifically, the user drops the sample and reporter solutions on the microfluidic chip that flows through the chip's channels and they are merged to produce electrochemical reaction. This electrical signal is transferred to another chip, which includes a microcontroller in order to process the incoming signals. The results of the data processing can be observed in the smartphone's display. As it was mentioned before, a micro-USB port

using the Universal Asynchronous Receiver/Transmitter (UART) protocol, connects the external device and the smartphone. Finally, the microcontroller processes and sends the data in the smartphone in real-time.

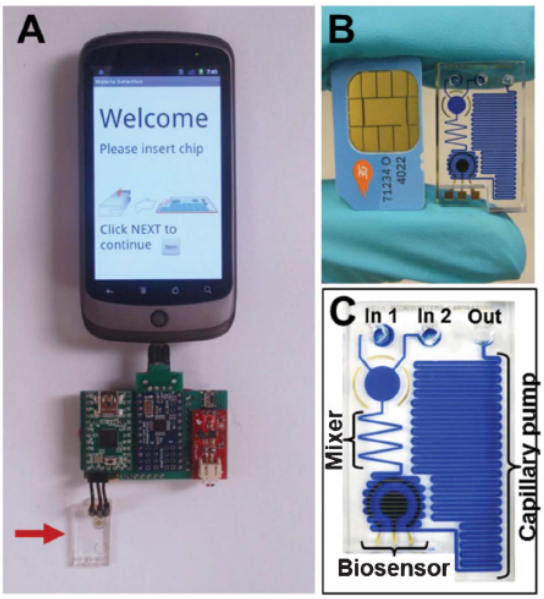

Figure 2.16: Immunoassay detection PCB device (78).

The microfluidic chip is designed and fabricated for the needs of this device providing stable flow rate. As it is observed in Figure 2.16, the chip consists of two inlets, a mixer, a biosensor, a capillary pump and an outlet. The radius of the inlets and outlet is 0.5 mm and the samples can be pipetted or dropped in inlets, simultaneously or separately. Then the samples flow and mix through the hydrophilic microfluidic channels until they reach the desired solution. The chip can be filled by the samples using channels with 100 μm height and 400 μm width, in only few minutes. The electrochemical sensors use gold electrodes that were fabricated on glass substrate (78).

The external device of the application, except the microfluidic chip, is designed using Altium designer program and it is based on PCB technology. The unoccupied areas on top and bottom layer of the PCB are covered by a copper and they are electrically grounded and connected to 3.3 Volts, respectively.

This application detects PfHRP2 following few biological steps. In the beginning, PfHRP2 capture antibody are immobilized on the gold electrode allowing the PfHRP2 antigen to bind on it. PfHRP2 detection antibody can bind to the gold surface through the PfHRP2 antigen and capture antibody. The negligible current is generated when the PfHRP2 detection antibody is absented. As final step, TMB/H_2O_2 substrate is added applying a bias voltage to the electrochemical biosensor. Then current is provided measuring the concentration of PfHRP2 protein in the sample.

Finally, the device can be connected with a smartphone, which is running only Android Operating System and it can be improved using wireless protocol in order to transfer the data from the microcontroller to the smartphone. This project outweighs in comparison with the commercial ELISAs, because it needs significantly less time (15 minutes) than the other (2-3 hours). Except of the positive and negative readout detection of the immunoassay, this device can provide a quantitative measurement (78). Furthermore, this platform can be used to detect malaria infection.

The above application provides an electrochemical detection on a smartphone that is consisted of two parts, the electronic device and the microfluidic one. Furthermore, it could use the processing power of the smartphone using less electronic components. The microfluidic design could change using a different design for the capillary pump increasing the flow rate a fact that reduces the time of the test. Finally, the main drawback of this application is the precision of the biosensor. When the same biological measurement is repeated the measured value is changed (high variability of the data) fact that does not provide clear changes in adjacent concentration ranges.

One year later (2014), Sun et al. designed another project based on an external device, which consists of an electronic board and a commercial available screen-printed electrode biosensor by DropSens.The project focus on the electronics comprising two potentiostats with different characteristics that are used for electrochemical experiments in order to detect biomarkers quantitative (79). The device is connected with the smartphone and is powered by it, through a standard 3.5 mm audio jack. The main advantages of this project are that leverages the capabilities of the smartphone as the battery, the computational power and the display. Moreover, the use of the audio jack is preferred for the connection than the classic USB by allowing the device to be used by any smartphone without needing to change the hardware. In Figure 2.17, the external device and the result of the measurement on the smartphone's display is observed.

Figure 2.17: POC Electrochemical biosensor based on smartphone (79).

The audio jack connector, which is used for the data transmission is consisted of four channels (Left and Right channel, Microphone input and Common channel). In this application, the left channel powers up the device from the smartphone's battery and the right channel and the microphone to receive and send data to the smartphone, respectively. The main electronic components, that the device contains, are the microcontroller, the potentiostat, the voltage to a specific frequency signal converter and the power harvest (79). First of all, the power harvest uses MOSFET H-Bridge and Schottky diode in a specific topology converting the phone's power to 4V for the microcontroller. The microcontroller is connected with the phone by the 3.5 mm audio jack, receiving the trigger to generate a PWM signal and an ADC to control the integrator's output (voltage waveform) that is sent to a potentiostat. The microcontroller that is chosen, receives 4 Volts power supply, uses the internal oscillator and has 10-bit ADC having 4mV resolution. The clock frequency is 500 kHz, keeping the power consumption as less as possible. Furthermore, the biological reaction creates a potential between the electrodes. The potentiostat controls the potential of the reaction and measures the current that is generated. Finally, the voltage waveform is converted to a frequency, in order to be transmitted to the smartphone by the audio jack (79).

This application presents the comparison of two different potentiostat's architectures using a standalone electronic board and a commercial disposable biosensor. One of the challenges of POC diagnostic devices is the sensitivity, accuracy and repeatability of the biosensor for complicated biological experiments (couple of steps as the ELISA). The current biosensor is developed for simple biological experiments without microfluidics channels for more complicated experiments. Furthermore, this board uses jack connector which allows to connect the device with any smartphone, but jack connector has limit at the level of the power that it can be harvested by a smartphone and it is less than a USB connector. In addition, any smartphone provides different power to an external device through the jack connector. Finally, the cost of the device is almost $30, which is still expensive for POC diagnostic devices.

In 2017, Chen et al. developed a smartphone-aided diagnostic platform for the detection of infectious diseases (80). The platform consists of the microfluidic chip, the hand-held "cradle" and a smartphone. The smartphone-based instrument has been designed for the detection of four infectious respiratory diseases (*Streptococcus equi*, *Streptococcus zooepidemicus*, and *Equine herpesvirus (EHV-1 and EHV-4)*) (see Figure 2.18).

A silicon-based chip (25 mm x 15 mm) was fabricated with 10 parallel flow channels. Different primers were uniform deposited on channels surfaces for the detection of the aforementioned diseases. Then a droplet of blood sample (15 μm) was placed through pipet injection in the microfluidic chip and separated in 10 distributed channels. The blood sample was mixed with the primers in each microchannel into a mixing chamber and then was amplified (Loop-Mediated Isothermal Amplification, LAMP) for 30 minutes. After the LAMP step conducted on a hot plate, the microfluidic chip was inserted

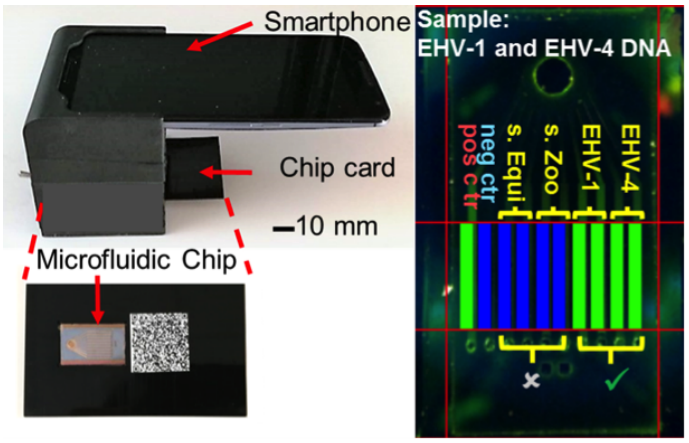

Figure 2.18: Smartphone-aided instrument for infectious diseases detection (80).

into the cradle reader on top of its internal heater. Then the smartphone's camera captured fluorescent images using crable's LEDs through an optical emission filter. These images were analysed by an image processing software, detecting potential *infectious diseases*. The software provides a result in few seconds allowing the user to share the data of the measurement with an expert or store them in a cloud database. Figure 2.19 illustrates analytically the steps of infectious diseases detection using smartphone's processing power and the internal camera. The platform provides rapid results with limit of detection close to laboratory methods keeping the cost of the device low.

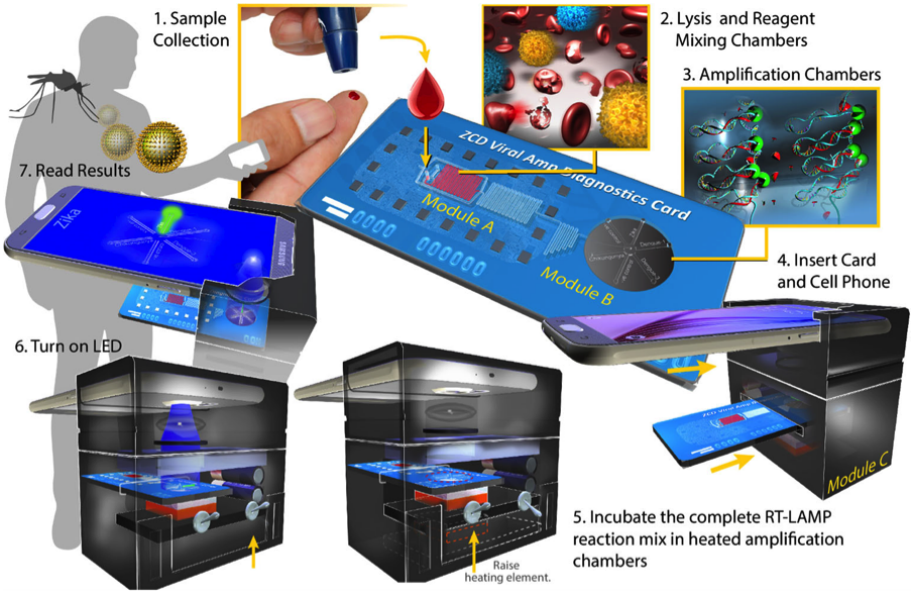

Figure 2.19: A simple schematic diagram of Smartphone-based instrument for infectious pathogens detection (80).

In 2018, Orth et al. (81) presented a smartphone-based dual-mode microscopy using the in-built smartphone's flash and ambient light. This work shows a 3D printed microscope that allows the capturing of bright and dark pictures without requiring an external light source (flash). The geometry of the 3D-printed device has been designed allowing the ambient light to illuminate the sample and creating diffuse transmission illumination using an internal refection. This geometry allows to observe sample (cells in media etc.) with refractive index contrast or low absorption fact that prevents the sample from being detected under a light field operation.

In Figure 2.20, a novel 3D-printed microscope is presented. The microscope uses internal illumination tunnels without requiring an external LED or electrical connection with a smartphone. Camera's flash is transmitted through a tunnel (blue arrows Figure 2.20A-C) and is reflected on the illusion backstop (gold in Figure 2.20A,D). Then the light is transmitted back to smartphone's camera via the sample and the objective lens (green arrows Figure 2.20A-C).

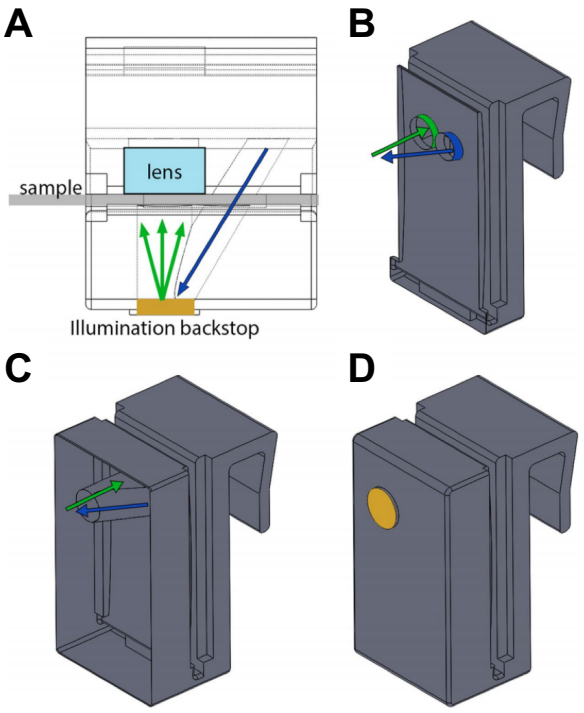

Figure 2.20: A 3D-printed microscope. A) An internal view of the illumination tunnel, B) A cross-section view of the illumination tunnel (external of the microscope), C) A cross-section view of the illumination tunnel (internal of the microscope) and D) The entire 3D-printed microscope (81).

Figure 2.21 shows the different steps of the smartphone microscope implementation. The objective lens is inserted and fitted into the friction-fit recess. The smartphone is placed into the microscope verifying that the camera is fitted over the objective lens. Furthermore, the sample slide is placed on microscope under the objective lens (Figure 2.21E). Finally, the smartphone's camera mode is activated having enabled the flash.

Figure 2.21F presents an image of Lilium with scale bar 1mm (scale bar of magnified image is 50 μm).

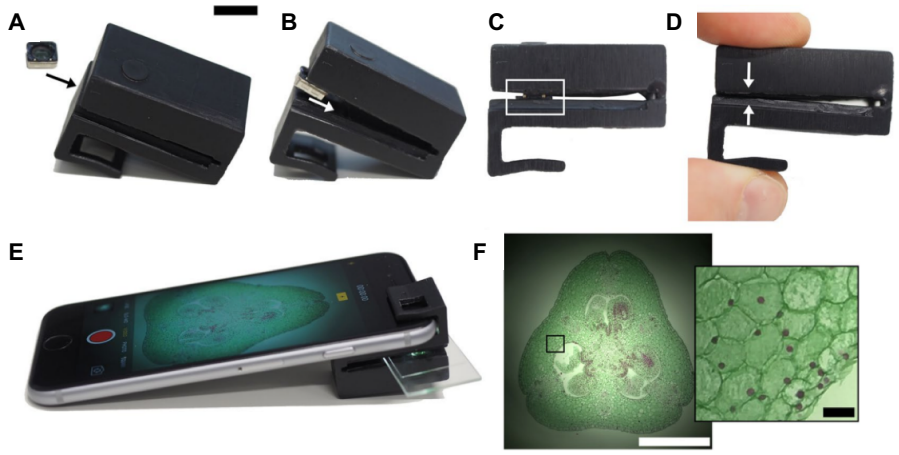

Figure 2.21: A 3D-printed microscope and smartphone assembly. A) Insert the objective lens into the microscope, B) Place the objective lens further into the recess, C) Verify the objective lens is pushed into friction-fit recess, D) Squeeze the microscope, E) Insert the smartphone and the sample into the microscope and F) Observe the captured image using the flash mode of the smartphone's camera (81).

This work shows a simple microscope device that exploits the advantage of the integrated illumination due to microscope's design. The cost of the device is kept low due to low cost 3D-printing material and the fact that no external LEDs are required. The 3D-printed microscope can be used in various applications such as detection zooplankton and visualization of cell nuclei in unlabelled cells. However, different positions of the camera depending on where is placed on a smartphone or multi-cameras on new smartphones, could cause problems between the alignment of the camera and the objective lens.

Zeng et al. (82) demonstrated a PoC smartphone-based Raman analyser with paper-based surface-enhanced Raman spectroscopy (SERS). This investigation proposes a nylon paper-based SERS chip, which has been created by absorbed silver nanoparticles within the microporous structure of a membrane. The membrane can be cut in small pieces and be stuck on a glass slide (see Figure 2.22A). The nylon membrane could also be used to detect specific molecules. Furthermore, the device consists of a smartphone-based Raman analyzer (CloudMinds Inc.) using a laser of 785 nm (100 mW and acquisition time 10 sec). Figure 2.22B shows the SERS chip placed into the Raman analyzer, which is connected to a smartphone. The data are presented in real-time through an App. The device has been used detecting different concentrations of Rhodamine 6G (RH6G), crystal violet and malachite green (MG). The measurements of each experiments was repeated 10 times. The LoD is 10 pmol for both crystal violet (standard deviation 5%) and MG, and 1 pmol for RH6G (standard deviation 11%).

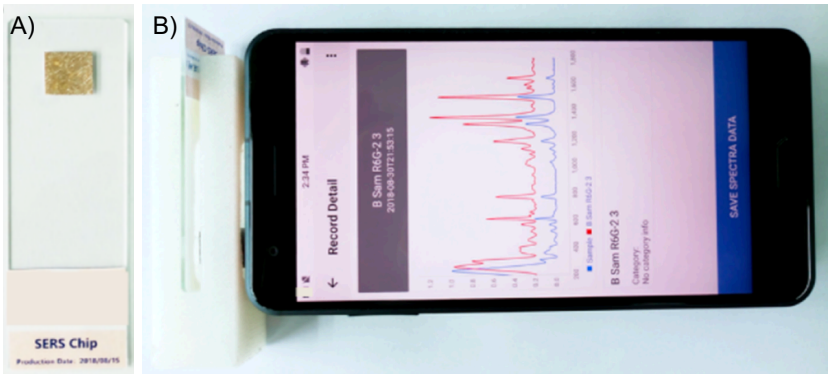

Figure 2.22: A) SERS chip on glass surface and B) SERS detection with the smartphone-based Raman analyzer (82).

POC diagnostic devices attract the interest of companies that are investing in them. These companies produce low cost devices that informs the patient primarily for their health status. For instance, iHealth features devices as glucose meters ($17), blood pressure monitors ($80), wireless scales ($70) and fitness ($70) (see Figure 2.23) (83). The products can be connected with a smartphone (android or iPhone) through Bluetooth protocol or jack connector. iHealth provides a specific mobile application for each product allowing to store the data in a history file. Because of the previous, it can be observed that there is a general interest to invest in an modern health system based on the devices that are common used (smartphones).

Figure 2.23: Smartphone-aided Health Care Products: A) Blood pressure monitor, B) Wireless scale, C) Glucose meter and D) Fitness (83).

Chapter 3

Smartphone-aided bio-instrumentation platform

3.1 Design of PCB implementation

This work demonstrates the capability of a portable bioinstrumentation board that receives amperometric signals from our PCB-based sensors. The signal is then digitised and relayed to a smartphone by standard serial protocol. The board is powered by the smartphone and a bespoke App processes received data to display signals in real-time over a graphical interface. Data can be stored in internal smartphone memory allowing the user to send or share data with other users or clinical staff. As such, this system lends itself favourably to the generation of sub-clinical prognostic metadata that could be evinced through App communication with a central database. The board covers a wide range of the input signal (from -2.5 mA to +2.5 mA) with adequate resolution, it is lightweight and portable, and the App can run on any modern Android smartphone (version 5.0 or later).

The fabricated bio-instrumentation board needs to have certain properties, in order to fully comply with the requirements of the "*eELISA*" technique and smartphone integration. It needs to have relatively small footprint to miniaturise the size of the board, minute power demands (less than 80mA) and be able to read electrochemical data accurately and in a low-noise manner (see section 4.1) (73). Taking the above into consideration, a careful selection of off-the-shelf components has been made. The analogue front-end of the board features eight low-noise amplifiers (low input voltage noise $9\text{nV}/\sqrt{Hz}$) (LMP7704) configured in a standard TIA topology, coupled to low-leakage, small R_{ON} resistance switch ICs, able to provide four distinct amperometric sensing ranges. A fully-differential, eight channel, 16-bit resolution voltage-input ADC has been employed for the digitisation of the converted current values received from the analogue

front-end. The ADC operates with a bipolar power supply (±2.5V) allowing the detection of both reduction and oxidation currents of electrochemical reactions. The digitised data are subsequently been sent to a USB-to-UART interface chip (FT232R) and then to the coupled smartphone device. Finally, for the appropriate biasing of the PCB-based amperometric sensors, a 12-bit DAC (AD5724) has been employed, connected to standard three-electrode potentiostat circuitry. The components of the current version board were chosen in order to cover any possible range of measurements (over-engineered) according to the literature due to the unknown electrical characteristics of the biosensor depending on its structure (topology, geometry and material) (73).

The current thesis used the same amperometric topology (TIA), with Papadimitriou electronic's board (73), to detect the current signal from the electrochemical reaction. However, this work improved the system including switches fact that increased the resolution from 122nA to 122 pA. This change allows to detect the small differences among the concentrations. For instance, several electrochemical reactions on section 4.3 shows that the step between low concentrations is close to 50nA -100nA. This small step cannot be detected using 122nA resolution. In addition, this electronic platform is designed to be powered by a smartphone (portable). It does not need an external power supply as the aforementioned Papadimitriou board. A simplified schematic diagram of the proposed circuit architecture can be found in Figure 3.1. The fabricated 4-layer PCB is shown in Figure 3.2.

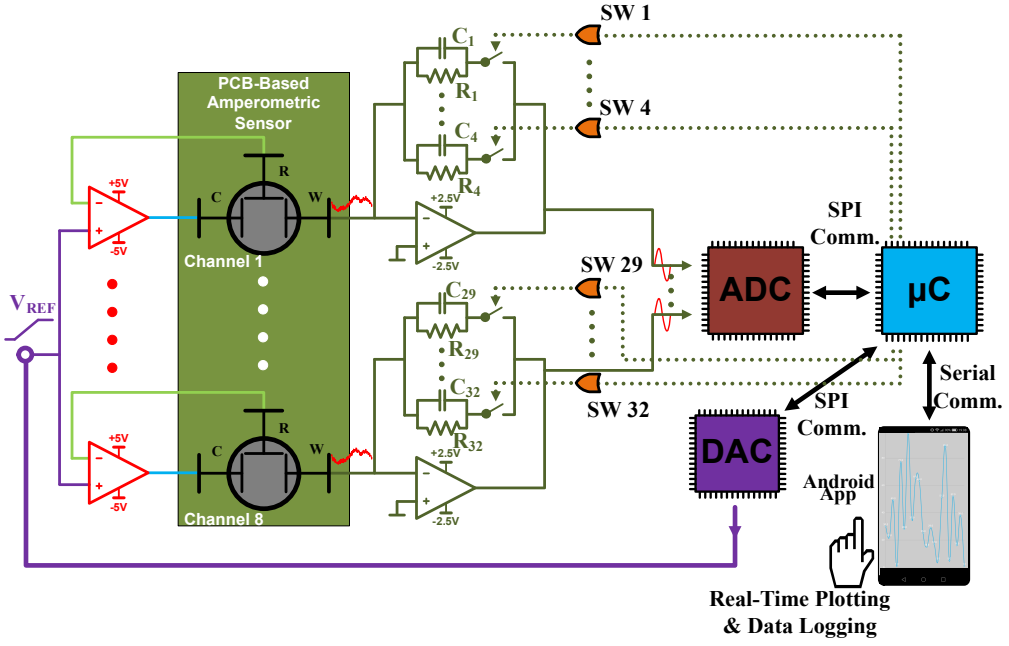

Figure 3.1: A simplified schematic diagram of the fabricated bioinstrumentation board that interfaces with the PCB-based sensor.

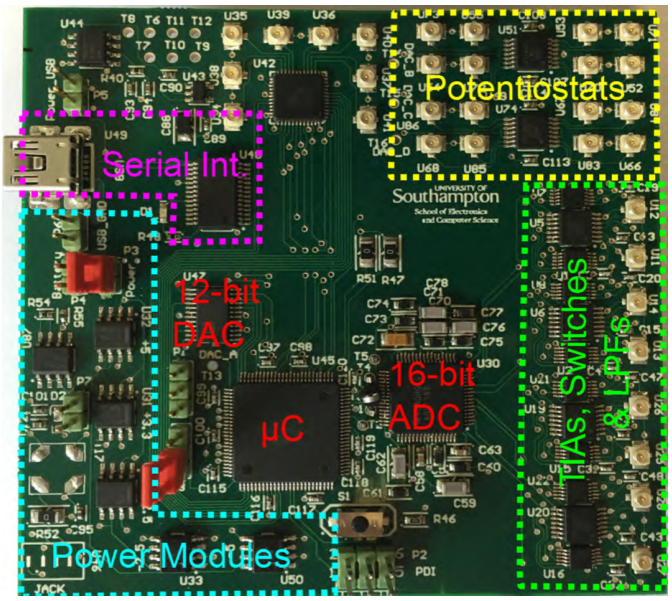

Figure 3.2: The smartphone-aided "*eELISA*" bioinstrumentation board.

Using a 32MHz ATxmega microcontroller, the system is able to constantly monitor the current ranges of the electrochemical reaction and "*select*" the optimum detection range by activating appropriate switch ICs, which employ optimal value feedback resistors to the TIA setup. All 8 current input channels are fully independent, therefore, they can read multiple reaction currents simultaneously from different sensors, operating at different ranges. In addition, the board offers the option to the user to perform a cyclic voltammetry (CV) calibration before every measurement, if necessary, by sweeping the voltage of the on-board DAC from positive (+2.5V) to negative values (-2.5V) and vice versa. A summary of the board characteristics can be found in the inclusive Table 3.1

Table 3.1: Bio-instrumentation Board's Characteristics

Input current range (mA)	±2.5
Min. current resolution (pA)	122
ADC range (V)	±2.5
ADC resolution (bit)	16
ADC sample rate (kSPS)	0.125-8
DAC resolution (bit)	12
DAC output settling time (μs)	10 typ.
Board dimensions (mm)	84 x 93
PCB-sensing platform dimensions (mm)	40 x 90
DSP unit	ATxmega128A1 - 32MHz
Total current consumption (mA)	$\sim$ 80
Power supply	5V (Battery or USB)

The board was designed in order to also be connected and send the data to a smartphone through a standard 3.5 mm audio Jack connector converting the digital signals to analogue and following the Frequency Shift keying (FSK) protocol (84). FSK protocol works converting the digital data to sine waves with discrete frequencies. The internal DAC of the μC has already programmed to send sine waves with constant amplitude and different frequencies (up to 10 kHz) that depend on the digital data (0 or 1). The analogue signal from the internal DAC has tested using an oscilloscope to verify that the communication between the board and a smartphone will work properly. This connection allows to exploit smartphone's capabilities without the need to change the hardware. However, the small amount of power that the board can harvest from a smartphone to powered up without external power source, does not allow this connection for higher-power systems.

3.1.1 Layout of board

Figure 3.3 shows the top layer of the board, which was designed in Altium professional designer and how the components were connected to each other. The board uses the above components for the aforementioned reasons and for proper system operation. In this layer we can observe the USB, Program / Debug Interface (PDI), UFL (Input / Output connectors) and JACK connectors, DDC 118, μC, ADS 1198, switches, regulators and inverters. At the right side of the Figure there are 8 UFL connectors (U11 - U14, U25 – U28) that are connected to the ADS 1198 through switches and amplifiers converting the current signal to voltage one. Furthermore, at the top side of the Figure, the connectors U34 – U41 are used as input for the DDC 118 without needing any conversion. Finally, there are 16 extra UFL connectors in this layer, which are used as reference and counter electrode for the biological experiments.

The other side of the board is consisted of through holes via, UFL connectors as counter and reference electrodes, capacitors and resistors (see Figure 3.4). Furthermore, in this side there are test points that are used to confirm the correct communication of the μC with the DDC 118 and the ADS 1198.

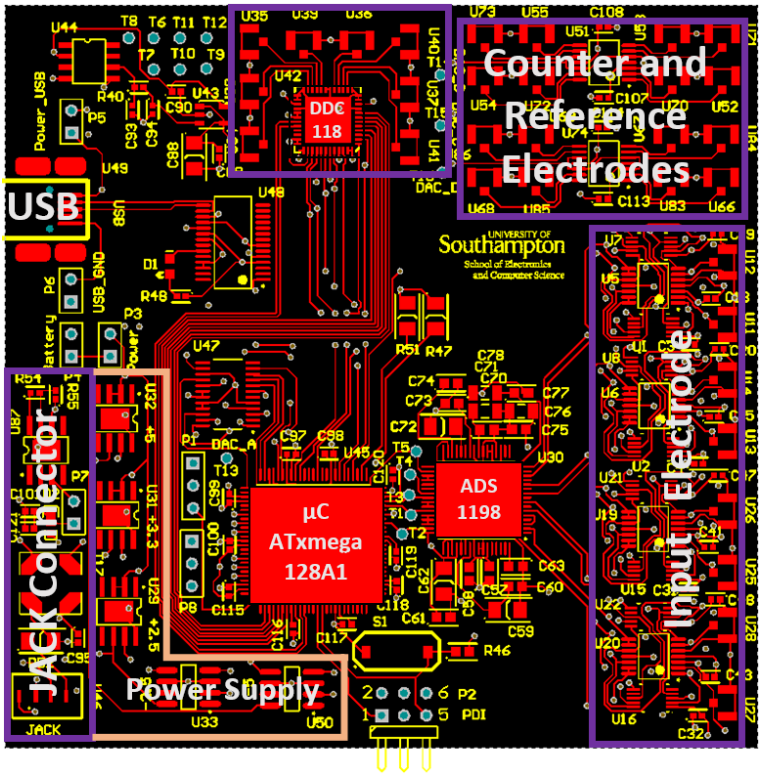

Figure 3.3: Top Layer of the Board.

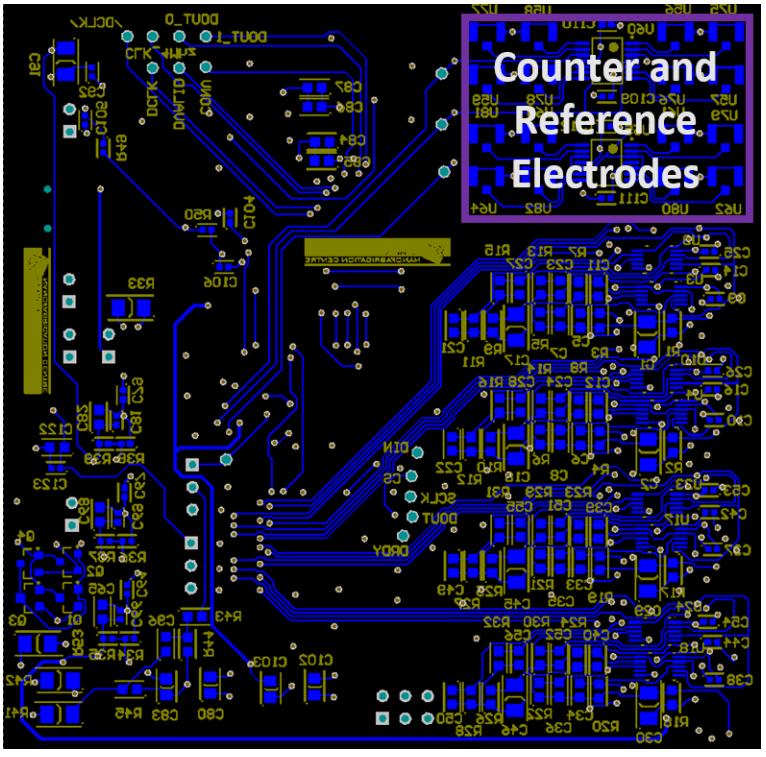

Figure 3.4: Bottom Layer of the Board.

3.2 Android-based App

The bio-instrumentation board digitise the sensor's signal relaying to a smartphone device. The smartphone device receives the digitised data from the instrumentation board through a USB port using a Serial interface and then displayed the processed data through an App. The data are monitored in real-time presenting the actual measurement of the sensor. In the beginning, IOS was chosen using the Xcode platform. IOS requires to be an Apple Developer member handling confidential information of Apple devices, increasing the complexity of the App. On the other side, Android Studio is an open-source platform providing examples and scripts that are open for everyone. For this reason, the App was decided to be built on Android Studio. The App can be installed in any android based smartphones that use version 5.0 or later. Figure 3.5 shows two snapshots of the designed App for the smartphone-aided "*eELISA*". On the left side, the welcoming screen can be seen, where the user can add and store personal identification details creating a file with the personal information and the recorded measurements. The right side illustrates a snapshot of a real-time electrochemical measurement. The App allows the storage of biochemical data on the device's internal or external memory, once measurement is complete. In addition, the App offers the flexibility to the user of sharing the measurements with private doctors or clinical experts. Once the measurement is complete, according to the measurement's value, the App suggests to the user if the data should be shared with the clinical expert or not. The app does not provide the probability of suffering by TB. It shares the measurement with an expert and shows the detected concentration to the patient. Finally, the current version is only in English and does not detect the location of the user.

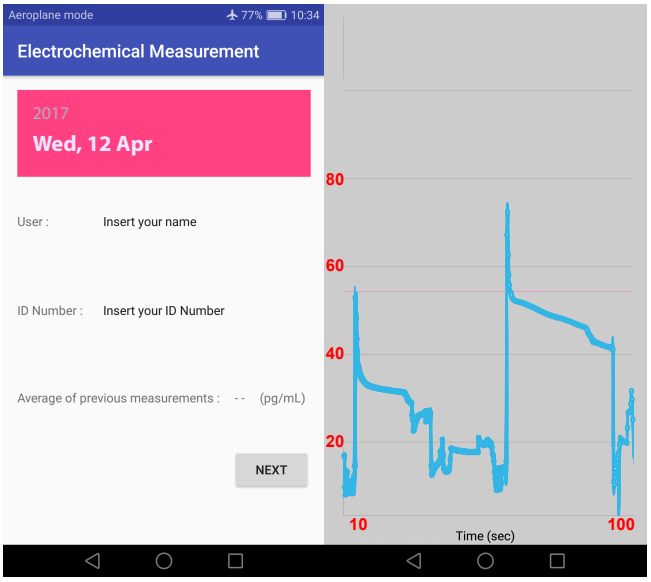

Figure 3.5: Two snapshots of the designed Android-based App. On the left, the welcoming screen can be seen, while on the right a snapshot of a real-time NaCl measurement can be found.

3.3 PCB-Based Sensing Platform

3.3.1 Commercial manufacturing PCB-Based Sensing Platform

The sensing platform was designed by Prodromakis group and manufactured by PCB manufacturing company (Newbury) (18). This platform consists of working, counter and reference electrodes embedded at the PCB surface during standard manufacturing processes. Working and counter electrodes are gold while the silver reference electrode is converted to Ag|AgCl by treatment with 30% Sodium Hypochlorite, ensuring its stability throughout the presented experiments (see Figure 3.6A). The PCB-based biosensing platform consists of 3 working electrodes having square geometry (1 mm x 1.3 mm). For this analysis a PMMA mould is used to cover the sensing area, while PDMS is poured onto the PCB to produce fluidic wells. A PMMA cover encloses the system to generate an amperometric sensing cell. Sample is introduced into the sensing well through a syringe and remained in the cell until the amperometric measurement is completed. A laser cutter (Epilog Laser) was used to create fluidic wells on PMMA. Different values of power or speed created a wider or narrower channel of fluid well. The optimal parameters to create a 1.3 mm x 8 mm fluidic well on PMMA (3 mm width) are 1200 dpi, vector speed 15% and vector power 20%. Three alternative working electrode positions are included to improve performance across a wide range reporter component concentrations. Figure 3.6B shows the bottom side of the commercial manufacturing sensor that includes UFL connectors in order to transfer the converted biological signal to the bio-instrumentation board. The whole assembly is clamped within an aluminium frame (see Figure 3.6C).

The geometry and the size of the commercial manufacturing PCB-based biosensing platform is not appropriate for high sensitive systems and integration with microfluidics due to the dimensions of the electrodes. According to the literature, some parameters of the electrodes as the size, geometry, surface structure and material, play main role in electrochemistry. Microscale electrodes allow to measure in pico to micro current ranges (pA - μA) with rapidly response in applied potential changes increasing the sensitivity of detection in ultralow concentrations (74). Most importantly, the total volume sample and the time of the measurement that the above sensor's design requires, are 200 μl and 2 minutes, respectively. As it will be discussed later, the values of theses parameters are significantly reduced minimizing the size of the sensor.

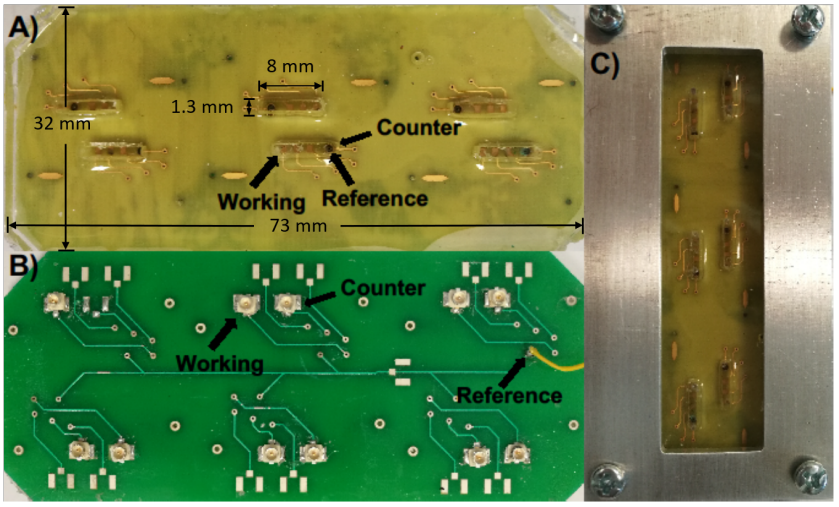

Figure 3.6: The proposed PCB-based sensing platform. A) The top view of the sensor with its three electrodes, B) the bottom view of the sensor with its three electrodes and C) the final assembly clamped within an aluminium frame.

3.3.2 Biosensors Geometries and Clean-room Fabrication technique

For the purpose of this thesis, in order to investigate the dependence between geometry and materials on their sensitivity, accuracy and precision, different biosensors were designed.

Figure 3.7 shows several cleanroom mask designs with different sensing surface geometries. The sizes of the new electrodes are significantly smaller than the previous ones (320 μm - 900 μm width of microfluidic channel). These designs consist of two separate masks, the first one containing the Reference Electrodes (RE) presented in grey, and the Counter and Working Electrodes (CE and WE respectively), in green. The RE will be fabricated with silver material. However, the WE and the CE will be fabricated using gold material. These masks include several size and electrode distance combinations, by keeping the same geometry, and designs with different geometries.

Figure 3.8 shows the different designed biosensor surfaces. The design in Figure 3.8E is similar to the aforementioned commercial manufacturing sensing platform in terms of the size and the distances among the electrodes expecting almost the same sensitivity. Figure 3.8F keeps the same shape increasing the distance among the electrodes studying how the distance of the electrode effects the electrochemical reactions. The rest of the designs have been chosen having as criteria the uniformity of the counter electrode (left electrode in each sensor) relatively to the working electrode (centre electrode in each sensor).

Figure 3.8A is a commercial available amperometric technique-based sensor by DropSens using the same design and size (85). The purpose is to investigate the accuracy and

sensitivity of a commercial available sensor in the electrochemical reactions of this thesis. The design in Figure 3.8D is the same as the previous one changing the size of the counter electrode. The expected result of the sensor is to reduce the sensitivity, since the counter electrode is much smaller than the working electrode, fact that made the counter electrode unable to feed the working electrode with the electrons if requested. In contrast to Figure 3.8A, in Figure 3.8C except the uniformity of the RE and CE with respect to WE, this sensor keeps the sizes of the RE and CE same. This sensor allows the analysis of how the size of the RE effects the measurements. Figure 3.8B shows a sensor with uniform CE and RE relatively to the WE. In this sensor, according to literature review, the size of the WE has been chosen to be smaller than the CE (74). Counter electrode should be large enough to provide current to potentiostat keeping maintain the RE-WE potential difference. Due to the uniformity of the design and the ration between WE and CE, the sensor in Figure 3.8B was expected to have the best sensitivity. Finally, an extra reason for choosing these designs is that they can be fabricated commercially. The purpose is that the biosensor can be a commercial product without needing facilities and tools of a clean-room laboratory.

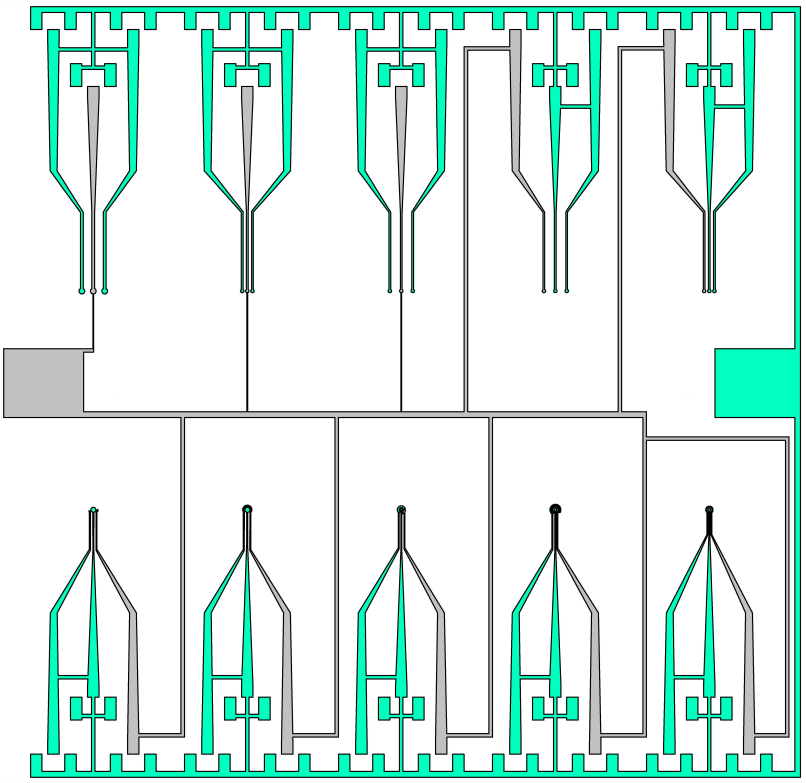

Figure 3.7: Different Biosensors Geometries (mask size 70mm x 70mm).

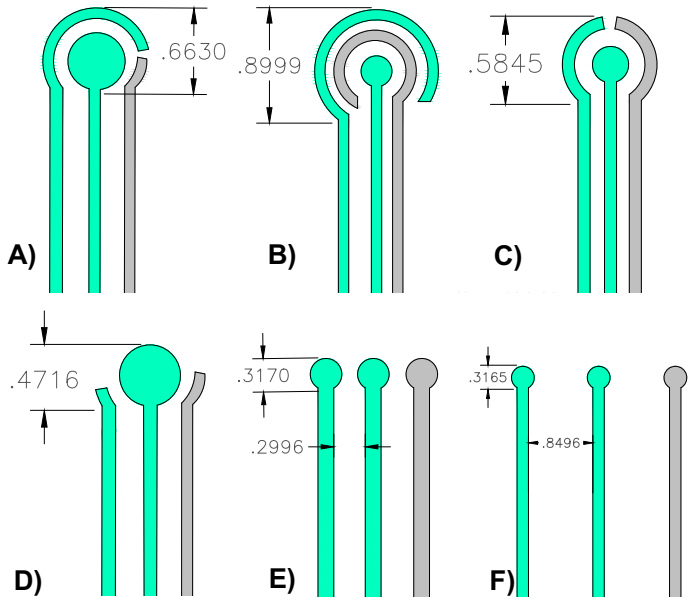

Figure 3.8: Different Biosensors Geometries (mm scale).

For the fabrication of electrodes on the FR-4 material, lift-off and wet-etching techniques could be used. However, lift-off technique was chosen, since it is much safer than wet-etching. Furthermore, wet-etching is not recommended for Au material due to the poor adhesion of the resist masks (86). In the fabrication sensor, an FR-4 material is used as substrate. The fabrication of the sensor's electrodes consists of a series of different steps. The main fabrication steps are photolithography, O_2 plasma etching, deposition and the lift-off process(see Figure 3.9).

- **Preparation of wafers**

The fabrication procedure starts with the cleaning of the FR-4 substrate's surface. The FR-4 wafer should be cleaned using acetone and the isopropanol removing all the dust and particles of the FR-4 surface. Then the wafer is baked into the oven (120 °C) for 10 minutes in order for the surface to dry (dehydration procedure). When these steps are completed, the substrate (FR-4) is ready for the deposition steps.

- **Photoresist deposition**

The first step of the lift-off process is photoresist deposition (see Figure 3.9). The photoresist, which is used for the needs of this fabrication process is the AZ 2070 (negative photoresist). The UV light beam transfers the pattern of the mask to photoresist, keeping the parts of the photoresist after the developing step, parts that were exposed to UV

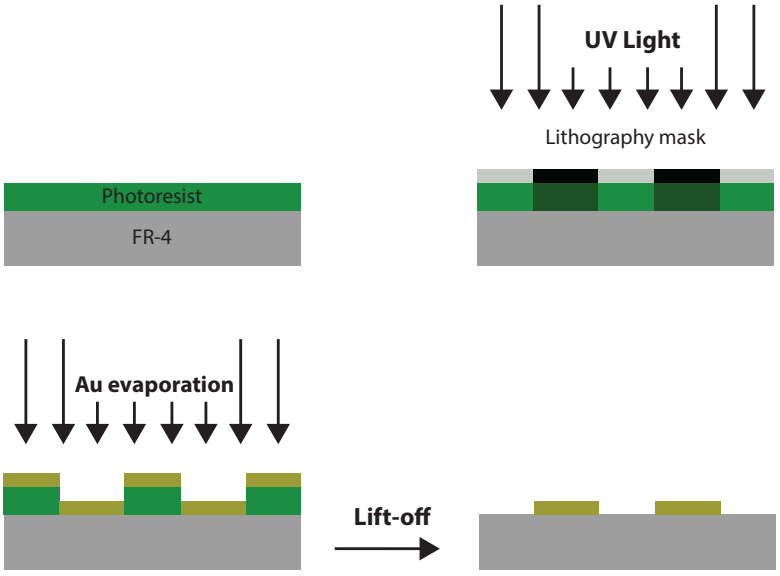

Figure 3.9: Lift-off precess steps.

light (negative photoresist). In contrast, positive photoresist can be dissolved by developer only in the area that UV light has been exposed. The uniformity of the AZ 2070 deposition is achieved by using the spinner instrument that allows the modification of the thickness of the photoresist, changing specific parameters as the time and the speed of the spinning. Spinner's parameters modified using 3000rpm (revolution per minute) for 30 seconds for film thickness 7 μm. This thickness of the film has been chosen as it is significantly thicker than the metal (Au or Ag) deposition thickness (100 nm). This difference between the photoresist film thickness and the metal deposition one, verify that the photoresist film, in the final lift-off step, will be removed properly without the removal of unwanted parts of the metal deposition. After the spinning step the wafer is baked in the hotplate for 1 minute at 110 °C, drying the photoresist. Then the wafer is ready for the photolithography step transferring the mask's pattern to the wafer's surface.

- **Optical lithography**

In the photolithography step, a 5 inch maskholder is used as the substrate wafer is 4 inch. In Figure 3.7 with the green colour the fist mask that was used for the patterning of the working and the counter electrodes can be detected. These electrodes are in the same mask because they follow the same lithography steps with the same targets. The lithography step was repeated over 10 times (using different FR-4 wafers), changing the exposure time (5 sec to 10 sec) and contact modes (between the mask and the wafer) in order to optimise the transferring of the mask's pattern to the substrate's surface. During these experiments, it was observed that when the exposure time was close to

5 sec or 10 sec the photoresist was removed less (under exposure-time) or more (over exposure-time), respectively, comparing to design pattern. The transferred pattern on the wafer was analysed through a microscope when the developer step ends. Finally, the best exposure time is 8.5 sec. in hard contact mode (contact force 1,100 mbar). When the lithography step ends the wafer is transferred to hotplate and is baked under the same circumstances as above. Finally, the wafer is sinking into the developer (AZ 726 MIF) for 1 minute and then is washed well and blow dried with N_2 gun. Figure 3.10 shows that the lithography pattern of WE and CE were transferred properly on the wafer using the correct development-time (without distorting the designs due to over or under development-time).

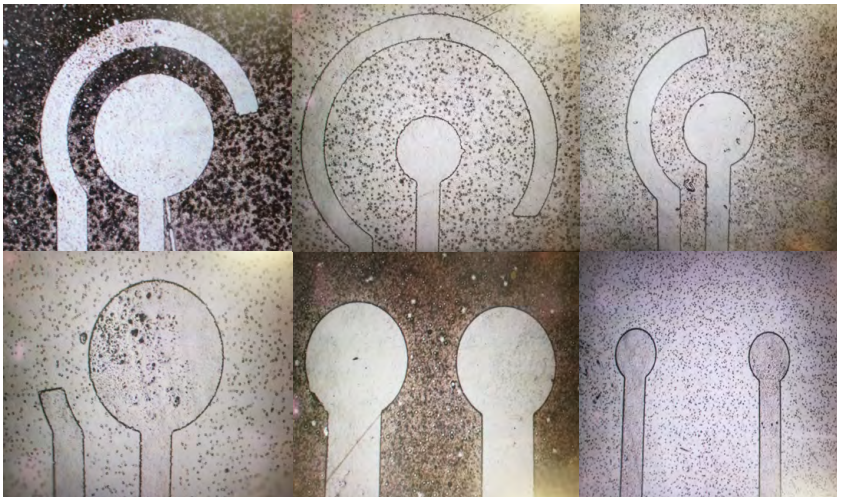

Figure 3.10: Photolithography pattern of Working and Counter electrodes.

- **Deposition of Au electrodes**

The following steps of the electrodes' fabrication are the O_2 plasma etching and the metal deposition. The O_2 plasma etching is used to clear the deposition area from any particles that remained from previous steps. Furthermore, hitting the FR-4 surface with O_2 plasma increases the roughness on the substrate's surface, a fact that helps the metal stick better on the substrate. There are two deposition techniques; the evaporation and the sputtering technique. Each technique provides advantages and disadvantages, relevant to the energy of atoms, grain size and adhesion (87). As the minimum feature size of these electrodes are few decades of μm, the resolution that is required appears to be less than the resolution both techniques provide. Both techniques have been used for electrodes fabrication providing the same uniformity and thickness. However, most of the times, for the Au deposition the AJA Orion Sputtering instrument was used for reasons of instrument's and Au target's availability. According to literature review, an adhesive layer of Cr (10 nm) was used between the substrate and the Au deposition film (100nm) (88). For both Cr and Au targets the deposition rate was 0.1nm/sec.

- **Lift-off process**

Finally the wafer consists of the substrate (FR-4), the area of the photoresist that is exposed to UV light and the metal layer. The final step is to remove the photoresist keeping only the area of the metal layer, which is attached to the surface and form the electrodes pattern (Lift-off process). The wafer with the metal layer is sank into the N-Methyl-2-pyrrolidone (NMP, C_5H_9NO) compound for 4 hours.

- **Ag deposition steps**

The same steps that were followed for the gold electrodes deposition was also followed for the deposition of the Ag electrode (photoresist deposition, hotplate, photolithography, development, Sputtering and Lift-off). In Figure 3.7 the second mask for the Ag electrodes with grey colour is presented. This mask was aligned with the previous electrodes using alignment marks (crosses in different sizes). The alignment marks of the masks were designed in order to provide the option of depositing Au or Ag as the first step. The thickness of the Ag layer is 100 nm keeping the Cr (10 nm) as adhesive layer (89; 90; 91). The sizes of the electrodes in Figure 3.10 and Figure 3.11 are the same as they are presented in Figure 3.8. Figure 3.11 shows the final step of three different sensor's designs. Each sensor consists of two Au electrodes (working and counter) and one Ag electrode (reference).

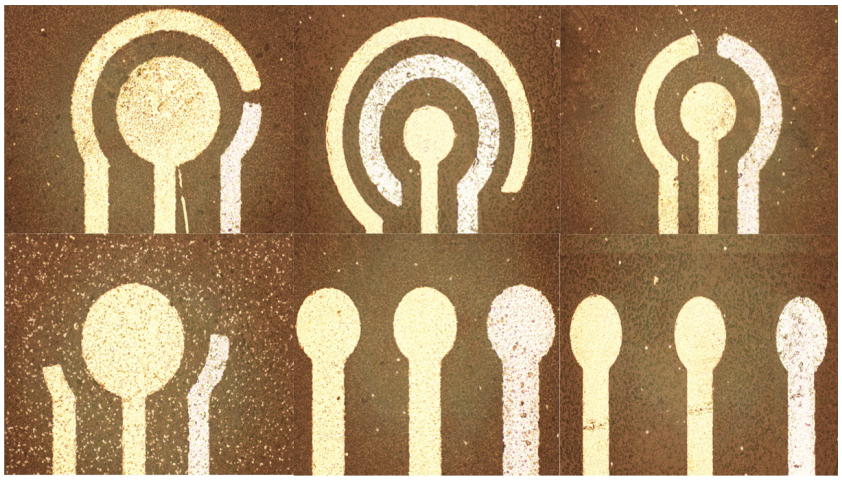

Figure 3.11: Fabrication of different sensor's designs.

- **Electroplating**

Finally, the electrodes have been fabricated with thickness close to 110 nm. However, the biological measurements require thicker electrodes as the electrochemical reaction has a clear affect on the electrodes surface. This reaction could either remove the metal electrodes or dissolve them. On the other hand, thicker electrodes can withstand longer in these phenomena. As the direct metal deposition (few μm thickness) is quite expensive through the evaporation or sputtering techniques (especially for Au metal), the electroplating technique was preferred. In both Au and Ag electroplating depositions, the FR-4 wafer (cathode) and a titanium anode coated with 2.5 μm of Pt were sank in gold and silver plating solution, respectively. The wafer and the anode net are placed in parallel into the solution increasing the uniformity of the deposition. Furthermore, a commercial reference electrode was sank into the solution among the aforementioned anode and cathode. Figure 3.12 shows the setup of the electroplating process. For the needs of this process a commercial potentiostat (PalmSens) was used, providing a constant current between the working and the counter wires (92). The working wire of the potentiostat (red) was connected to the anode, the counter to the cathode (black) and the reference wire to the reference electrode (blue). The range of the provided current varies depending in the deposition area and rate. Both masks of Au and Ag lithography step, have designed in order to connect the electrodes with a pad. This connection is necessary for the electroplating step as all the electrodes should characterised by the same potential. The potentiostat provides current to the area that has the same potential with the cathode's pad. Once the electroplating step ends, the connectivity between the counter and the working electrodes (Au electrodes) is interrupted as the electrodes should be independent for the biological measurements.

- **Atomic Force Microscopy (AFM)**

Atomic Force Microscopy (AFM) is a simple precise contact measurement technique, which allows the possibility of reaching an atomic resolution. This atomic level resolution was the fact that the AFM became an important tool, especially in Nanotechnology (93). In this thesis, an AFM (Multimode Nanoscopoe V, Veeco) was used, providing information about the surface topology of the FR-4 surface. The area of the sample that was scanned and captured was $60\mu m$ x $60\mu m$) (512 scanning lines, 0.6 Hz scanning rate). Furthermore, an Al-coated Tap300 Al-G tip was used measuring the surface's topology (resonance frequency 204-497 Hz, force constant 10-130 N/m). The measured topology of the area close to the electrode's surface, provides information about the thickness of the electrode after the electroplating step. The thickness of the electrode after the electroplating were measured twice in different wafers. Figure 3.13A and Figure 3.13B illustrate that the step between the FR-4 surface and the electrode surface is almost $2.5\mu m$ (AFM images were processed by Gwydditioin software). This slight divergence

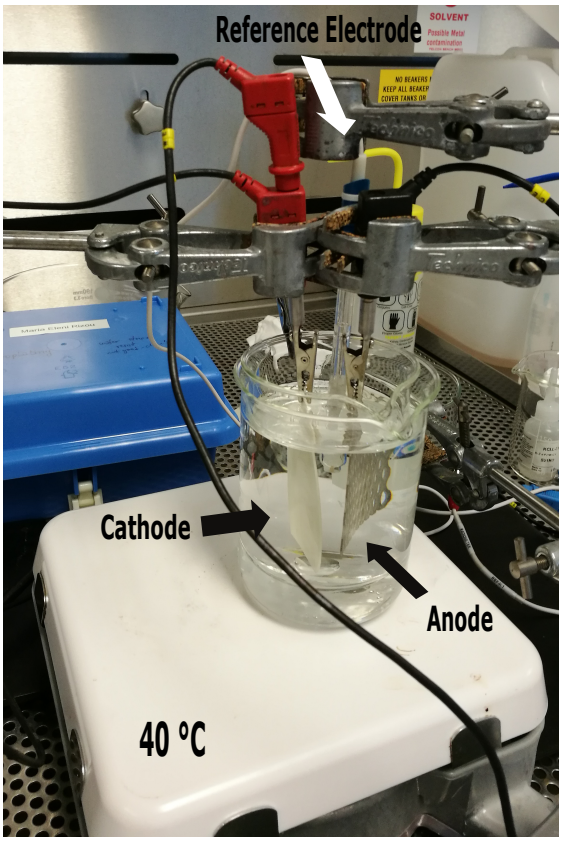

Figure 3.12: Electroplating setup.

of the two measurements could be attributed to the purity of the plating solution or to the contact between the electrodes of the potentiostat and the wafer. Furthermore, the roughness at the beginning of the sample could be due to its movement during the electroplating. This thickness verifies that in the previous electroplating steps, there was Au and Ag deposition on Au and Ag electrodes, respectively.

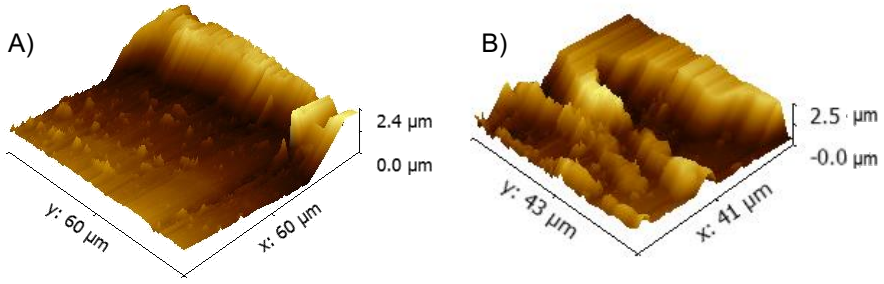

Figure 3.13: AFM height image of an Au electro-deposited on FR-4 substrate with thickness almost 2.5 μm.

- **Final assembly of PCB-based sensing platform**

The fabricated sensing platform is a single layer PCB with Au and Ag/AgCl plated electrodes. On the top side of the sensor's surface, there is PMMA laser-micromachined channel comprising of inlet and outlet holes in order to form fluidic. Sample was introduced through a hole in the PMMA cover and removed through another hole integrated after the sensing area. The flow rate of the sample was constantly 15 μl/min and introduced through a syringe pump (94). The idea was to create a microfluidic channel on the top of the sensor surface via PMMA. The same laser cutter (Epilog Laser) was used to create the microfluidic channel, an inlet and an outlet, as in the commercial sensor (see Figure 3.6). Epilog Engraver was used to design the pattern of the microchannels and the inlet/outlet on the PMMA surface. Both commercial and fabricated sensors used the same parameters for the patterning. Various parameters were used to properly transfer the pattern to PMMA. Parameter changes could cause the channel to leak. In addition, if the channel is too narrow, it would only be possible to use only part of the sensor. The optimal parameters are 1200 dpi, raster speed 50%, raster power 20%, vector speed 15% and vector power 20%. Figure 3.14 shows the PCB-based sensor consisting of three electrodes and the fluidic channel for the solution flow. The PCB-based sensor is the only disposable part of the bio-instrumentation platform. However, as shown in the next chapter, the same PCB-based sensor was used several times and purified with PBS after each use.

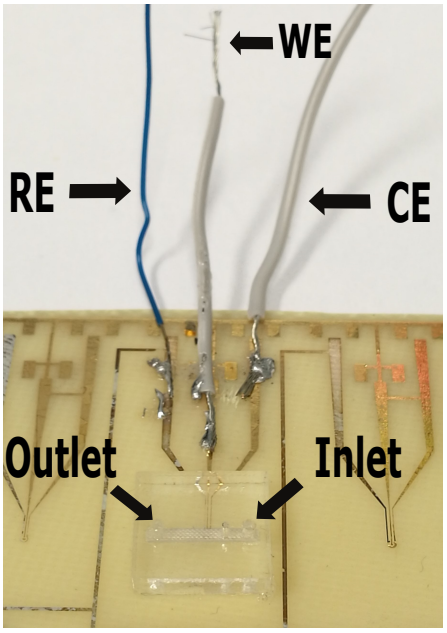

Figure 3.14: PCB-based sensing platform.

Chapter 4

Characterisation and Experimental measurements

4.1 Electronic Board Characterisation

Evans et al. and Papadimitriou et al. present an electronic board instrumentation that can cover a wide range of measurement (±2.5mA) keeping the range and the resolution of the measurements constant (16; 73). However, relevant researches show that the range of electrochemical reactions, as H_2O_2 and IFN-γ amperometric reactions, are few μA (14; 95). At these ranges a low resolution (few nA or lower) is required to detect accurately low concentration samples. The constant resolution is a limitation for detecting low concentration samples and for reaching LoD.

The electronic instrumentation platform of this thesis has been designed and programmed to read the current input signal and adapt the range, in real-time, optimizing the resolution. For initial electronic characterisation of the instrument, a high-precision Keithley 6221 AC/DC current source has been used. Primarily, the limits of each current sensing range have been investigated. Although, Table 4.1 provides the theoretical read-out limits of the instrument based on the ADC's capabilities ($V_{Ref}/(2^{15}-1)$), it was vital to identify the actual limitations of the device. Adequate resolution is an important board's feature, therefore, in Figure 4.1, low current measurements have been recorded, using the 4^{th} range of the board (R_4=1MΩ). Step changes of 500pA and 1nA have been used on a 100nA baseline DC signal. These step changes correspond to a resolution of 0.5% and 1% of the base signal, respectively. The recorded signals demonstrate clear distinction between each step. In addition, this instrumentation performs a current sweep experiment. The current source has been programmed to generate discrete steps from 10nA to 50μA, in an attempt to demonstrate in *real-time the automatic detection range algorithm* of the board. This algorithm detects the input signal and automatically changes the range, keeping the resolution high. The results are shown in Figure 4.2.

Furthermore, compared to the aforementioned board instrumentation, the current board can be actually portable without any external power supply needed.

Table 4.1: Summary of the characterisation experiments

	Programmable Current Ranges	
	Current Range	**Resolution**
R_1=1KΩ	± 2.5mA	122nA
R_2=10KΩ	± 250μA	12.2nA
R_3=100KΩ	± 25μA	1.22nA
R_4=1MΩ	± 2.5 μA	122pA

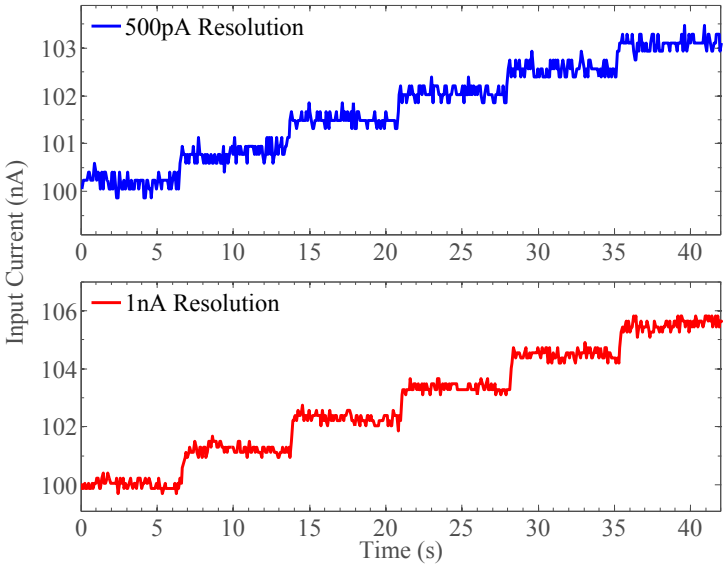

Figure 4.1: Investigation of the resolution properties of the instrument. The graphs demonstrate adequate, visible readings with 500pA and 1nA step changes.

The instrumentation board also consisted of an in-build potentiostat for the needs of the biological measurements. Figure 4.3 shows the potentiostat's changes of the provided potential and the received input signals (by Keithley 6221 AC/DC current source). The potentiostat has been tested receiving manually (see Figure 4.3A) or by default sine current input signals (see Figure 4.3B) in several frequencies, while simultaneously the potentiostat provides constantly different potentials in real-time.

Finally, Moschou et al. shows an PCB-based IFN-γ immunosensor with amperometric detection using a commercial electronic PCB platform. Compared to this thesis' instrumentation board, the commercial PCB-based platform is disadvantaged because it needs an external power supply and is expensive for POC diagnostic devices (14).

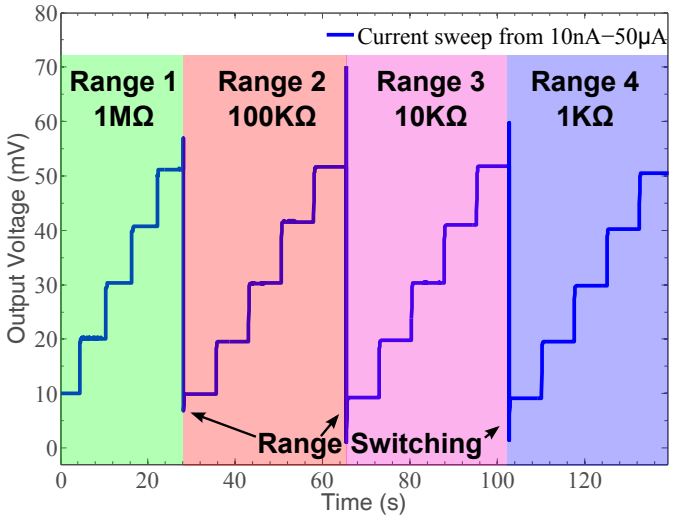

Figure 4.2: Automatic adaptation of the instrument's current reading range, as the input current increases from 10nA - 50μA.

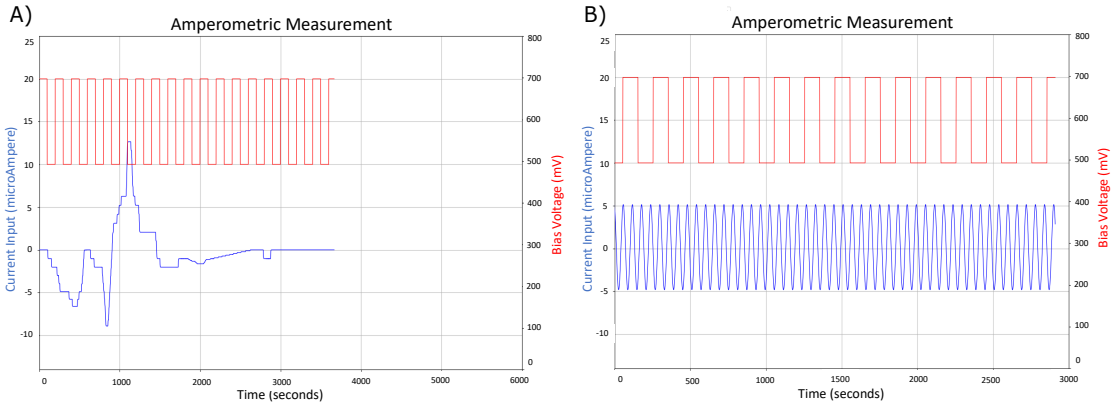

Figure 4.3: Potentiostat characterisation: A) Manual current input and B) Standard sine wave.

4.2 Cyclic Voltammetry

Cyclic Voltammetry is used to provide information about the sensor's surface, estimating the electroactive surface's area on gold electrodes. Potessium Fericyanide compound is indicated for the study of an electrochemically reversible redox system. Figure 4.4 illustrates the CV of the Potassium Ferricyanide solution (6.4 mM) with voltage sweeps from +0.1 V to +0.5 V (scan rate 0.05 V/s). The figure shows the peaks of the oxidase/reduction current in reversible reaction. This reversibility of the reaction allows the disclosure of information relevant to the sensor's behaviour. Furthermore, there seems to be no shift of the peak potential after 10 repeats of the Potassium Ferricyanide CV. Fact that proves the sensor could be used for several measurements as the electrochemically active area of the sensor behaves properly. In this electrochemical reaction as in

the following reactions, the sensor in Figure 3.8B was used.

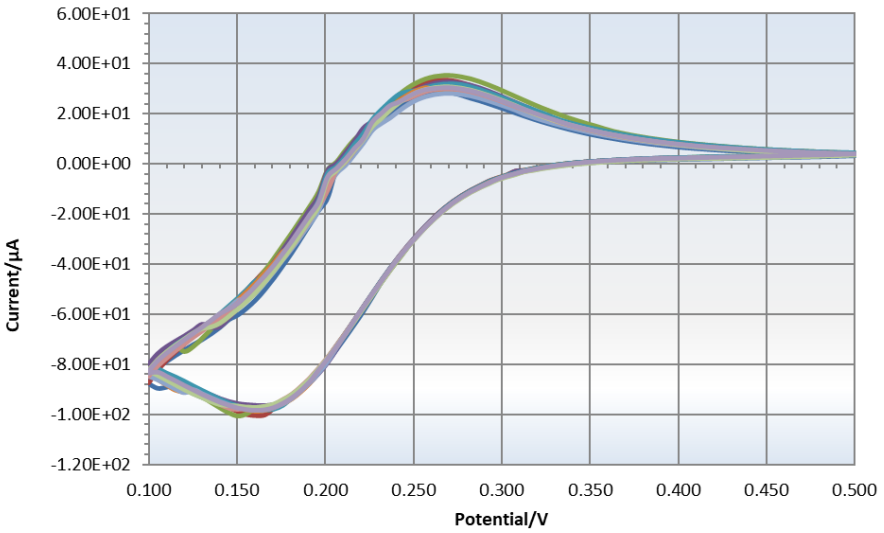

Figure 4.4: Cyclic Voltammetry of gold electrodes in Ferricyanide solution.

Figure 4.5 presents the CV of of 6.4 mM H_2O_2 in different scan rates. The figure shows that the increase of the scan rate of the measurement increases the total current too. In a low scan rate measurement, the diffusion layer will grow further than in a high scan rate, a fact that reduces the flux to the electrode's surface (96). In Figure 4.5, for each scan rate, the experiment was implemented 10 times.

Figure 4.6 illustrates the CV of H_2O_2 in different concentrations keeping the scan rate constant (0.05 V/sec) in a log2 dilution scheme. This figure presents that the peak current is proportional to solution's concentration as it is expected by Randles-Sevcik equation (see equation 2.5). The range of the concentrations is 0.4 mM to 12.8 mM observing higher current as the concentration increases.

The active area of the electrode was calculated and verified through the equation 2.6, exploiting information of the above electrochemical reaction (see Figure 4.4). In this experiment, 6.4 * 10^{-6} mol/cm^3 and 0.05 V/s were used for the concentration of the solution and the scan rate of the measurement, respectively. In addition, the current of the reaction (i_p) was measured 10^{-4} A. Relevant research shows that cyclic voltammetry of Ferricyanide reaction uses one electron transferred (n) and diffusion coefficient equal with 7.25 10^{-6} cm^2/s (97). According to the equation 2.6 and the above parameters, the area of the electrode that occurs on the reaction was calculated 0.0963 cm^2 (9.63 mm^2). However, the theoretical value of area of the sensors slightly differs (9.4 mm^2). The area on Figure 3.7 was calculated by Autocad designer using only 2 dimensions. This small variation should be due to the fact that the equation calculates the actual electroactive surface of the fabricated sensor (3D) instead of the theoretical area provided by the Autocad.

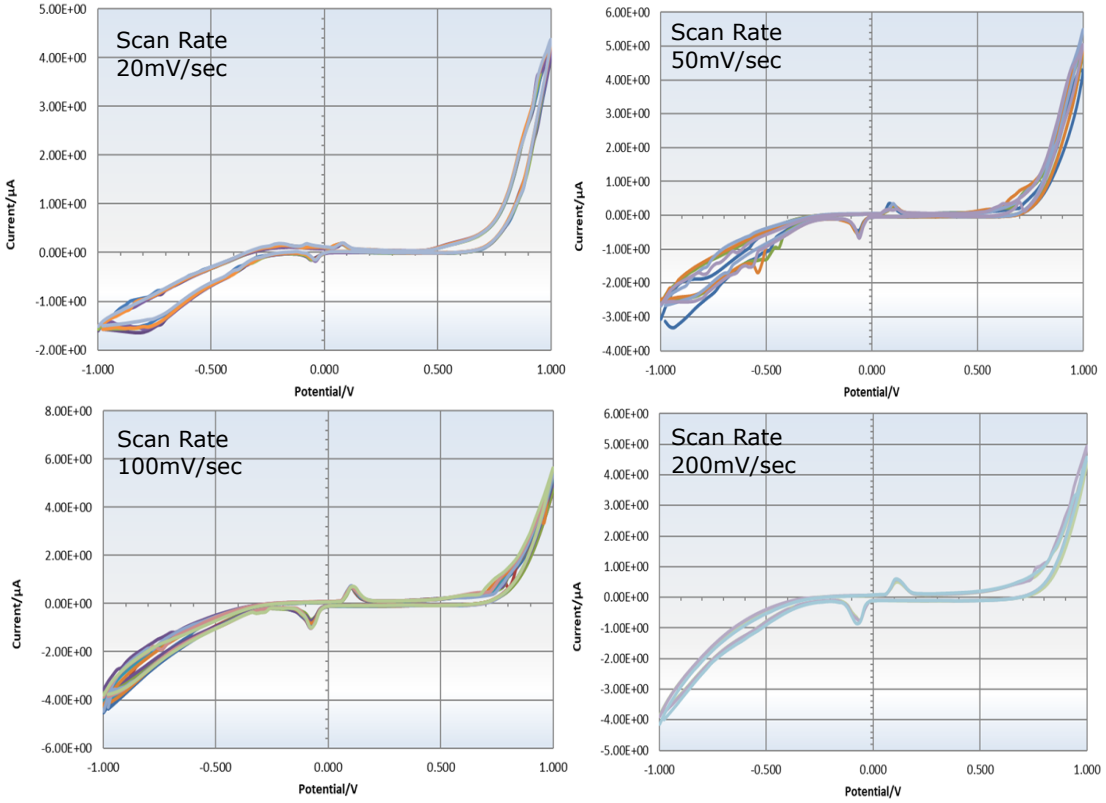

Figure 4.5: Cyclic Voltammetry of 6.4 mM H_2O_2 in different scan rates.

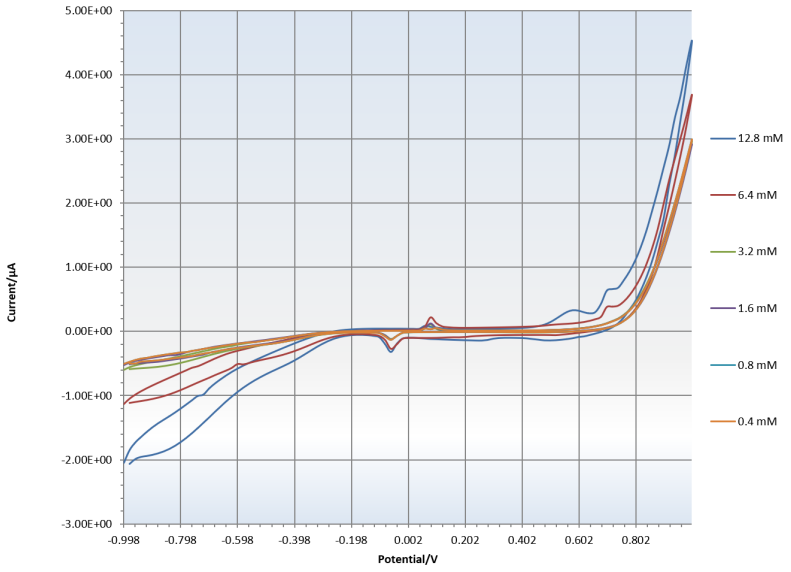

Figure 4.6: Cyclic Voltammetry of different concentrations of H_2O_2.

4.3 Biological Measurements

NaCl Measurements

NaCl concentration was assayed amperometrically across a range of concentrations to complement data showing bio-instrumentation processing of artificially generated signals. In this experiment, a wide range of NaCl electrochemical reaction attempted to be covered by randomly selecting 500mM as a high concentration in order to investigate how the amperometric sensor behaves in this reaction. A 500mM NaCl solution was diluted across ten samples in a $\log_2$ dilution scheme. Samples were introduced to the sensor of Figure 3.6 via the upper port and cleared from the system through a trans-PCB via. We observed linear relationships between NaCl concentration and current magnitude for high and low salt concentration schemes (see Figure 4.7). It could be argued that when viewed together the data suggests an exponential relationship. The linearity of a sensor usually is preferred because of its mathematical simplicity. However, nowadays the Digital Signal Processing (DSP) and the microprocessors allow to calculate more complicate responses of the sensors as an exponential response. The repeatability and the stability of the sensor are more important parameters for the characterisation of the sensor. These parameters will be studied further below by presenting experiments with repeated measurements.

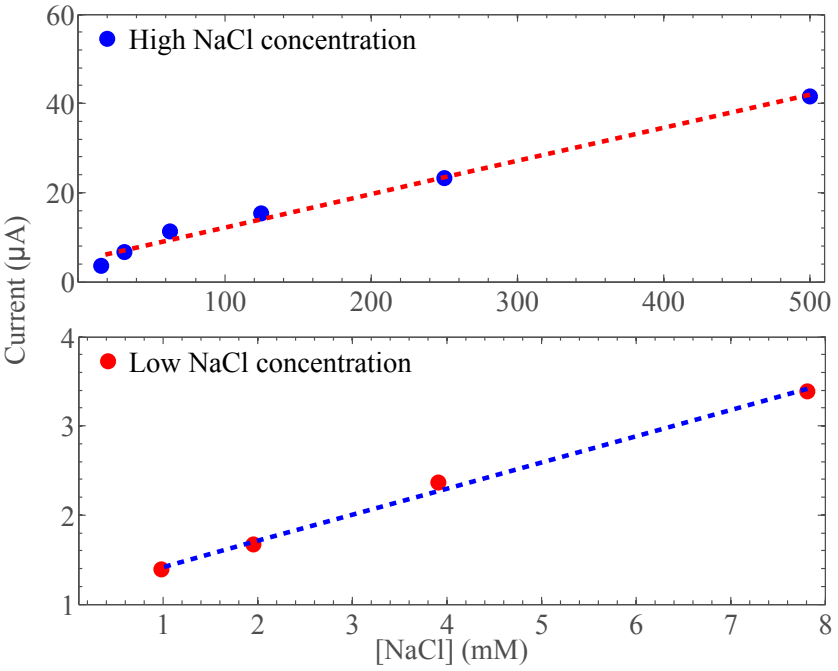

Figure 4.7: Amperometric measurement of NaCl concentrations (high and low) with the fabricated board. The system exhibits high degree of linearity with coefficients of determination (R^2) equal to 0.9883 and 0.9950 for the high and low NaCl concentration measurements, respectively (OPC voltage: -600mV).

H_2O_2 Measurements

Many colorimetric detection systems employ a TMB substrate converted to a di-imine product by the HRP enzyme. HRP is conjugated to detect antibodies and is thus proportional to target biomarker concentrations in immunochemical assay systems. In the enzymatic conversion of TMB, HRP consumes H_2O_2, so in excess substrate H_2O_2 concentrations are also proportional to those of the target biomarker. Using the electrochemical cell and fluidics described previously, we demonstrate amperometric signal magnitude proportional to titrated H_2O_2 concentrations. H_2O_2 was diluted in 10mM HEPES buffer from a top concentration of 10mM across six points in a $\log_2$ scheme (6.4mM H_2O_2 highest concentration). Amperometric assessment returns a broadly linear relationship between H_2O_2 concentration and measured current, as shown in Figure 4.8. These amperometric measurements show that the sensitivity of the commercial fabricated sensor is close to 236 nA/mM. Furthermore, the H_2O_2 measurement was repeated using the fabricated sensor providing similar linearity between the solution's concentration and the measured current, as the commercial sensor (see Figure 4.9). The sensitivity of this fabricated sensor is 173.1 nA/mM. However, the linearity of the measured data was increased further when the Open Circuit (OPC) voltage changed from -600 mV to -800 mV (see Figure 4.10) keeping the sensitivity almost the same 172.5 nA/mM. According to cyclic voltammetry of the H_2O_2 in 50 mV/s (see Figure 4.6), the curves show almost constant current in the potential close to -800 mV instead to -600 mV. The variation of the current close to -600 mV OPC voltage effects to the precision of the measurement. Although commercial sensor measurements (sensitivity 236 nA/mM) show better sensitivity than the fabricated sensor (172.5 nA/mM), nevertheless the fabricated sensor reached lower LoD (commercial sensor: 0.7 mM and fabricated sensor: 0.3 mM). The electrochemical reactions on Figures 4.8 to 4.10 were performed using 8 replicates of the same sensor (Figure 3.8B) for each experiment. The same fabricated sensing platform was used for HRP and TMB concentrations, which are presented in the following sections.

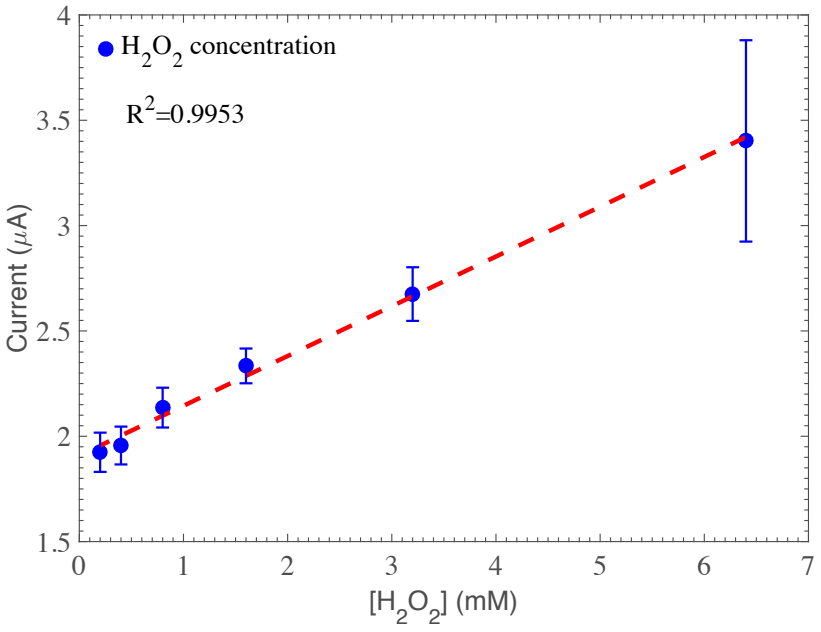

Figure 4.8: Amperometric measurement of H_2O_2 concentrations, using the commercial PCB-based sensor of Figure 3.6. The system exhibits high degree of linearity with coefficient of determination (R^2) equal to 0.9953 (OPC voltage: -600mV).

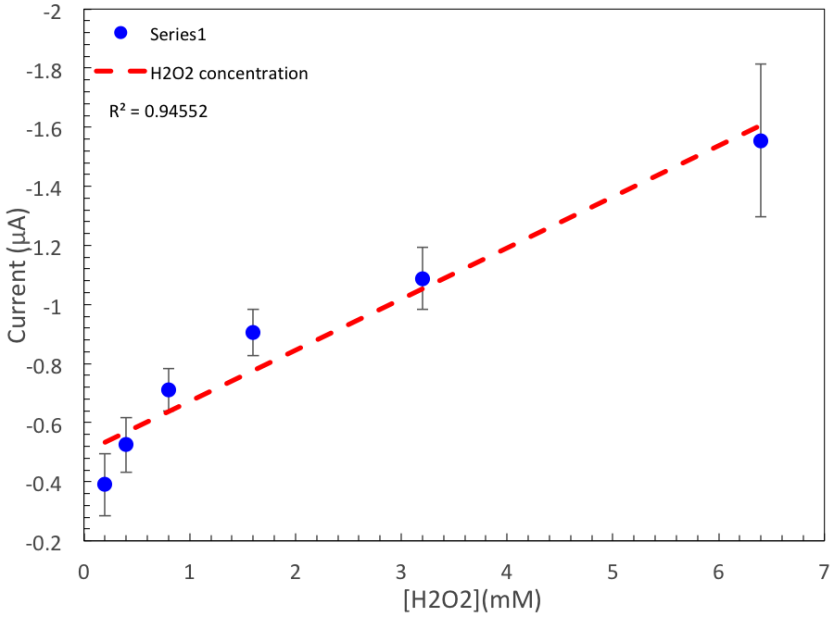

Figure 4.9: Amperometric measurement of H_2O_2 concentrations, using the fabricated PCB-based sensor of Figure 3.14. Again, the system exhibits high degree of linearity with coefficient of determination (R^2) equal to 0.94552 (OPC voltage: -600mV).

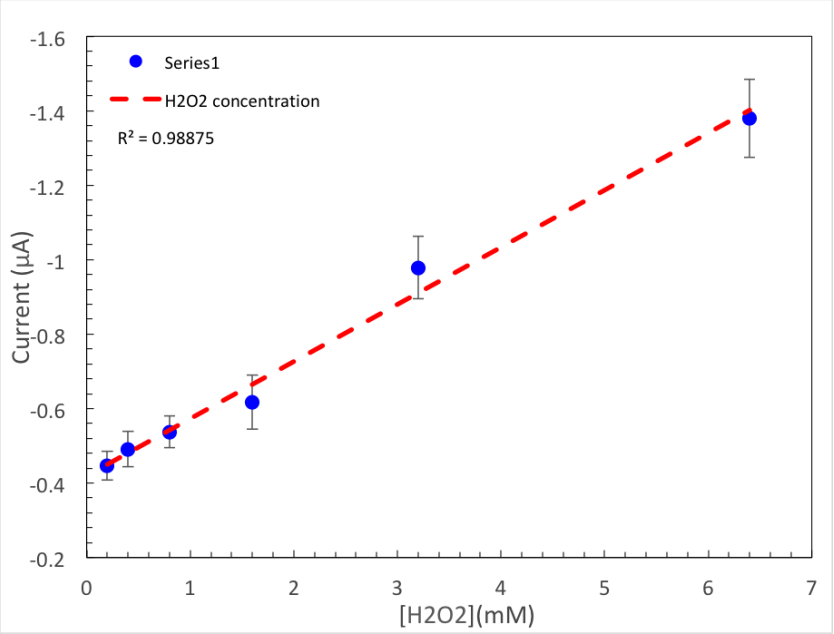

Figure 4.10: Amperometric measurement of H_2O_2 concentrations, using the fabricated PCB-based sensor of Figure 3.14. The system shows a further increase in linearity with coefficient of determination (R^2) equal to 0.98875 (OPC voltage: -800mV).

The same electrochemical experiment was repeated in sensing platforms with different geometries using the same highest concentration ($\log_2$ scheme) and OPC (-800mV). In section 3.3.2 was described the expected response of each design. Figure4.11 presents how the different designs effect the amperometric measurements. On Figures 4.11A/B, an amperometric measurement of a commercially design sensor and a sensor design with symmetrical RE and CE are presented. The sensors show similar sensitivity (A:131.1 nA/mM and B:123.7 nA/mM) to the above measurements; however, due to the high standard deviation, the samples concentration steps are not distinguished for both sensors designs. As it can been observed on Figure 3.8, the amperometric measurement on Figure 3.8C design (see Figure4.11B) shows better linearity (0.9726) comparing to the others. Figure4.11C presents a distinguished steps for low concentrations; however, tends to be saturated at high concentrations (sensitivity 71.2 nA/mM). This may be due to the small size of the CE relative to the WE (see Figure 3.8D). Finally the last measurements used similar designs, differing only in the distance of the electrodes. Both sensors cannot detect the low concentrations (sensitivities D: 94.7 nA/mM and E:103.2 nA/mM). Especially, Figure 3.8E shows that the sensor is not able to detect different concentration at the range 1,5mM - 4mM. The sensitivities of these graphs were calculated choosing the linear parts from each curve, found the slop for each part and then the average value (98). The measurements on Figure 3.8 were performed using 8 replicates of the each sensor.

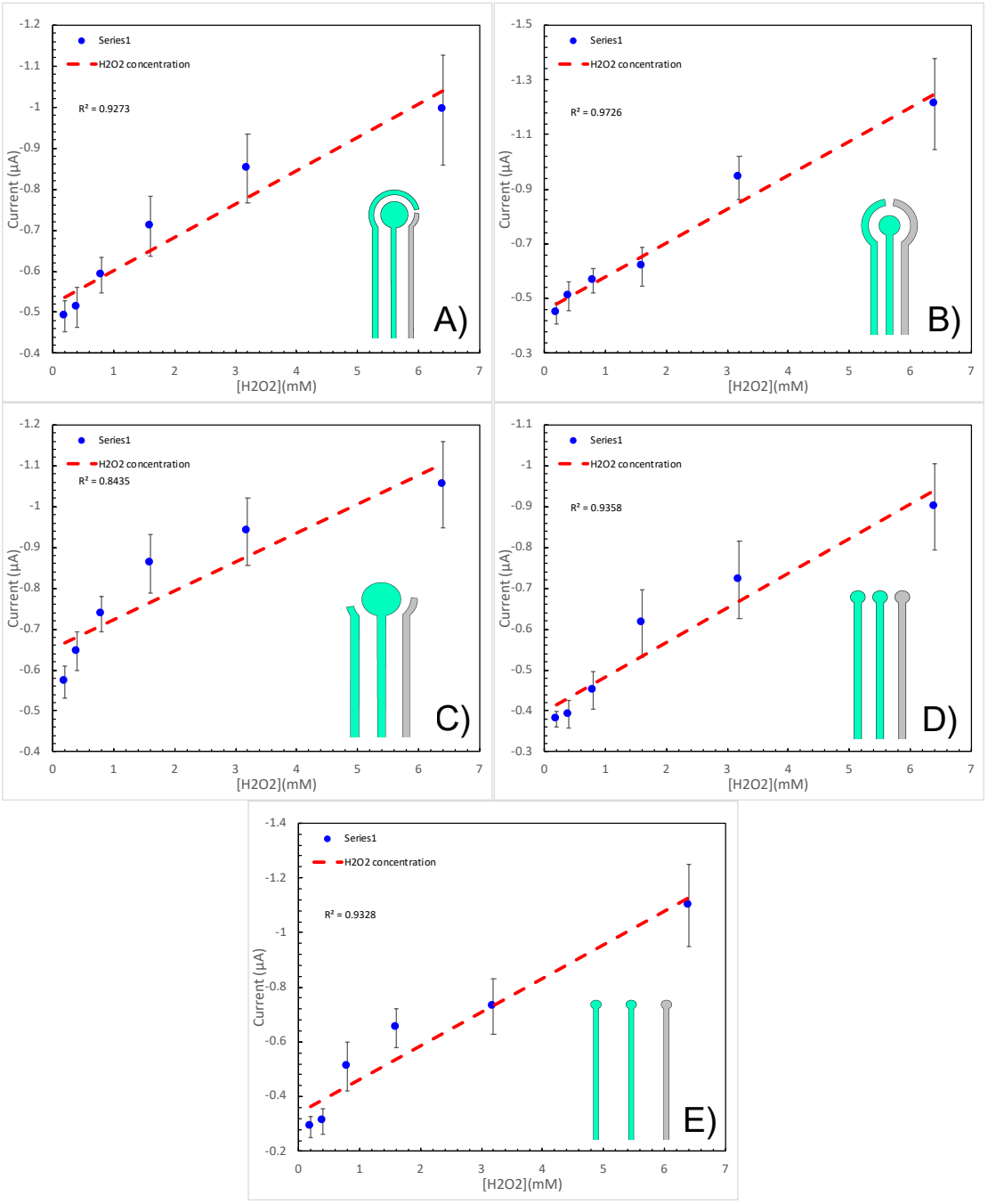

Figure 4.11: Amperometric measurement of H_2O_2 concentrations, using different biosensors geometries of the fabricated PCB-based sensors of Figure 3.8(OPC voltage: -800mV): A)Figure 3.8A, B)Figure 3.8C, C)Figure 3.8D, D)Figure 3.8E and E)Figure 3.8F.

The total volume sample and the time for each of the aforementioned measurements are 15 μl and 60 seconds. These parameters are significant lower than the commercial manufactured sensing platform (200 μl and 2 minutes).

HRP Measurements

Overall, this thesis is targeted on the measurements of concentrations of different biological samples (HRP and TMB) on a PCB-based biosensor platform using the amperometric technique and reducing the amount of sample (15 μl) and the detection time (60 seconds). Furthermore, this bio-instrument platform could be also used for more complicate ELISA-based targets as the IFN-γ in a clinically relevant range (14 pg/ml). An investigation conducted prior to this thesis measured a TMB product and IFN-γ concentrations (16). As a first step in this investigation, a simpler assay (TMB product) was measured colorimetrically. The TMB assay was prepared adding 5 μl of H_2O_2 to a TMB substrate (according to relevant guidelines, TMB tablet (Sigma-Aldritch T5525) in 10 ml of de-ionized water), and 5 μl 1 mg/ml of HPR solution (R + D Biosystems). However, following the aforementioned protocol, the colour of the sample did not change properly, which means there was an incomplete (inadequate) biochemical reaction into the solution (binding between the HRP and the TMB substrate). According to the protocol of the TMB substrate (Sigma-Aldritch T5525), the table has to be dissolved in a 1 ml of DMSO and a 9 ml of Phosphate Citrate Buffer (PBS) instead of 10 ml of de-ionised water (a guide following the above relevant work). The TMB tablet was dissolved in both a DI water and DMSO allowing an inter-comparison of these two protocols. The solutions were next centrifuged in 16,000 RCF for 3 minutes. Figure 4.12A shows that in DI water case, some particles of the tablet did not liquefied in contrast to DMSO case (see also Figure 4.12B). Figure 4.13 demonstrates the TMB product solutions for different HRP concentrations (TMB table dissolved in DMSO). The experiment was repeated 8 times in different rows of standard 96-well plates (see Figure 4.14). HRP's maximum concentration is 1.25 μg/ml diluted in a $\log_2$ dilution scheme.

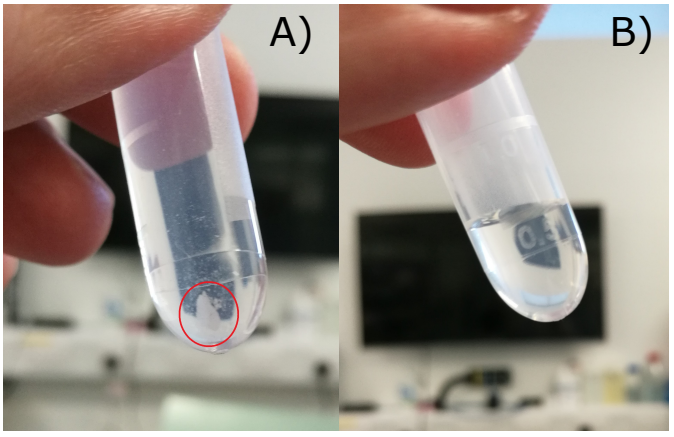

Figure 4.12: TMB tablet dissolved in: A)DI water and B)DMSO.

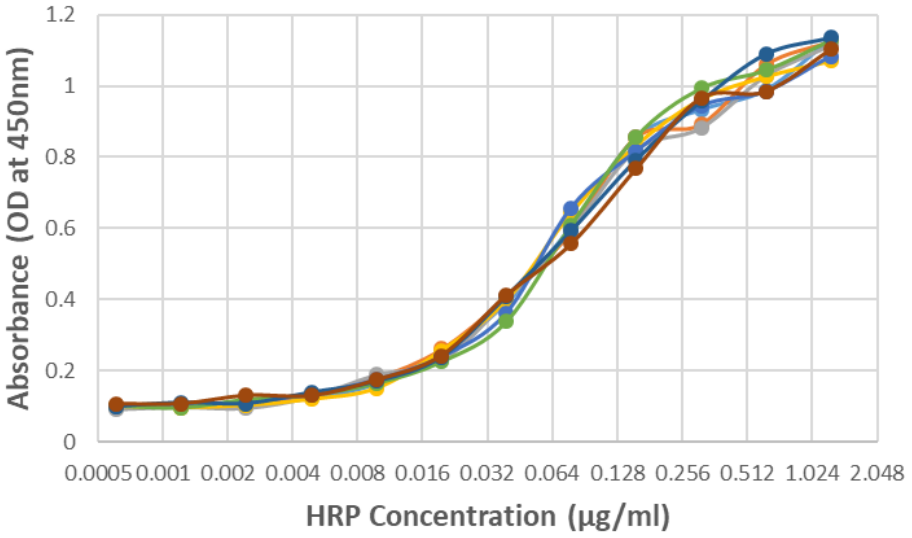

Figure 4.13: Colorimetric detection of HRP concentrations.

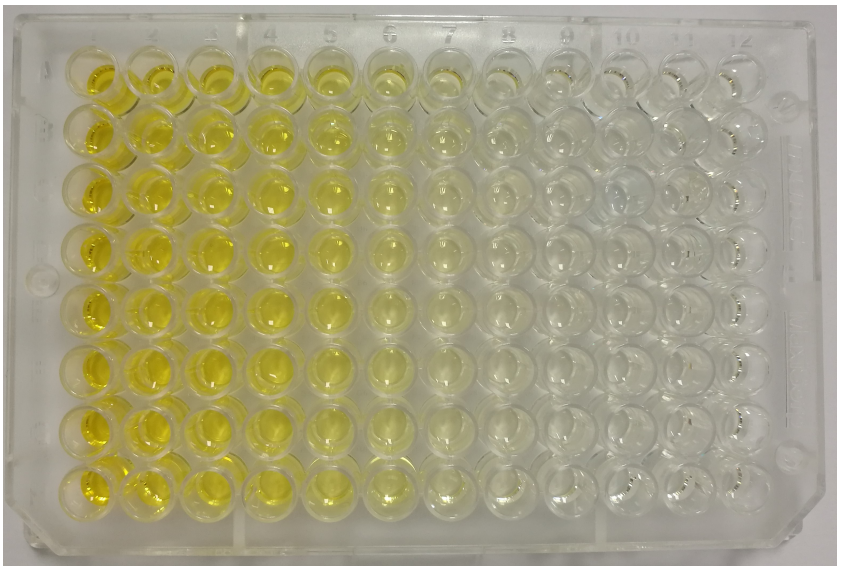

Figure 4.14: Biological plate including TMB and HRP solutions.

Figure 4.15 presents the comparison between the colorimetric (see Figure 4.13) and the amperometric detection method of HRP measurements. The left Y-axis (orange) shows the absorbance in 450 nm using the colorimetric method and how the colour of the sample changes for different concentrations. In the other side of the Y-axis (blue) there is an illustration of the results of the measurements (using amperometric method) and is also depicted how the current varied from these HRP concentrations. According to equation 2.3, the LoD of the colorimetric and the amperometric methods are 48.828 μg/ml and 97.65 μg/ml, respectively. Finally, both colorimetric and amperometric data correlate well with HRP concentrations.

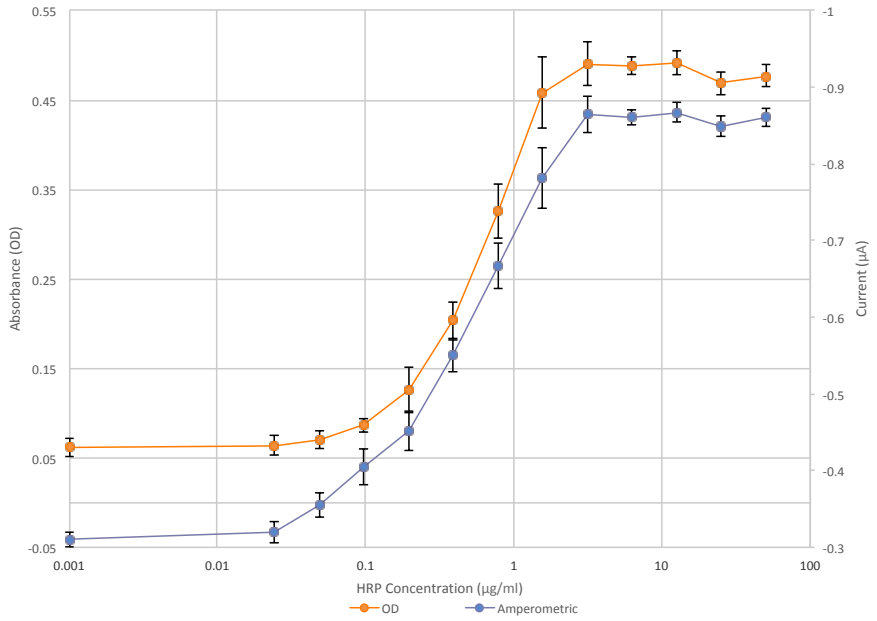

Figure 4.15: Comparison of colorimetric and amperometric detection of HRP concentrations.

TMB Measurements

TMB is a common reporter for ELISA colorimetric detection, thus, this detection system is appropriate for the replacement of colorimetry in standard TMB-based diagnostics. Figure 4.16A presents the typical Michaelis-Menten curve with TMB as substrate. Michaelis-Menten curve shows the substrate concentration as function of the reaction rate. As it can be observed in Figure 4.16A, increasing the concentration of the substrate means an increase of the velocity of the reaction (6 repeats with the same sensor (Figure 3.8B)). In addition, the curve provides information about the kinetic parameters of the enzyme, as the Michaelis constant (K_M) and the maximum reaction rate (V_{max}). K_M is the concentration of the substrate, when the velocity reaches the half of the V_{max}. According to the graph, Michaelis constant was obtained 0.25 mM as the maximum velocity is close to $2.5*10^{-8}$Msec^{-1}. The measured TMB samples were prepared using the aforementioned TMB tablet by Sigma (in a $\log_2$ dilution scheme), with 1 mM H_2O_2 and 1 ng/ml of HRP. Figure 4.16B shows the Lineweaver-Burk plot of the enzymatic reaction. Finally, the velocity curve was calculated from time-dependent absorbance changes at 600 nm.

The same concentration and dilution steps of TMB substrate were repeated measuring the response of the enzymatic reaction (HRP with TMB/H_2O_2) amperometrically. The reaction that occurs between the TMB solution and the electrode is observed in Equation 4.1. The TMB substrate (mediator) contributes to the electrons transfer between the enzyme and the electrode, as the direct carriage is not easy (99).

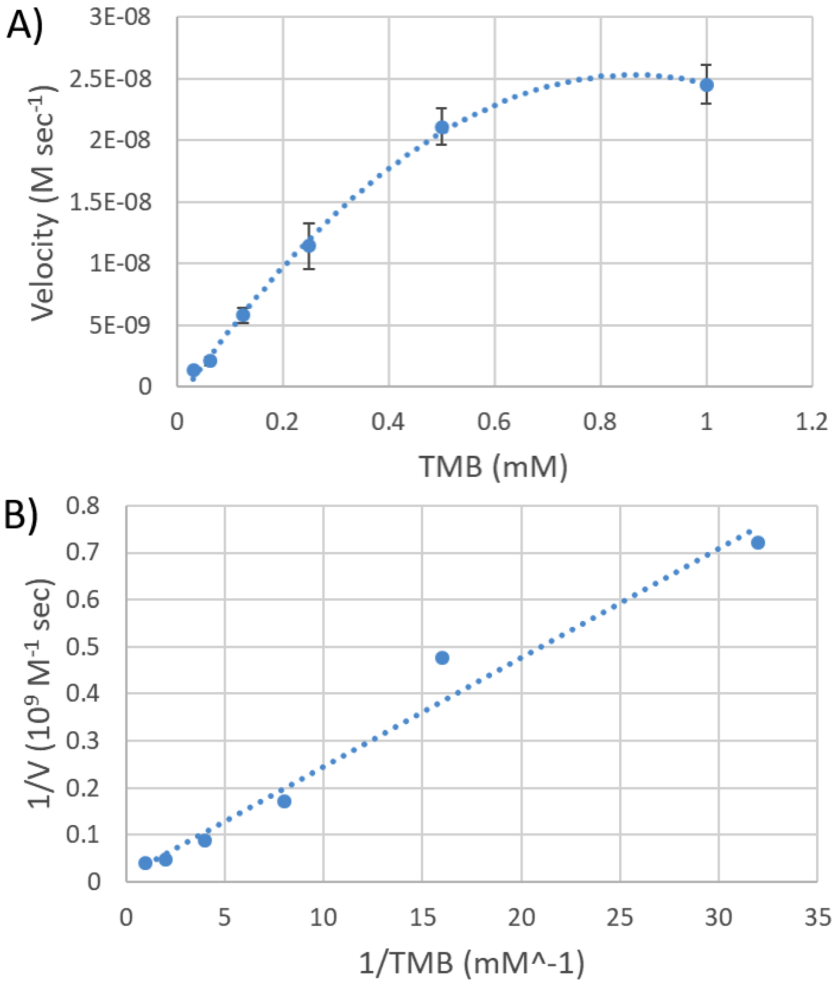

Figure 4.16: Steady-state kinetic assay and catalytic mechanism of TMB.

$$TMB_{ox} + 2H^{+} + 2e \rightarrow TMB_{red} \tag{4.1}$$

Figure 4.17 illustrates the electrochemical response of the enzymatic reaction. As it is observed, when the sample flows on the sensor's surface (0 sec.), a high current is produced and then is sharply decreased providing a constant current. The graph shows that by increasing the TMB concentration, a higher constant current is provided, fact that is also verified by the equation 4.1. Furthermore, this Figure presents the fact that when the solution passes on the sensor's surface, takes about 10 seconds in order to reach the constant value for each concentration. This time is significantly lower than the colorimetric technique (15 minutes).

In Figure 4.18 the relationship of the TMB concentration is presented against the constant current produced by each concentration (6 repeats with the same sensor (Figure 3.8B)). The graph shows that there is high linearity between the TMB concentrations and the current with coefficient of determination (R^2) equal to 0.96306. Furthermore, the measurement presents high sensitivity 289.4 nA/mM and LoD 31.125 μM. These

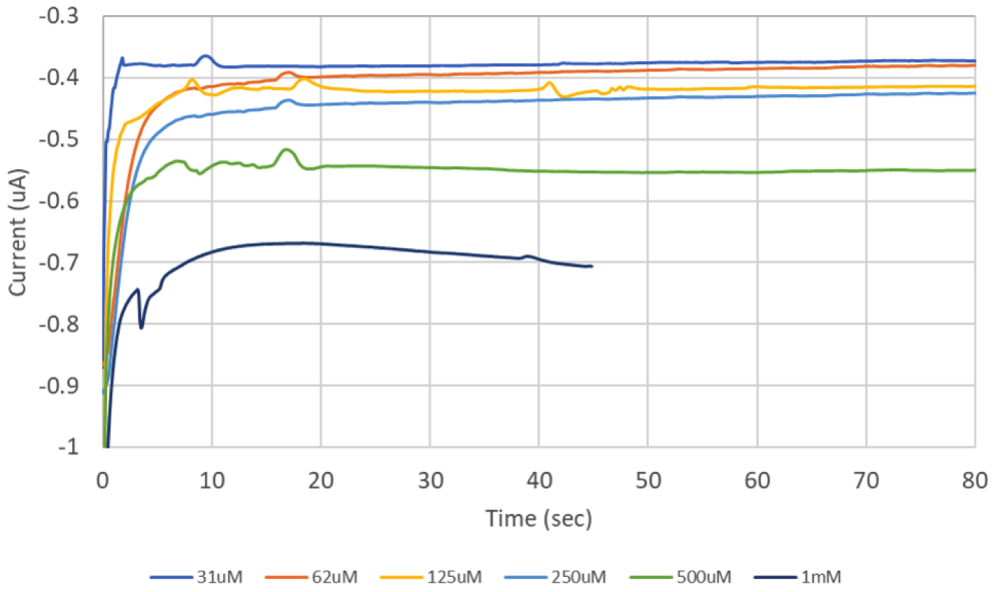

Figure 4.17: Current-time curve corresponding to TMB concentrations (31.25 μM - 1 mM).

results are encouraging enough and show that this bio-instrumentation platform can also be used for more complicated ELISA-based experiments with the amperometric technique reducing the time and the total amount of the sample.

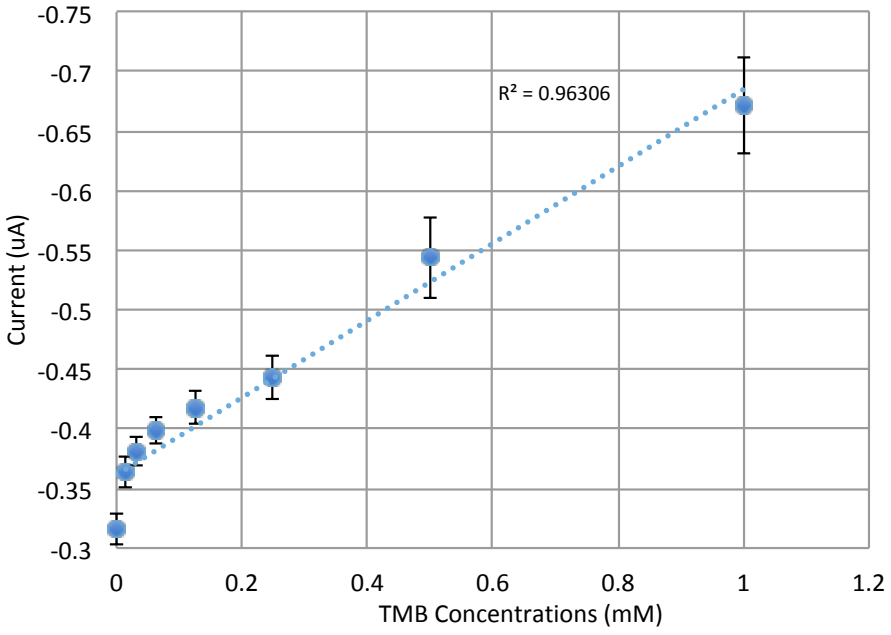

Figure 4.18: Amperometric detection of TMB concentrations (15.625 μM - 1 mM).

IFN-γ Measurements

As a next step, a commercial IFN-γ assay kit produced by R+D Biosystems (Human IFN-γ DuoSet ELISA) was used to measure different concentrations of IFN-γ target. This assay uses the sandwich ELISA method consisting of several steps (see Figure 4.19). Following the protocol of the previous investigation, the experiments take place in standard 96-well plates using $100\mu l$ volumes based on a standard ELISA analysis. Figure 4.20 shows several repeats (different colours) of a IFN-γ target detection at 450 nm absorbance using the Promega GloMax spectrometer. Figure 4.20A presents a small absorbance range with optical density of about 0.2 using maximum concentration of IFN-γ 2,048 pg/ml. This range was due to the fact that the concentration of the detection antibody (220 ng/ml) was 4.5 times lower than the protocol's suggestion (1 μg/ml) which results into less bindings between the detection antibody and the assay target (IFN-γ). After several repetitive experiments, it is observed that the standard curve reaches the linear portion, but it does not reach the saturation one. The protocol of the DuoSet kit suggests as a maximum IFN-γ concentration of 1024 pg/ml. However, all the experiment at Figure 4.20 have as highest concentration 2048 pg/ml except from the results in Figure 4.20C, which have maximum at 4096 pg/ml (4 times higher than the concentration in the DuoSet kit). The problem was overcome as at the TMB product assay when the TMB tablet was dissolved in a DMSO solution. Finally, Figure 4.21 shows the standard curve of the colorimetric detection of the IFN-γ concentrations in a $\log_2$ dilution scheme (maximum concentration at 1024 pg/ml). Figure 4.21 presents the curves of the IFN-γ assay following the same protocol's steps, yet dissolving the TMB tablet in a DI water and DMSO. When the tablet was liquidated in DMSO, the curve reached the saturation segment, in contrast to having the tablet liquidated in the DI water, which reached only part of the linear portion of the standard curve. Furthermore, Figure 4.21 highlights the fact that the DMSO samples are more sensitive to the DI water samples, especially in low IFN-γ concentrations. Figure 4.21 experiment was performed using 4 replicates of the same sensor (Figure 3.8B) for both DMSO and DI. Finally, according to the clinical range of this target, which is 0.35 IU/ml (14 pg/ml), the Limit of Detection and the high sensitivity in low concentrations of the IFN-γ are important for diagnostic devices (100).

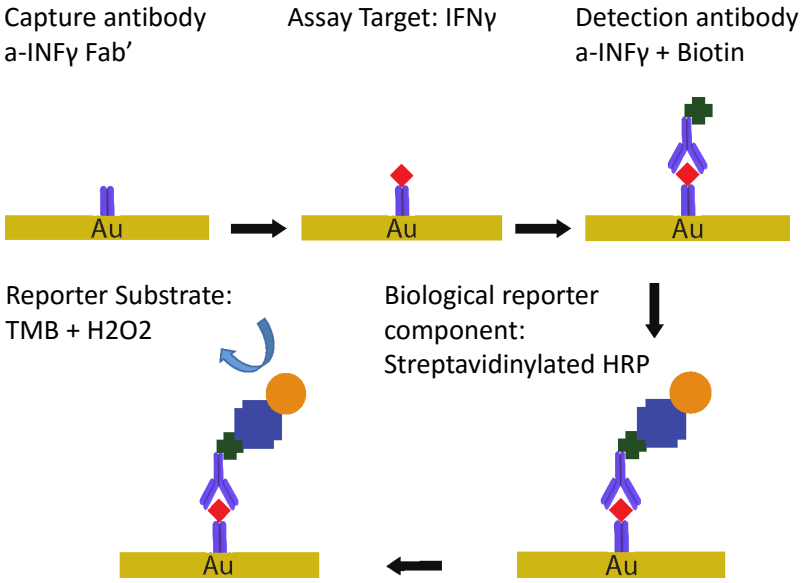

Figure 4.19: Standard ELISA detection method.

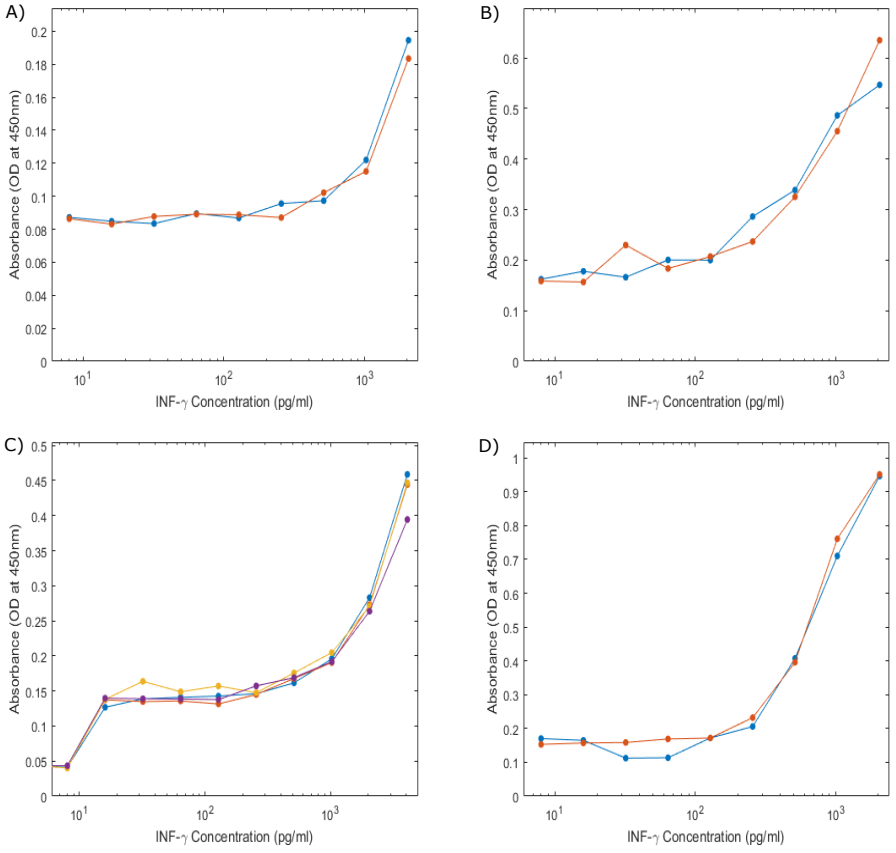

Figure 4.20: Colorimetric measurements detecting different IFN-γ concentrations.

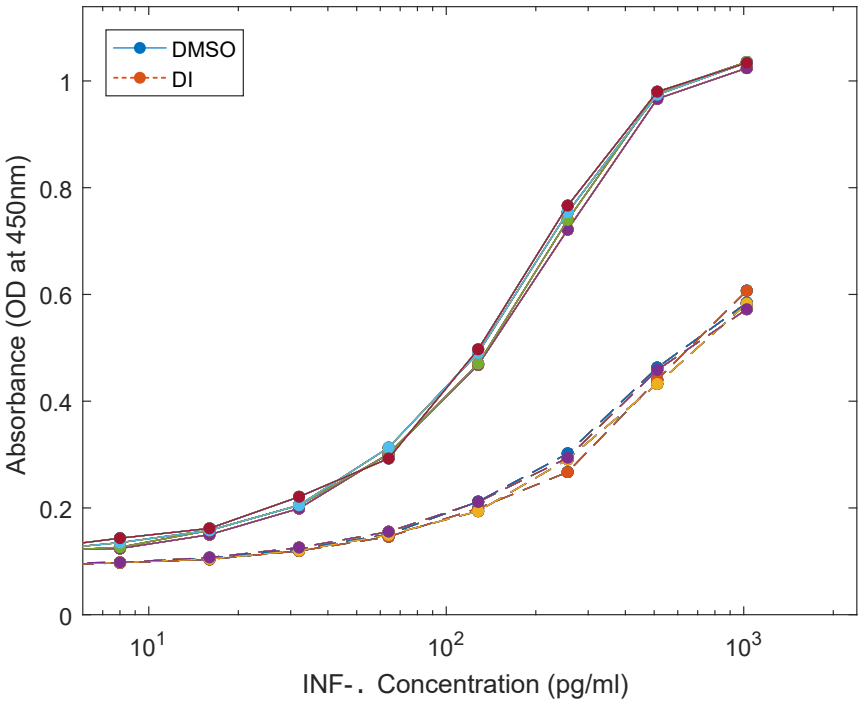

Figure 4.21: Colorimetric measurements detecting different IFN-γ concentrations dissolving TMB tablet in DMSO and DI.

4.4 Comparison with other relevant studies

In this thesis, a Lab-on-PCB platform for PoC diagnostic devices is demonstrated. The platform consists of a PCB-based electronic board, microfluidics and amperometric topology sensor. The platform was used to measure different concentrations of various samples (such as NaCl, H_2O_2, HRP and TMB) and further to provide the real-time results on a smartphone through an App. Similar investigations have been performed based on the same approach (Lab-on-PCB platform).

In Evans et al. (15) the current range of the IFN-γ measurement was 90 nA to 160 nA (2048 pg/ml to 40pg/ml IFN-γ concentration, respectively). However, the demonstrated data shows 10 nA signal different among the concentration range, when the ideal resolution of this electronic platform is 122 nA (much higher than the signal different). Furthermore, the TMB tablet was dissolved into 10 ml of deionised water instead of DMSO (DMSO suggested by *"Sigma Aldrich"* protocol), a fact that it does not allow the TMB tablet to be properly dissolved (the tablet is only partially dissolved). The current thesis platform outweighs the above platform due to higher signal resolution (122 pA), smaller sample volume (15 μl instead of 200 μl), no need for a power supply equipment (powered by a smartphone while monitoring the data in real-time), and a

"Sigma Aldrich" protocol to properly dissolve the TMB tablet. Another similar approach by Moschou et al. shows a PCB-based platform for TB diagnosis that uses a commercially available IFN-γ assay. This approach demonstrates the limit of detection of IFN-γ measurements using both colorimetric (LOD=28.22 pg/ml) and amperometric techniques (LOD=126.75 pg/ml). The LOD of the amperometric technique is 5 times higher than the colorimetric one, but this can be improved by minimizing the dimensions of the sensor (74). Nevertheless, this project requires a lab equipment to read the electronic signal that the PCB-sensor produces and lacks of microfluidic channels to set a complete Lab-on-PCB application such as a PoC diagnostic device. In contrast, this thesis presents a Lab-on-PCB platform that is independent of an external power supply equipment and uses a PCB-based microfluidic channel, which is necessary for an IFN-γ PoC diagnostic device due to the various sample steps (ELISA protocol).

Nowadays, the most common commercially available TB diagnostic test is the Skin Test (Mantoux). TST is an inexpensive diagnostic method to detect TB. A small amount of tuberculin is injected intradermally to the lowest part of the patient's arm. After 48 to 72 hours, the patient should visit again the clinician expert to check if a hard or swelling area appears. In the case that the skin changed in that area, the clinician expert will measure the size of that hard or swelling area (101). TST is the predominant method for TB detection, since it does not require bulky lab equipment and is low cost (2£-5£ in India) (102). However, this method does not provide information about the type of the TB disease (active or latent), is inaccurate (false positive and negative results) (9; 103) and requires 3 days for the results. In contrast, IGRA method can provide the result in 24 hours, has higher accuracy, is specified for latent TB and does not require a second visit for the patient. Especially, this thesis addresses the limitations that other IGRA applications have: 1) uses a portable Lab-on-PCB platform that consists of PCB-based electronic, microfluidic and sensor instrumentations, and 2) uses an android based smartphone (no external power supply or another bulky equipment). Furthermore, this platform keeps the cost low due to the inexpensive PCB material.

Chapter 5

Conclusions and Future work

5.1 Overview and Contributions of the accomplished work

This thesis presents a portable diagnostic framework suitable for measurements of H_2O_2, HRP and TMB concentrations, relevant to industry's standard colorimetric assay protocols. The connectivity of a smartphone with an electronic platform through the phone's USB port using a standard serial interface is demonstrated. The device is portable and power overheads are easily satisfied with the use of a standard smartphone battery. Amperometric measurement capability is demonstrated in four distinct regions between -2.5mA and +2.5mA. The electronic instrumentation platform is programmed to identify in real-time the input signal and change the range optimizing the resolution of the measurements (up to 122 pA). The associated App was designed to be easy-to-use. The successful demonstration of amperometric sensing cells, signal digitisation and processing via the bio-instrumentation platform, smartphone integration read-out, confirm the feasibility of a future fully integrated PoC diagnostic technology, including the PCB-based microfluidics.

Furthermore, in this thesis, the fabrication and the characterisation of the PCB-based electrochemical biosensors (see Figure 3.8) are performed. The purpose of these designs is to study the effect of the size and shape of the electrode on accuracy and sensitivity. The design shows the best performance with sensitivity 172.5 nA/mM and standard deviation allowing the distinct detection of different concentrations (see Figure 3.8B). This design uses a much bigger CE compared to WE, which allows the CE to provide electrodes to WE, if this is needed. However, all the other designs use a CE that is equal to or smaller than WE. These designs show significantly lower sensitivity (close to 100nA/nM) and higher standard deviation, which does not allow the concentration to be accurately detected.

The amperometric measurements of these designs show that minimizing the electrode size and creating microfluidic channels on the top of the sensor's surface results in increased sensitivity of the sensor and measurement of lower concentrations. Furthermore, the minimization of the sensor's size reduces the total amount of the sample (15 μl) and the total time of the measurement (60 sec.) of each measured sample.

In comparison to other relevant studies, this investigation presents a really portable bio -instrumentation platform exploiting smartphone's capabilities without requiring any external power supply. The ergonomic App allows to monitor, store and share in real-time the data of the biological measurement. Furthermore, the electronic instrumentation platform is designed and programmed to optimise the results of the measurements increasing also the resolution. An automatic detection range algorithm is programmed to recognise the input signal and automatically change the range keeping the resolution high (from 122nA to 122pA). Finally, a PCB-based electrochemical biosensor is fabricated and characterised. The uniformity of the design on the sensor's electrodes as well as the minimization of the sensor's size increase the limit of detection of the measurement reducing significantly the reaction time and the total amount of the sample. The reduction of the sample's volume and the detection time allows multiple measurements in few minutes, affecting the optimization of the accuracy.

5.2 Future work, ideas and applications

The experimental results of H_2O_2, HRP and TMB concentrations encourage further biological detections using the amperometric technique. The aforementioned platform performs a high sensitivity on the enzymatic reaction results, fact that motivates for further and more complicated ELISA-based enzymatic reactions.

In order to further improve the current platform, this thesis suggests the following:

- This bio-instrumentation platform could be used on similar biological enzymatic reactions, such as for TB disease, detecting different IFN-γ concentrations. According to the standard commercial available colorimetric technique, the concentration of the IFN-γ into solution is proportional to the enzymatic reaction.

- Furthermore, the electronic instrumentation platform offers 8 independent inputs allowing to detect 8 different or the same samples in parallel. This stimulation detection could be used for further improvement of the accuracy of the measurement (same sample), or for different samples reducing further the total detection time.

In order to further extend the current platform by adding new features, this thesis suggests the following:

- A future development could address a more complicated microfluidic design. This microfluidic device could incubate all the solutions of an ELISA process including also the wash steps. This design allows to run the whole process of an enzymatic reaction in a single device without an external intervention.

- The same sophisticated design could be utilised using passive microfluidic channels. This channels permit the solution to flow passively, without any requirement for external forced energy.

- The App could be improved by adding different languages (given the App is in developing countries) and requesting feedback at the end of the measurement for further improvement.

Finally, relevant studies showed that PCB-based PoC diagnostic devices, provide similar results to the conventional commercial colorimetric techniques. This thesis further enhances the capabilities of the PCB technology by combining the capabilities of a smartphone. The results of the biological measurements can be displayed on smartphone's screen through the App and exploit the aforementioned advantages of smartphone's potential.

Appendix A

Publication record

Conference Contributions:

- "Towards a smartphone-aided electronic ELISA for real-time electrochemical monitoring", Nikolaos G. Pechlivanidis, K. I. Papadimitriou, D. Evans, N. Vasilakis and T. Prodromakis, International Symposium on Circuits and Systems (ISCAS) Conference, IEEE, Baltimore, MD, USA, 2017. (Oral presentation)

Appendix B

Schematic of the bioinstrumentation board

Schematic diagram illustrates the connections among electronic components in a unique way. This connection could be presented used different schematic sheets declaring the inputs/outputs of each schematic sheet (see Figure B.1, Figure B.2, Figure B.3, Figure B.4, Figure B.5, Figure B.6, Figure B.7).

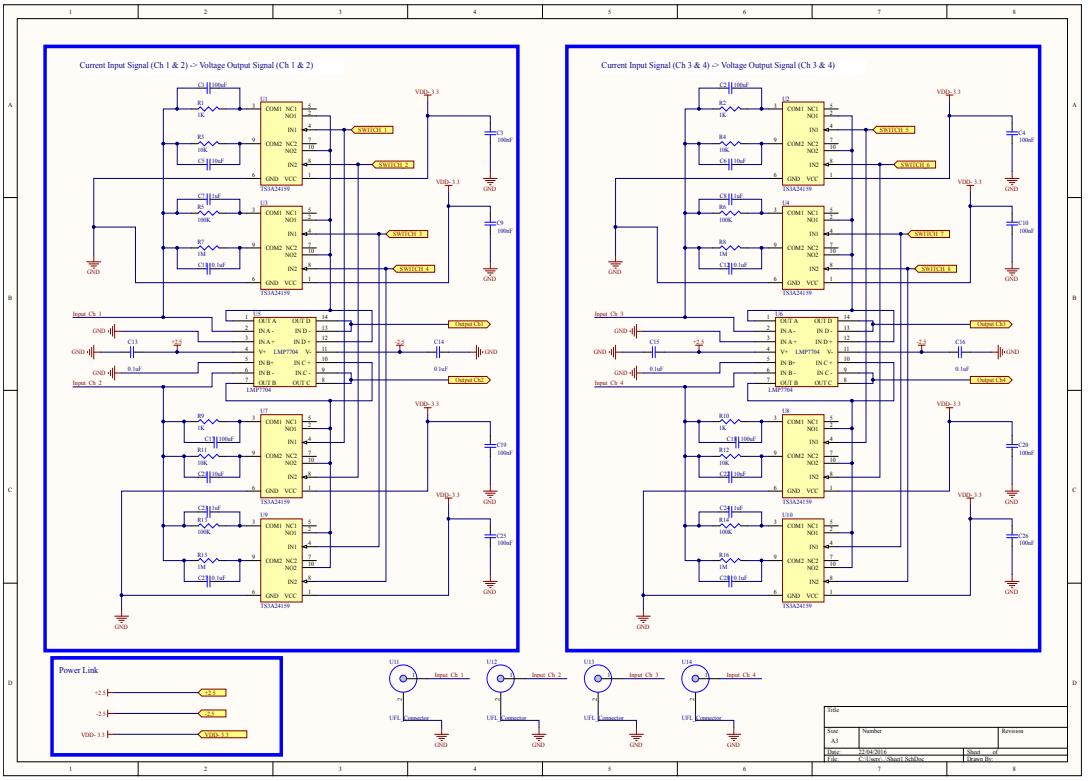

Figure B.1: Schematic diagram of the TIAs (Input Channels 1-4).

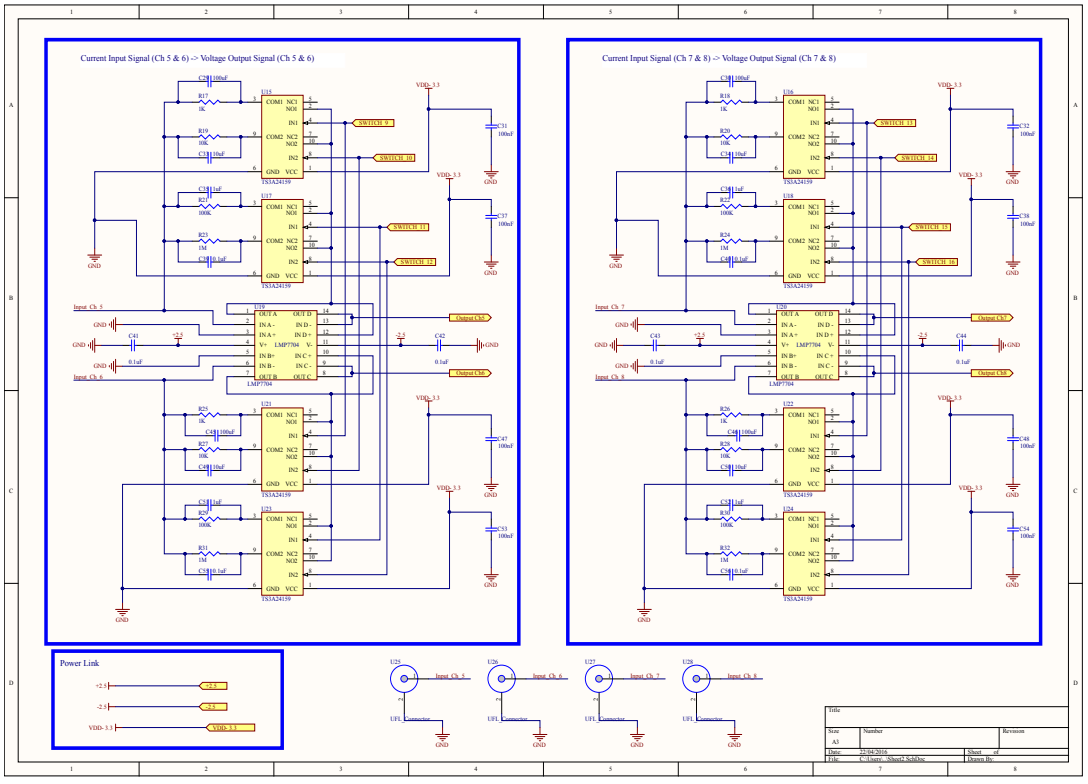

Figure B.2: Schematic diagram of the TIAs (Input Channels 5-8).

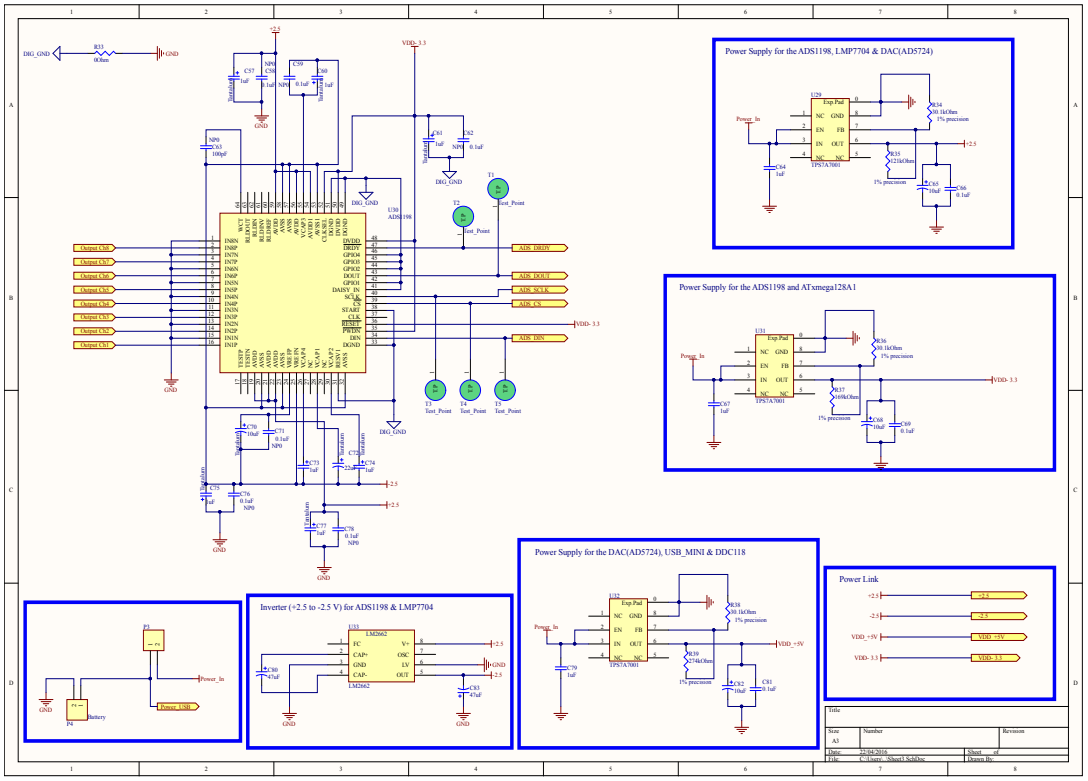

Figure B.3: Schematic diagram of ADC and Power Supplies/Inverter.

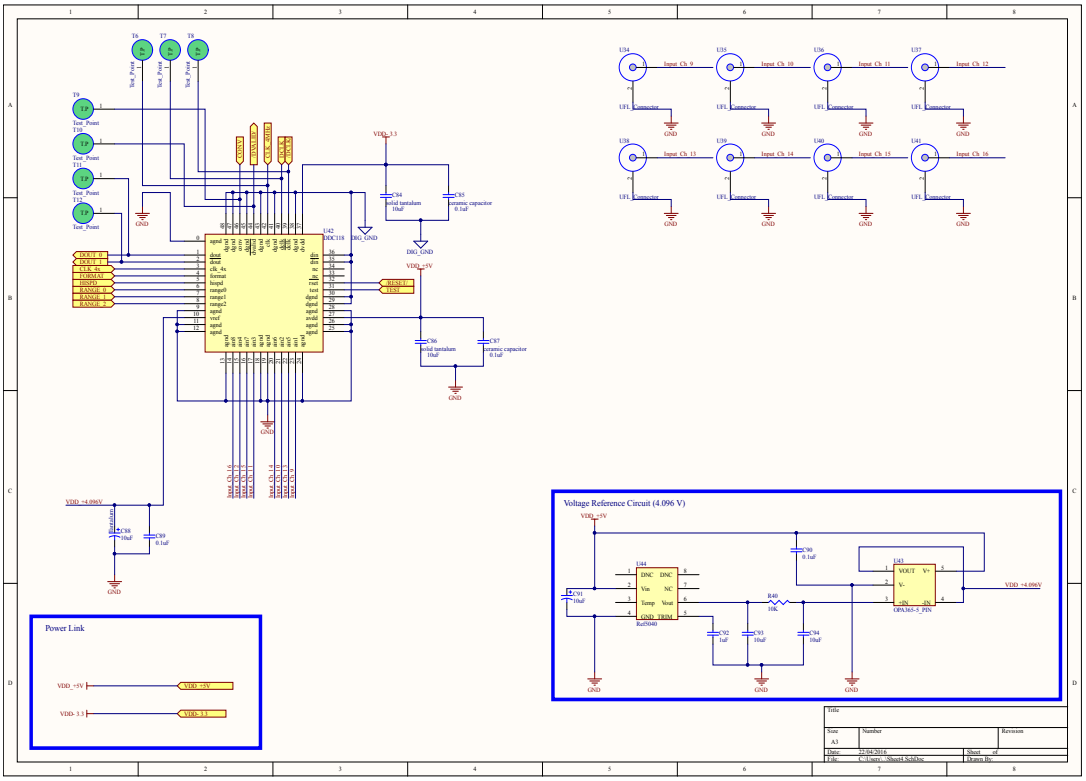

Figure B.4: Schematic diagram of the DDC118.

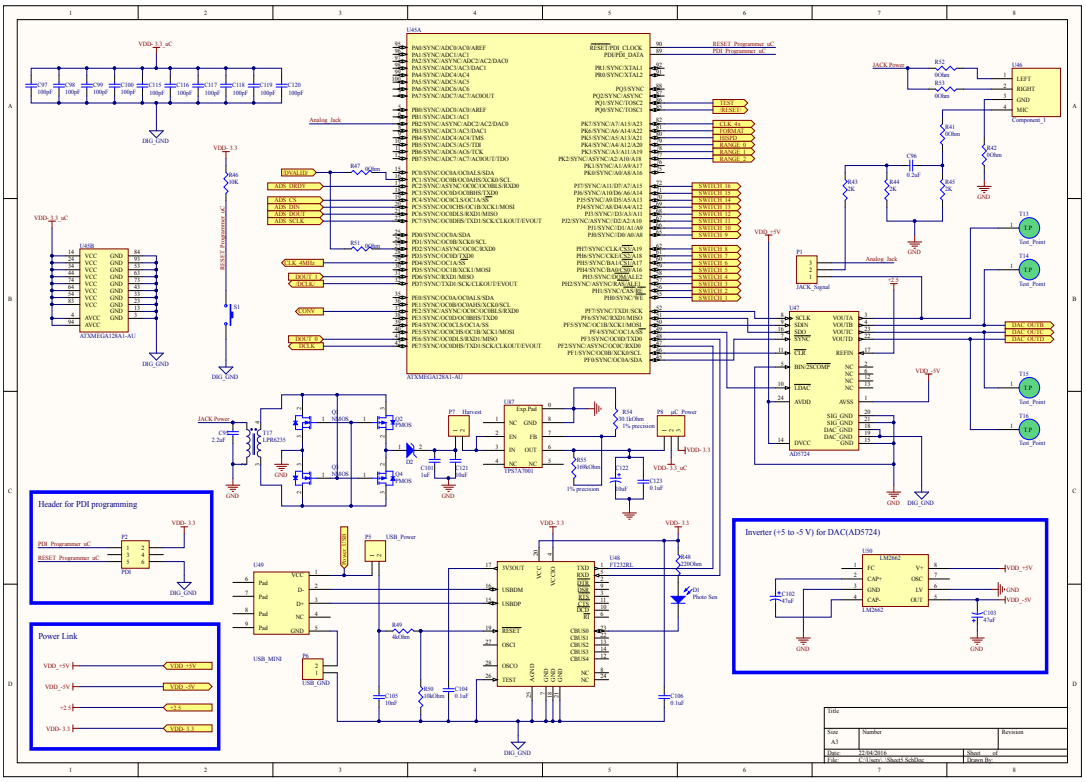

Figure B.5: Schematic diagram of the μC , USB/Jack connectors and DAC.

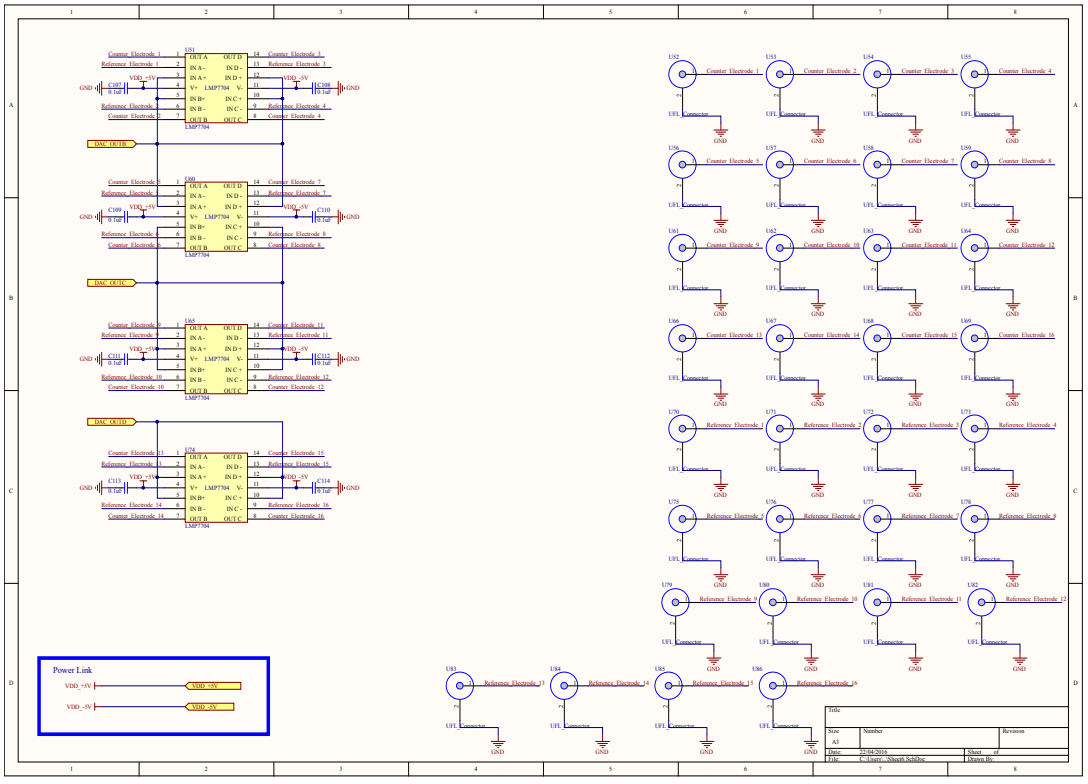

Figure B.6: Topology of the potentiostat and CE/RE connectors.

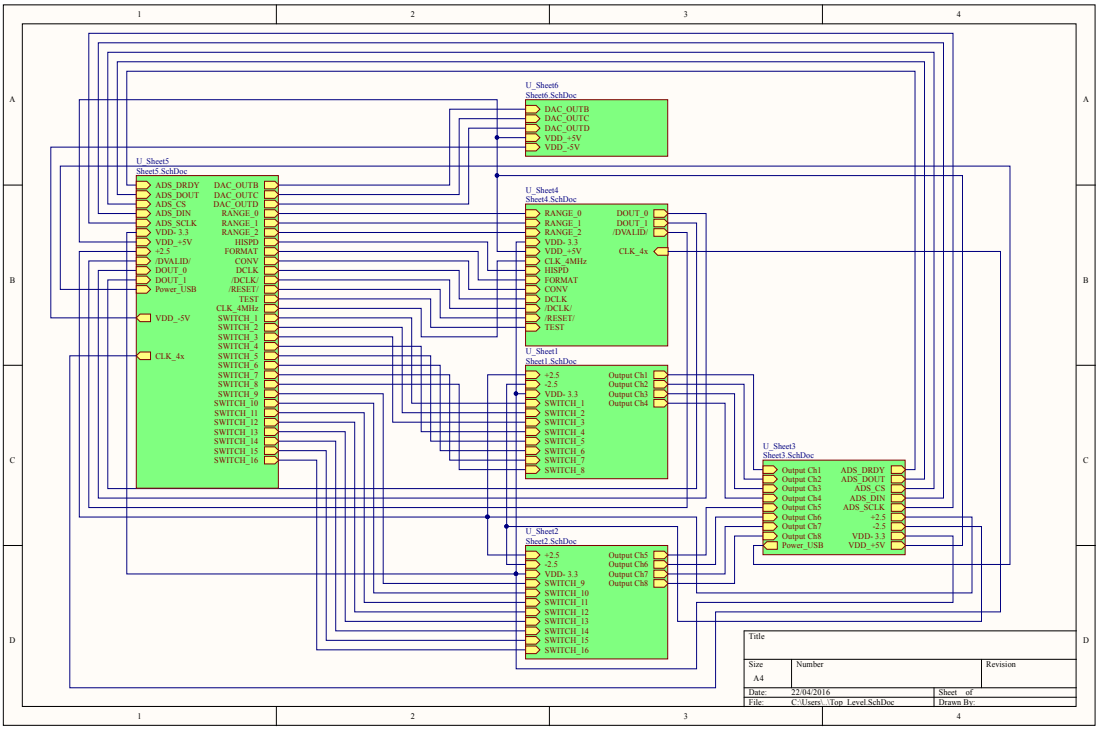

Figure B.7: Top schematic diagram of the bioinstrumentation board.

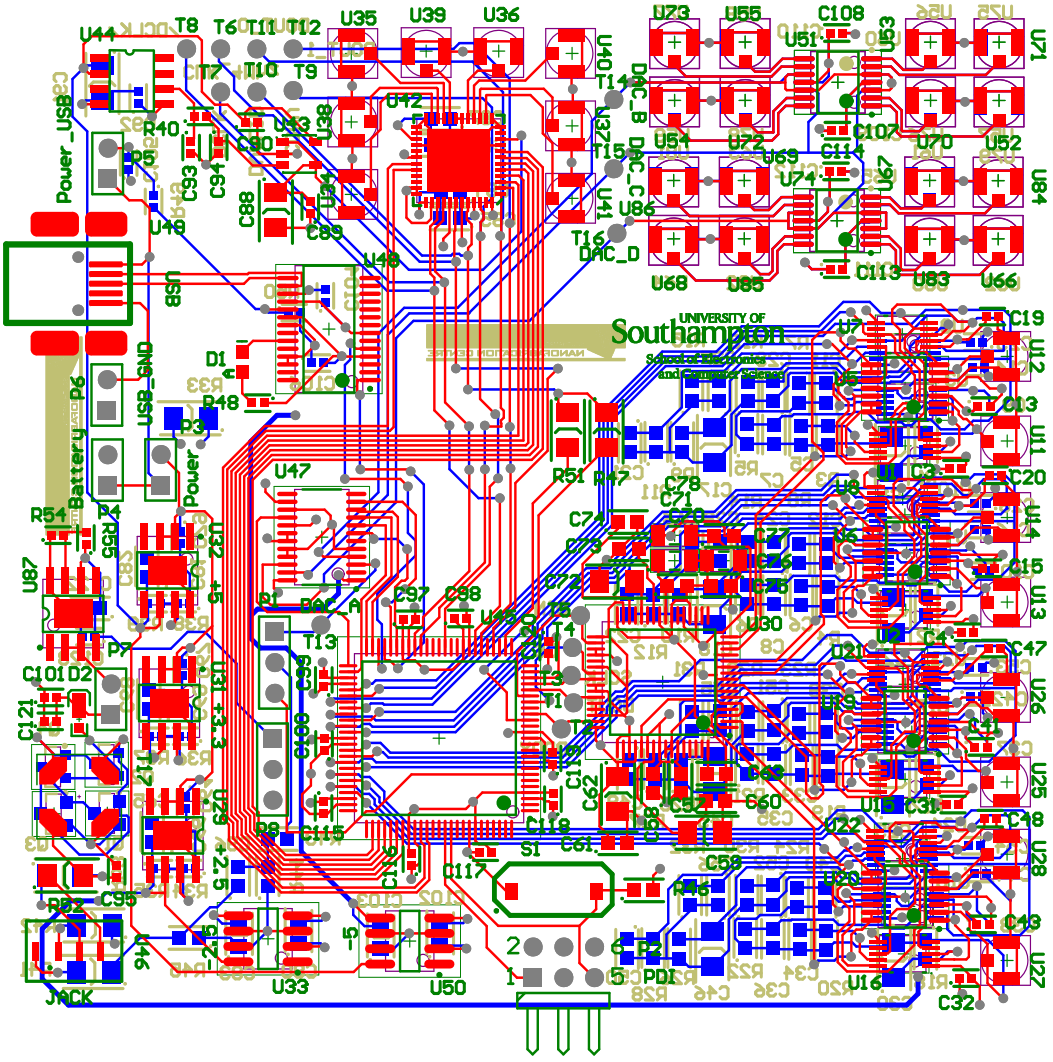

Figure B.8: 4-Layers layout of the bioinstrumentation board.

Appendix C

Biosensor Parameters Definitions

- **Accuracy:** describes how close is the measured value to the actual (true) value (36).
- **Precision:** describes the reproducibility of multiple measurements (36).
- **Sensitivity:** is the slope of a linear transfer function. It can also be described as the probability of test to be positive when disease present (36).
- **Selectivity:** presents the ability of the sensor to discriminate the needed response from the interfering inputs. (104).
- **Limit of Detection (LoD):** is the lowest concentration of an analyte, which it could be reliably distinguished and detected (105).
- **Low Cost:** is defined as less expensive than laboratory testing. (106).
- **Low Power Consumption:** is defined as power autonomy device. The device could be power free, powered by battery handheld or powered by a smartphone. (107).

References

[1] J. Howick, J. Cals, C. Jones, C. Price, A. Plüddemann, C. Heneghan, M. Berger, F. Buntinx, J. Hickner, W. Pace, T. Badrick, A. van den Bruel, C. Laurence, H. van Weert, E. van Severen, A. Parrella, and M. Thompson, "Current and future use of point-of-care tests in primary care: an international survey in australia, belgium, the netherlands, the uk and the usa," *BMJ Open*, vol. 4, no. 8, 2014.

[2] WHO, "WHO Call for Interest for Production of Open Point-of-Care Diagnostic Platforms Suitable for Low- and Middle-Income Countries," pp. 1–3, 2013. [Online]. Available: http://www.who.int/phi/Open{_}DX{_}Platform{_}WHO{_}Call{_}for{_}Interest.pdf

[3] D. Mabey, R. Peelin, A. Ustianowsk, and M. Perkin, "Tropical infectious diseases: Diagnostics for the developing world," *Nature reviews Microbiology*, vol. 2, no. 3, pp. 231–40, 2004. [Online]. Available: http://researchonline.lshtm.ac.uk/14771/

[4] A. Brunier and F. Chaib. (2017, March) Depression: let's talk says who, as depression tops list of causes of ill health. World Health Organization. [Online]. Available: http://www.who.int/mediacentre/news/releases/2017/world-health-day/en/

[5] WHO. (2017) Tuberculosis. [Online]. Available: http://www.who.int/mediacentre/factsheets/fs104/en/

[6] U. Secretariat, W. H. Organization *et al.* (2015) Tuberculosis: Diagnostics technology and market landscape. [Online]. Available: http://unitaid.org/assets/Tuberculosis_diagnostics_technology_and_market_landscape_4th_edition_Oct_2015-1.pdf

[7] (2012, July) The tuberculosis diagnostics pipeline. TAG Treatment Action Group. [Online]. Available: https://www.treatmentactiongroup.org/resources/pipeline-report/2012-pipeline-report/the-tuberculosis-diagnostics-pipeline/

[8] S. K. Srivastava, C. J. Van Rijn, and M. A. Jongsma, "Biosensor-based detection of tuberculosis," *RSC advances*, vol. 6, no. 22, pp. 17 759–17 771, 2016.

[9] N. P. Pai and M. Pai, "Point-of-care diagnostics for hiv and tuberculosis: landscape, pipeline, and unmet needs," *Discovery medicine*, vol. 13, no. 68, pp. 35–45, 2012.

[10] A. Bhimji, A. A. Zaragoza, L. S. Live, and S. O. Kelley, "Electrochemical enzyme-linked immunosorbent assay featuring proximal reagent generation: Detection of human immunodeficiency virus antibodies in clinical samples," *Analytical chemistry*, vol. 85, no. 14, pp. 6813–6819, 2013.

[11] H.-y. Tseng, "Development of Printed-Circuit-Board Based Industry-Compatible Point-of-Care Biosensing and Bioprocessing Technology with Applications," Ph.D. dissertation, 2015.

[12] W. Liang Li, S. Babikian, L. Guann-Pyng, and M. Bachman, "Microfluidic printed circuit boards," *2011 IEEE 61st Electronic Components and Technology Conference (ECTC)*, pp. 1576–1581, 2011.

[13] TECBRIDGE. (2017) Printed circuit board pcb instant price calculator. [Online]. Available: http://www.tecbridgecircuits.co.uk/priceform.php

[14] D. Moschou, L. Greathead, P. Pantelidis, P. Kelleher, H. Morgan, and T. Prodromakis, "Amperometric ifn-γ immunosensors with commercially fabricated pcb sensing electrodes," *Biosensors and Bioelectronics*, vol. 86, pp. 805–810, 2016.

[15] D. Evans, K. I. Papadimitriou, N. Vasilakis, P. Pantelidis, P. Kelleher, H. Morgan, and T. Prodromakis, "A novel microfluidic point-of-care biosensor system on printed circuit board for cytokine detection," *Sensors*, vol. 18, no. 11, 2018. [Online]. Available: https://www.mdpi.com/1424-8220/18/11/4011

[16] D. Evans, K. I. Papadimitriou, L. Greathead, N. Vasilakis, P. Pantelidis, P. Kelleher, H. Morgan, and T. Prodromakis, "An assay system for point-of-care diagnosis of tuberculosis using commercially manufactured pcb technology," *Scientific Reports*, 2017.

[17] Y. Hu, S. Sharma, J. Weatherwax, A. Cass, and P. Georgiou, "A portable multi-channel potentiostat for real-time amperometric measurement of multi-electrode sensor arrays," in *2016 IEEE International Symposium on Circuits and Systems (ISCAS)*, May 2016, pp. 1306–1309.

[18] N. G. Pechlivanidis, K. I. Papadimitriou, D. Evans, N. Vasilakis, and T. Prodromakis, "Towards a smartphone-aided electronic elisa for real-time electrochemical monitoring," in *International Symposium on Circuits and Systems (ISCAS), 2017 IEEE*. IEEE, 2017.

[19] G. Kost, "Guidelines for point-of-care testing. improving patient outcomes," *American journal of clinical pathology*, vol. 104, no. 4 Suppl 1, October 1995. [Online]. Available: http://europepmc.org/abstract/MED/7484942

[20] I. M. B. IMB, "Guidelines for safe and effective management and use of point of care testing in primary and community care," 2010.

[21] R. F. Louie, Z. Tang, D. G. Shelby, and G. J. Kost, "Point-of-Care Testing: Millennium Technology for Critical Care," *Lab Medicine*, vol. 31, no. 7, pp. 402–408, 2000. [Online]. Available: http://labmed.ascpjournals.org/content/31/7/402.abstract

[22] D. Unold and J. H. Nichols, "Point-of-Care Testing: Needs, Opportunity, and Innovation, 3rd Edition, by Christopher P. Price, Andrew St John, and Larry J. Kricka, eds." *Clinical chemistry*, vol. 56, pp. 1893–1894, 2010.

[23] P. N. Nge, C. I. Rogers, and A. T. Woolley, "Advances in microfluidic materials, functions, integration, and applications," *Chemical Reviews*, vol. 113, no. 4, pp. 2550–2583, 2013.

[24] J. Hu, S. Wang, L. Wang, F. Li, B. Pingguan-Murphy, T. J. Lu, and F. Xu, "Advances in paper-based point-of-care diagnostics," *Biosensors and Bioelectronics*, vol. 54, no. November, pp. 585–597, 2013.

[25] N. Guo, K. Cheung, H. T. Wong, and D. Ho, "CMOS time-resolved, contact, and multispectral fluorescence imaging for DNA molecular diagnostics," *Sensors*, vol. 14, no. 11, pp. 20 602–20 619, 2014.

[26] A. St John and C. P. Price, "Existing and Emerging Technologies for Point-of-Care Testing." *The Clinical biochemist. Reviews / Australian Association of Clinical Biochemists*, vol. 35, no. 3, pp. 155–67, 2014. [Online]. Available: http://www.pubmedcentral.nih.gov/articlerender.fcgi?artid=4204237{&}tool=pmcentrez{&}rendertype=abstract

[27] M. Medina-Sanchez, C. Martinez-Domingo, E. Ramon, S. Miserere, A. Alcalde-Aragones, J. Carrabina, and A. Merkoci, "Inkjet printed fet for biosensing applications," *16th International Conference on Miniaturized Systems for Chemistry and Life Sciences*, 2012.

[28] J. Li, F. Rossignol, and J. Macdonald, "Inkjet printing for biosensor fabrication: combining chemistry and technology for advanced manufacturing," *Lab on a Chip*, vol. 15, no. 12, pp. 2538–2558, 2015.

[29] R. Borkar, M. Bohr, and S. Jourdan, "Advancing Moore's Law on 2014!" *Intel*, pp. 1–86, 2014. [Online]. Available: http://www.intel.com/content/dam/www/public/us/en/documents/presentation/advancing-moores-law-in-2014-presentation.pdf

[30] Y. H. Ghallab and W. Badawy, *Lab-on-a-chip: techniques, circuits, and biomedical applications*. Artech House, 2010.

[31] F. B. Myers, R. H. Henrikson, J. Bone, and L. P. Lee, "A Handheld Point-of-Care Genomic Diagnostic System," *PLoS ONE*, vol. 8, no. 8, pp. 1–10, 2013.

[32] M. Pohanka and P. Skládal, "Electrochemical biosensors–principles and applications," *J. Appl. Biomed*, vol. 6, no. 2, pp. 57–64, 2008.

[33] J. P. Villagrasa, J. Colomer-Farrarons, and P. L. Miribel, *Bioelectronics for Amperometric Biosensors*. INTECH Open Access Publisher, 2013.

[34] M. Hiraiwa, J.-H. Kim, H.-B. Lee, S. Inoue, A. L. Becker, K. M. Weigel, G. A. Cangelosi, K.-H. Lee, and J.-H. Chung, "Amperometric immunosensor for rapid detection of mycobacterium tuberculosis," *Journal of Micromechanics and Microengineering*, vol. 25, no. 5, p. 055013, 2015.

[35] A. A. P. Ferreira, C. V. Uliana, M. de Souza Castilho, N. C. Pesquero, M. V. Foguel, G. P. dos Santos, C. S. Fugivara, A. V. Benedetti, and H. Yamanaka, "Amperometric biosensor for diagnosis of disease," in *State of the Art in Biosensors-Environmental and Medical Applications*. InTech, 2013.

[36] R. R. Pethig and S. Smith, *Introductory Bioelectronics: For Engineers and Physical Scientists*. John Wiley & Sons, 2012.

[37] C. V. Sapan, R. L. Lundblad, and N. C. Price, "Colorimetric protein assay techniques," *Biotechnology and applied Biochemistry*, vol. 29, no. 2, pp. 99–108, 1999.

[38] N. Nazeer. (2017) Spectrophotometry at a glance. [Online]. Available: http://slideplayer.com/slide/10410627/

[39] L. R. Volpatti and A. K. Yetisen, "Commercialization of microfluidic devices," *Lab on a Chip*, vol. 12, pp. 2118–2134, 2012.

[40] B. Michaels. (2010) Channelling Microfluidic Devices into Point of Care Diagnostics. Medical Product Manufacturing News. [Online]. Available: http://www.qmed.com/mpmn/article/channeling-microfluidic-devices-point-care-diagnostics

[41] M. Rhee, "Advanced components of microfluidic systems for bioanalytical applications," Ph.D. dissertation, University of Michigan, 2009.

[42] S. C. Terry, J. H. Jerman, and J. B. Angell, "A gas chromatographic air analyzer fabricated on a silicon wafer," *IEEE Transactions on Electron Devices*, vol. 26, no. 12, pp. 1880–1886, 1979.

[43] A. Wego and L. Pagel, "Self-filling micropump based on PCB technology," *Sensors and Actuators, A: Physical*, vol. 88, no. 3, pp. 220–226, 2000.

[44] D. Pagonis, A. Petropoulos, and G. Kaltsas, "A pumping actuator implemented on a pcb substrate by employing water electrolysis," *Microelectronic Engineering*, vol. 95, pp. 65 – 70, 2012. [Online]. Available: http://www.sciencedirect.com/science/article/pii/S0167931712000263

[45] N. Vasilakis, K. I. Papadimitriou, H. Morgan, and T. Prodromakis, "High-performance pcb-based capillary pumps for affordable point-of-care diagnostics," *Microfluidics and Nanofluidics*, vol. 21, no. 6, p. 103, 2017.

[46] N. Vasilakis, K. Papadimitriou, D. Evans, H. Morgan, and T. Prodromakis, "The lab-on-pcb framework for affordable, electronic-based point-of-care diagnostics: From design to manufacturing," in *Healthcare Innovation Point-Of-Care Technologies Conference (HI-POCT), 2016 IEEE*. IEEE, 2016, pp. 126–129.

[47] E. Berthier, E. W. K. Young, and D. Beebe, "Engineers are from PDMS-land, Biologists are from Polystyrenia," *Lab on a Chip*, vol. 12, no. 7, p. 1224, 2012. [Online]. Available: http://dx.doi.org/10.1039/C2LC20982A

[48] K. Yoshihisa, A. Yoshimura, Y. Shibamori, K. Fuchigami, and N. Kubota, "Hydrophilic modification of plastic surface by using microwave plasma irradiation," *IHI Eng. Rev*, vol. 46, no. 1, pp. 29–33, 2013.

[49] N. S. Lynn and D. S. Dandy, "Passive microfluidic pumping using coupled capillary/evaporation effects." *Lab on a chip*, vol. 9, no. 23, pp. 3422–3429, 2009. [Online]. Available: http://www.pubmedcentral.nih.gov/articlerender.fcgi?artid=2827300{&}tool=pmcentrez{&}rendertype=abstract

[50] A. Wego and L. Pagel, "A self-filling micropump based on pcb technology," *Sensors and Actuators A: Physical*, vol. 88, no. 3, pp. 220–226, 2001.

[51] J. Z. Kubicek-Sutherland, D. M. Vu, H. M. Mendez, S. Jakhar, and H. Mukundan, "Detection of lipid and amphiphilic biomarkers for disease diagnostics," *Biosensors*, vol. 7, no. 3, p. 25, 2017.

[52] GamryInstruments. (2014) Basics of electrochemical impedance spectroscopy. [Online]. Available: https://www.slideshare.net/GamryInstruments/basics-of-electrochemical-impedance-spectroscopy

[53] D. N. Ford, "Printed Circuit Board," vol. 2, pp. 1–5, 2014. [Online]. Available: http://www.madehow.com/Volume-2/Printed-Circuit-Board.html

[54] T. Nikola, "PCB Material," pp. 1–5, 2013. [Online]. Available: http://www.bitweenie.com/listings/pcb-materials/

[55] S. Biological. (2017) Elisa applications. [Online]. Available: http://www.elisa-antibody.com/ELISA-applications

[56] R. Gutlapalli, A. Sykam, S. P. Tenali, P. Chandran, S. Suneetha, and L. M. Suneetha, "Detection of tuberculosis in hiv co-infected individuals: Use of multiple elisa responses to 38kda, lipoarabinomannan and esat6 of m. tuberculosis," *Journal of clinical and diagnostic research: JCDR*, vol. 10, no. 2, 2016.

[57] BOSTER. (2017) Elisa principle-immunoassays. [Online]. Available: https://www.bosterbio.com/protocol-and-troubleshooting/elisa-principle

[58] S. Wang, F. Inci, G. De Libero, A. Singhal, and U. Demirci, "Point-of-care assays for tuberculosis: role of nanotechnology microfluidics," *Biotechnology advances*, vol. 31, no. 4, pp. 438–449, 2013.

[59] W. Jing, X. Jiang, W. Zhao, S. Liu, X. Cheng, and G. Sui, "Microfluidic platform for direct capture and analysis of airborne mycobacterium tuberculosis," *Analytical chemistry*, vol. 86, no. 12, pp. 5815–5821, 2014.

[60] WHO. (2011) Same-day diagnosis of tuberculosis by microscopy. [Online]. Available: http://apps.who.int/iris/bitstream/10665/44603/1/9789241501606_eng.pdf

[61] W. H. Organization *et al.*, "Commercial serodiagnostic tests for diagnosis of tuberculosis: policy statement," 2011.

[62] Cigna. (2016) Tuberculin skin test. [Online]. Available: https://www.cigna.com/healthwellness/hw/medical-tests/tuberculin-skin-test-hw203560

[63] B. Malhotra, "Guidelines for intensified tuberculosis case-finding and isoniazid preventative therapy for people living with hiv in resource-constrained settings," 2011.

[64] W. H. Organization. (2017, March) Blood tests recommended over skin tests to check for tb in most cases. LAB TESTS ONLINE AACC. [Online]. Available: http://www.who.int/mediacentre/news/releases/2017/world-health-day/en/

[65] W. H. Organization *et al.*, "Use of tuberculosis interferon-gamma release assays (igras) in low-and middle-income countries: policy statement," 2011.

[66] A. Trajman, R. Steffen, and D. Menzies, "Interferon-gamma release assays versus tuberculin skin testing for the diagnosis of latent tuberculosis infection: an overview of the evidence," *Pulmonary medicine*, vol. 2013, 2013.

[67] J. A. Sánchez, O. Henry, H. Joda, B. W. Solnestam, L. Kvastad, E. Johansson, P. Akan, J. Lundeberg, N. Lladach, D. Ramakrishnan *et al.*, "Multiplex pcb-based electrochemical detection of cancer biomarkers using mlpa-barcode approach," *Biosensors and Bioelectronics*, vol. 82, pp. 224–232, 2016.

[68] D. Moschou and A. Tserepi, "The lab-on-pcb approach: tackling the μtas commercial upscaling bottleneck," *Lab Chip*, vol. 17, pp. 1388–1405, 2017. [Online]. Available: http://dx.doi.org/10.1039/C7LC00121E

[69] M. Backer, D. Rakowski, A. Poghossian, M. Biselli, P. Wagner, and M. J. Schoning, "Chip-based amperometric enzyme sensor system for monitoring of bioprocesses

by flow-injection analysis," *Journal of biotechnology*, vol. 163, no. 4, pp. 371–376, 2013.

[70] C. D. Chin, S. Y. Chin, T. Laksanasopin, and S. K. Sia, "Low-Cost Microdevices for Point-of-Care Testing," *Biological andMedical Physics, Biomedical Engineering*, pp. 3–22, 2013. [Online]. Available: http://link.springer.com/10.1007/978-3-642-29268-2

[71] A. W. Martinez, S. T. Phillips, and G. M. Whitesides, "Three-dimensional microfluidic devices fabricated in layered paper and tape." *Proceedings of the National Academy of Sciences of the United States of America*, vol. 105, no. 50, pp. 19 606–19 611, 2008.

[72] W. Zhao, S. Tian, L. Huang, K. Liu, and L. Dong, "The review of lab-on-pcb for biomedical application," *ELECTROPHORESIS*, vol. n/a, no. n/a. [Online]. Available: https://onlinelibrary.wiley.com/doi/abs/10.1002/elps.201900444

[73] K. I. Papadimitriou, D. Evans, H. Morgan, and T. Prodromakis, "A pcb-based electronic elisa system for rapid, portable infectious disease diagnosis," in *Biomedical Circuits and Systems Conference (BioCAS), 2016 IEEE*. IEEE, 2016, pp. 1–4.

[74] D. G. Rackus, M. H. Shamsi, and A. R. Wheeler, "Electrochemistry, biosensors and microfluidics: a convergence of fields," *Chemical Society Reviews*, vol. 44, no. 15, pp. 5320–5340, 2015.

[75] L. Shen, J. A. Hagen, and I. Papautsky, "Point-of-care colorimetric detection with a smartphone," *Lab on a Chip*, vol. 12, no. 21, pp. 4240–4243, 2012.

[76] a. R. J. Mitchell and P. Le Page, "Living with the handheld ECG," *BMJ Innovations*, pp. 1–3, 2015. [Online]. Available: http://innovations.bmj.com/lookup/doi/10.1136/bmjinnov-2014-000029

[77] A. Pal, A. Sinha, A. Dutta Choudhury, T. Chattopadyay, and A. Visvanathan, "A Robust Heart Rate Detection Using Smart-phone Video," *Proceedings of the 3rd ACM MobiHoc Workshop on Pervasive Wireless Healthcare*, pp. 43–48, 2013. [Online]. Available: http://doi.acm.org/10.1145/2491148.2491156

[78] P. B. Lillehoj, M.-C. Huang, N. Truong, and C.-M. Ho, "Rapid electrochemical detection on a mobile phone." *Lab on a chip*, vol. 13, no. 15, pp. 2950–5, 2013. [Online]. Available: http://www.ncbi.nlm.nih.gov/pubmed/23689554

[79] A. Sun, T. Wambach, a. G. Venkatesh, and D. a. Hall, "A Low-Cost Smartphone-Based Electrochemical Biosensor for Point-of-Care Diagnostics," *IEEE Biomedied Circuits and Systems*, pp. 312–315, 2015.

[80] W. Chen, H. Yu, F. Sun, A. Ornob, R. Brisbin, A. Ganguli, V. Vemuri, P. Strzebonski, G. Cui, K. J. Allen *et al.*, "Mobile platform for multiplexed detection and differentiation of disease-specific nucleic acid sequences, using microfluidic loop-mediated isothermal amplification and smartphone detection," *Analytical chemistry*, vol. 89, no. 21, pp. 11 219–11 226, 2017.

[81] A. Orth, E. R. Wilson, J. Thompson, and B. C. Gibson, "A dual-mode mobile phone microscope using the onboard camera flash and ambient light," *Scientific reports*, vol. 8, no. 1, p. 3298, 2018.

[82] F. Zeng, W. Duan, B. Zhu, T. Mu, L. Zhu, J. Guo, and X. Ma, "Based versatile surface-enhanced raman spectroscopy chip with smartphone-based raman analyzer for point-of-care application," *Analytical chemistry*, vol. 91, no. 1, pp. 1064–1070, 2018.

[83] iHealth. (2017) Modern healthcare realized. [Online]. Available: https://ihealthlabs.com/

[84] Y.-S. Kuo, S. Verma, T. Schmid, and P. Dutta, "Hijacking power and bandwidth from the mobile phone's audio interface," *Proceedings of the First ACM Symposium on Computing for Development - ACM DEV '10*, p. 1, 2010. [Online]. Available: http://dl.acm.org/citation.cfm?id=1926180.1926210

[85] DropSens. (2018) Screen-printed electrodes (spes). [Online]. Available: http://www.dropsens.com/en/screen_printed_electrodes_pag.html

[86] MicroChemicals. (2019) Lift-off. [Online]. Available: https://www.microchemicals.eu/technical_information/lift_off_photoresist.pdf

[87] J. H. Lee, K. S. Hwang, T. S. Kim, J. W. Seong, K. H. Yoon, and S. Y. Ahn, "Effect of oxygen plasma treatment on adhesion improvement of au deposited on pa-c substrates," *Journal of the Korean Physical Society*, vol. 44, no. 5, pp. 1177–1181, 2004.

[88] C. A. Goss, D. H. Charych, and M. Majda, "Application of (3-mercaptopropyl) trimethoxysilane as a molecular adhesive in the fabrication of vapor-deposited gold electrodes on glass substrates," *Analytical Chemistry*, vol. 63, no. 1, pp. 85–88, 1991.

[89] H. Suzuki, H. Shiroishi, S. Sasaki, and I. Karube, "Microfabricated liquid junction ag/agcl reference electrode and its application to a one-chip potentiometric sensor," *Analytical Chemistry*, vol. 71, no. 22, pp. 5069–5075, 1999. [Online]. Available: https://doi.org/10.1021/ac990437t

[90] T. Rahman and T. Ichiki, "Fabrication and characterization of a stabilized thin film ag/agcl reference electrode modified with self-assembled monolayer of alkane

thiol chains for rapid biosensing applications," *Sensors*, vol. 17, no. 10, p. 2326, 2017.

[91] S. Gernet, M. Koudelka, and N. De Rooij, "Fabrication and characterization of a planar electrochemical cell and its application as a glucose sensor," *Sensors and Actuators*, vol. 18, no. 1, pp. 59–70, 1989.

[92] PalmSens. (2018) Palmsens3 potentiostat. [Online]. Available: https://www.palmsens.com/software/ps-trace/

[93] A. Touhami, B. Nysten, and Y. F. Dufrêne, "Nanoscale mapping of the elasticity of microbial cells by atomic force microscopy," *Langmuir*, vol. 19, no. 11, pp. 4539–4543, 2003.

[94] Syringe-Pump. (2019) Harvard apparatus 11 plus syringe pump. [Online]. Available: https://conquerscientific.com/product/harvard-apparatus-pump-ii-syringe-pump/

[95] Y. Wang, G. Mazurek, and E. Alocilja, "Measurement of interferon gamma concentration using an electrochemical immunosensor," *Journal of The Electrochemical Society*, vol. 163, pp. B140–B145, 01 2016.

[96] D. A. C. Fisher. (2018) Linear sweep and cyclic voltametry: The principles. [Online]. Available: https://www.ceb.cam.ac.uk/research/groups/rg-eme/teaching-notes/linear-sweep-and-cyclic-voltametry-the-principles

[97] S. Menolasina, "Electrochemical studies of fe (cn) 6 (4-)/fe (cn) 6 (3-) on gold ultramicroelectrodes varying the concentrations of kf as supporting electrolyte," *Revista Técnica de la Facultad de Ingeniería Universidad del Zulia*, vol. 28, no. 2, pp. 159–168, 2005.

[98] S. Mohanty and R. Codell, "Sensitivity analysis methods for identifying influential parameters in a problem with a large number of random variables," *WIT Transactions on Modelling and Simulation*, vol. 31, 2002.

[99] A. Saleh Ahammad, "Hydrogen peroxide biosensors based on horseradish peroxidase and hemoglobin," *J Biosens Bioelectron S*, vol. 9, p. 2, 2013.

[100] M. Druszczynska, M. Wlodarczyk, G. Kielnierowski, M. Kawka, and W. Rudnicka, "Two-year follow-up study of mycobacterium tuberculosis antigen-driven ifn-γ responses and macrophage scd14 levels after tuberculosis contact," *Indian journal of microbiology*, vol. 56, no. 2, pp. 205–213, 2016.

[101] S. Nayak and B. Acharjya, "Mantoux test and its interpretation," *Indian dermatology online journal*, vol. 3, no. 1, p. 2, 2012.

[102] (2020) Mantoux test cost. Medifee. [Online]. Available: https://www.medifee.com/tests/mantoux-cost/

[103] M. Arias-Guillén, M. M. S. Menéndez], M. Alperi, S. Riestra, M. T. G. Budiño], M. M. García-Clemente, S. Martínez-González, A. I. Enríquez, R. Alonso-Arias, J. J. P. Gutiérrez], M. Santibáñez, P. Coto-Segura, P. M. Camblor, L. García-Alfonso, I. Morante, and P. Escalante, "High rates of tuberculin skin test positivity due to methotrexate therapy: False positive results?" *Seminars in Arthritis and Rheumatism*, vol. 48, no. 3, pp. 538 – 546, 2018. [Online]. Available: http://www.sciencedirect.com/science/article/pii/S0049017217306522

[104] A. D'Amico and C. Di Natale, "A contribution on some basic definitions of sensors properties," *IEEE Sensors Journal*, vol. 1, no. 3, pp. 183–190, Oct 2001.

[105] G. Indrayanto, "Chapter five - validation of chromatographic methods of analysis: Application for drugs that derived from herbs," ser. Profiles of Drug Substances, Excipients and Related Methodology, H. G. Brittain, Ed. Academic Press, 2018, vol. 43, pp. 359 – 392. [Online]. Available: http://www.sciencedirect.com/science/article/pii/S1871512518300037

[106] A. El-Osta, M. Woringer, E. Pizzo, T. Verhoef, C. Dickie, M. Z. Ni, J. R. Huddy, M. Soljak, G. B. Hanna, and A. Majeed, "Does use of point-of-care testing improve cost-effectiveness of the nhs health check programme in the primary care setting? a cost-minimisation analysis," *BMJ Open*, vol. 7, no. 8, 2017. [Online]. Available: https://bmjopen.bmj.com/content/7/8/e015494

[107] S. Choi, "Powering point-of-care diagnostic devices," *Biotechnology Advances*, vol. 34, no. 3, pp. 321 – 330, 2016, trends in In Vitro Diagnostics and Mobile Healthcare. [Online]. Available: http://www.sciencedirect.com/science/article/pii/S0734975015300549